from which waste would first reach the shaf
were made using lithostatic and hydrostati
lower- and upper-bound limits for the travel
threshold concentrations were used, 10^{-10} cur
10^{-9} g/day for lead. The revised calculation
by Lappin et al. (1989), indicate that no
released into the Culebra Dolomite within the
years; release times range from 27,000 to >1
parameters used. These times are longer tha
al. (1989).

Issued by Sandia National Laboratories, operated for the United States Department of Energy by Sandia Corporation.

Printed in the United States of America. This report has been reproduced directly from the best available copy.

Available to DOE and DOE contractors from
Office of Scientific and Technical Information
PO Box 62
Oak Ridge, TN 37831

Prices available from (615) 576-8401, FTS 626-8401

Available to the public from
National Technical Information Service
US Department of Commerce
5285 Port Royal Rd
Springfield, VA 22161

NTIS price codes
Printed copy: A14
Microfiche copy: A01

SAND89-1996
Unlimited Release
Printed December 1990

SAND--89-1996

DE91 007150

SYSTEMS ANALYSIS, LONG-TERM RADIONUCLIDE TRANSPORT, AND DOSE ASSESSMENTS, WASTE ISOLATION PILOT PLANT (WIPP), SOUTHEASTERN NEW MEXICO; SEPTEMBER 1989

A. R. Lappin, R. L. Hunter, P. B. Davies, D. J. Borns,

M. Reeves*, J. Pickens*, and H. J. Iuzzolino**

*INTERA
**GEO-CENTERS, Inc.

Abstract

This study supports the Waste Isolation Pilot Plant (WIPP) Final Supplemental Environmental Impact Statement and has two main objectives. First, it describes current ideas about the characteristics and potential impacts of the disturbed-rock zone (DRZ) known to develop with time around excavations at the WIPP horizon. Second, it presents new calculations of radionuclide migration within and from the WIPP repository for steady-state undisturbed conditions and for two cases that consider human intrusion into the repository.

A DRZ will develop near underground openings in salt. At the WIPP, the presence of a DRZ has been confirmed by geophysical studies, gas-flow tests, and direct observations. The DRZ results from dilation and rapid strain rates near the excavation. The behavior of the DRZ may include slabbing of the roofs of rooms, entryways, and accessways. The DRZ will allow gas or brine from waste-emplacement panels to bypass panel seals and flow into adjacent portions of the underground workings unless preventive measures are taken. The DRZ may alter fluid-flow behavior within the Salado Formation near the repository and increase the flow of brine into the repository, but fractures within the DRZ should also provide significant storage capacity for gases that may be generated as a result of brine inflow.

Revised calculations of the undisturbed performance of the repository indicate that no radionuclides will be released into the Culebra Dolomite within the regulatory period of 10,000 years. Because no exposures to human beings are possible, no dose calculations are warranted.

The human-intrusion calculations included here assume a connection between the WIPP repository, an occurrence of pressurized brine within the underlying Castile Formation, and the overlying Culebra Dolomite. The calculations differ in three important ways from earlier calculations performed in support of the Draft Supplemental Environmental Impact Statement: two-dimensional contaminant transport within the Culebra is modeled more realistically; the new calculations use a revised Culebra transmissivity distribution; and the new calculations explicitly compare and contrast results of single- and double-porosity calculations. The improved calculations change the previous estimates of the consequences of human intrusion in several ways. For expected conditions within the Castile Formation, the repository, and the Culebra Dolomite, integrated releases at the WIPP site boundary are several orders of magnitude below those allowed by the present form of 40 CFR 191. For unlikely, degraded flow-and-transport conditions within the repository and the Culebra Dolomite, integrated releases at the WIPP site boundary at 10,000 years are calculated to be 3.2 times the limit presently set by 40 CFR 191 for releases with probabilities greater than 0.1 and less than the limit set for releases with probabilities less than 0.1. The calculated release at 5 km is 0.7 times that limit. Calculated individual 50-year dose commitments from daily ingestion of beef contaminated by Culebra ground waters are 7.9×10^{-7} mrem/50 years for expected conditions and 28 mrem/50 years for degraded conditions. Both dose commitments are lower than calculated earlier.

Acknowledgments

Van Kelley and Geoff Freeze of INTERA supported simulations of ground-water flow and transport for Chapter 4. Rob Rechard and Fred Mendenhall provided useful comments on the manuscript; editorial assistance was provided by Ed Lorusso. We appreciate the support of these colleagues.

CONTENTS

Page

EXECUTIVE SUMMARY xi

1.0 INTRODUCTION 1

2.0 DISTURBED ROCK ZONE (DRZ) 5

2.1 Description of the DRZ 9
2.1.1 Fracture Observations at WIPP 9
2.1.2 Fracture Pattern around Excavations 10
2.1.3 Observation of Hydrologic Effects of the DRZ 11
2.1.4 Mechanical Processes Active in the DRZ 12
2.1.5 Maximum Extent of the DRZ and Its Evolution Through Time 15

2.2 Possible Effects of the DRZ 16
2.2.1 Impacts on Seals 16
2.2.2 Impacts on Shaft Stations, Tramways, and Access Drifts 16
2.2.3 Impacts on General Structural Response of the Salado Formation 17
2.2.4 Impacts on the Hydrologic Response of the Salado Formation 18
2.2.5 Impacts on Gas and Brine Storage 19
2.2.6 Impacts of Ground Control Methods, Including Rock Bolting 20
2.2.7 Summary of Previous and Current Assumptions About the DRZ 20

3.0 RADIONUCLIDE TRANSPORT IN THE ABSENCE OF HUMAN INTRUSION 27

3.1 Description of Cases IA′ and IB′ 27

3.2 Results of NEFTRAN Calculations 31

4.0 CONTAMINANT TRANSPORT AND DOSES ARISING FROM HUMAN INTRUSION 33

4.1 Numerical Implementation of Post-Plugging Analysis 34
4.1.1 Modeling Approach 34
4.1.2 Two-Dimensional Calculations of Flow and Transport 39

4.2 Input Parameters for Post-Plugging Analysis 42
4.2.1 Brine-Reservoir Parameters 42
4.2.2 Intrusion-Borehole Parameters 42
4.2.3 Repository Source-Term Parameters 46
4.2.4 Culebra Parameters 51
4.2.4.1 Regional Flow Field 51
4.2.4.2 Culebra Transport Parameters 58

4.3 Post-Plugging Release to the Culebra Dolomite 58
4.3.1 Fluid and Waste Release to the Culebra Dolomite 58
4.3.2 Transport Pathways and Particle Travel Times in the Culebra 63

CONTENTS (concluded)

Page

4.3.3 Contaminant Transport for Case IIA' 65
4.3.4 Contaminant Transport for Case IIC' 73
4.3.4.1 Centerline Concentrations 73
4.3.4.2 Integrated Releases of Radionuclides 89
4.3.4.3 Radiation Doses 89

4.4 Other Consequences of Human Intrusion 92

5.0 SUMMARY 95

5.1 Disturbed Rock Zone 95

5.2 Cases IA' and IB', Undisturbed Performance 95

5.3 Cases IIA' and IIC', Effects of Human Intrusion 96
5.3.1 Doses Arising from Releases at the Head of the Intrusion Well 96
5.3.2 Doses Arising from Ingestion of Contaminated Beef 96
5.3.3 Integrated Releases 97

6.0 REFERENCES 99

APPENDIX A: UNPUBLISHED MEMORANDUM A-1

TABLES

Page

2-1. Current understanding of the DRZ, contrasted with the assumptions in the calculations of Lappin et al. (1989) 24

3-1. Numerical parameters used by NEFTRAN for Cases IA' and IB' 28

3-2. Retardation factors for use in Cases IA' and IB' 29

3-3. Arrival times at intermediate points between waste-disposal rooms and the Culebra Dolomite 30

4-1. Parameter base-case and range values selected for the hypothetical brine reservoir, Case II 44

4-2. Specifications for the intrusion borehole, Case II' 47

4-3. Mass inventory of radionuclide species and stable lead in the repository, Case II' 49

4-4. Repository parameters, Case II' 50

4-5. Parameter base-case and range values selected for the Culebra Dolomite, Case II' 52

4-6. Characteristics of the waste plume within the Culebra Dolomite from point of release to stock well 59

4-7. Free-water diffusion coefficients (cm^2/s) for radionuclides and stable lead, Case II 60

4-8. Times of source depletion, times to reach peak concentrations, and calculated peak concentrations, all at site boundary and stock well 64

4-9. Normalized integrated release at site boundary and stock well at 10,000 years, Case IIA' 72

4-10. Normalized integrated release at site boundary and stock well over 10,000 years, Case IIC' 88

4-11. Radionuclide concentrations (kg/kg brine) in the Culebra aquifer at the stock well at 10,000 years for all cases 90

4-12. Maximum 50-year committed effective dose equivalent after a 1-year exposure to contaminated beef 91

FIGURES

Page

1-1. Setting of the WIPP site relative to the northern Delaware Basin, showing selected geomorphic features and some boreholes..... 2

1-2. Generalized stratigraphic column of the Delaware Mountain Group and younger sedimentary rocks at and near the WIPP site..... 3

2-1. Map view of existing and planned underground workings..... 6

2-2. Geologic cross section at the repository horizon..... 7

2-3. Conditions around underground openings, shown in cross section..... 8

2-4. Generalized time-strain relationship for salt deformation, showing primary, secondary, and tertiary creep..... 13

2-5. Wall convergence in SPDV Room 1, with rates beginning to increase in early 1989..... 14

2-6. Cross section of rock-bolt installation in Panel 1..... 21

2-7. Horizontal plan of vertical rock-bolt pattern in roof of Panel 1... 22

3-1. Numerical flow-network input for simulation of Cases IA' and IB'..... 28

4-1. Schematic diagram of the brine-reservoir-breach release simulation..... 35

4-2. Model area, site boundary (projected land-withdrawal boundary), waste-panel layout, breach-borehole and stock-well locations, and transport pathways..... 36

4-3. Comparison of modeling assumptions and actual intrusion well..... 38

4-4. Schematic illustration of streamlines in a unidirectional flow field perturbed by an injection well..... 41

4-5. Schematic illustration of the two-dimensional grid for the Culebra Dolomite used for Case-II simulations using SWIFT II..... 43

4-6. Schematic illustration of intrusion borehole after plug emplacement..... 45

4-7. Distribution of Culebra transmissivities, as estimated by LaVenue et al. (1988) and used by Lappin et al. (1989)..... 53

4-8. Simulated flow field (Darcy velocities) for the Culebra Dolomite under undisturbed conditions, as estimated by LaVenue et al. (1988) and used by Lappin et al. (1989)..... 54

FIGURES (continued)

Page

4-9. Initial kriged transmissivity estimation errors in Culebra transmissivity distribution used in this report..... 55

4-10. Distribution of Culebra transmissivities, as estimated by LaVenue et al. (1990) and used in this report..... 56

4-11. Simulated flow field (Darcy velocities) for the Culebra Dolomite under undisturbed conditions, as estimated by LaVenue et al. (1990) and used in this report..... 57

4-12. Flow rates to the Culebra Dolomite from the intrusion borehole, Cases IIA' and IIC'..... 61

4-13. Concentration profiles along the plume centerline for stable Pb at 10,000 years, Case IIA'..... 66

4-14. Concentration profiles along the plume centerline for the ^{240}Pu decay chain at 10,000 years, Case IIA'..... 68

4-15. Concentration profiles along the plume centerline for the ^{239}Pu decay chain at 10,000 Years, Case IIA'..... 69

4-16. Concentration profiles along the plume centerline for the ^{238}Pu decay chain at 10,000 years, Case IIA'..... 70

4-17. Concentration profiles along the plume centerline for the ^{241}Am decay chain at 10,000 years, Case IIA'..... 71

4-18. Concentration profiles along the plume centerline for stable Pb at 10,000 years, Case IIC'..... 74

4-19. Breakthrough concentrations at stock well for stable Pb as a function of time, Case IIC'..... 75

4-20. Lateral concentration profile across contaminant plume at stock well for stable Pb at 10,000 years, Case IIC'..... 77

4-21. Concentration profiles along the plume centerline for the ^{240}Pu decay chain at 10,000 years, Case IIC'..... 79

4-22. Breakthrough concentrations at stock well for the ^{240}Pu decay chain as a function of time, Case IIC'..... 80

4-23. Concentration profiles along the plume centerline for the ^{239}Pu decay chain at 10,000 years, Case IIC'..... 81

4-24. Breakthrough concentrations at stock well for the ^{239}Pu decay chain as a function of time, Case IIC'..... 82

4-25. Concentration profiles along the plume centerline for the ^{238}Pu decay chain at 10,000 years, Case IIC'..... 83

FIGURES (concluded)

Page

4-26. Breakthrough concentrations at stock well for the ^{238}Pu decay chain as a function of time, Case IIC' 84

4-27. Concentration profiles along the plume centerline for the ^{241}Am decay chain at 10,000 years, Case IIC' 85

4-28. Breakthrough concentrations at stock well for the ^{241}Am decay chain as a function of time, Case IIC' 86

4-29. Breakthrough concentrations at stock well for ^{226}Ra as a function of free-water diffusivity, Case IIC' 87

4-30. Radiation doses to individuals who ingest contaminated beef from cattle watered at the stock well, Cases IIC and IIC' 93

EXECUTIVE SUMMARY

This report has been written in support of the Waste Isolation Pilot Plant (WIPP) Final Supplemental Environmental Impact Statement (FSEIS) (U.S. Dept. of Energy (DOE), 1990a). The report is a companion to a similar report (Lappin et al., 1989) completed in support of the WIPP Draft Supplemental Environmental Impact Statement (DSEIS) (DOE, 1989a). Draft chapters and final calculations from this report were distributed to Federal reading rooms as part of the public record prior to publication of the FSEIS. In order to maintain consistency with the FSEIS, information more recent than June 1989 is not included here. In general terms, the conceptual model of the expected behavior of the WIPP repository has not changed since the work of Lappin et al. (1989) and the publication of the WIPP DSEIS (DOE, 1989a). Only those conceptual or numerical aspects of the overall model that have changed have been revised for this report.

This report has two main objectives. First, it describes current thinking about the characteristics and potential effects of the disturbed-rock zone (DRZ) known to develop with time around excavations at the WIPP horizon. The DRZ may affect repository sealing and both the near-field structural response and fluid-flow response of the Salado Formation. The brief description of the DRZ by Lappin et al. (1989) is superseded here. Second, this report revises calculations of radionuclide migration within and from the WIPP repository for steady-state undisturbed conditions (Cases IA' and IB') and for two cases that consider human intrusion into the repository (Cases IIA' and IIC'). Both radionuclides and stable lead are considered. The hypothetical human intrusion by hydrocarbon-exploration drilling connects the WIPP with an underlying occurrence of pressurized brine in the Castile Formation and with the overlying Culebra Dolomite. Integrated radionuclide releases to the accessible environment and individual doses resulting from ingestion of contaminated beef are calculated.

Disturbed-Rock Zone

The far-field mechanical response of the Salado Formation to construction of the WIPP underground workings is expected to be dominated by creep closure of a coherent rock mass. Long-term containment of waste within the Salado Formation is expected to result from compaction of waste and backfill by creep closure and minimization of waste/backfill permeability. However, the time-dependent development of a DRZ is inherent in the near-field domain around underground openings in salt unless mechanical closure of the openings is prevented.

The near-field domain is defined here as the volume within which the intrinsic hydrologic and mechanical properties of the Salado have been changed. In 1988, the DRZ was 2 to 4 m thick in rooms excavated in 1983. It should reach its maximum extent in twenty years or less. In the long term, the DRZ will decrease in size and its connectivity will be greatly reduced in response to far-field creep closure and backpressure exerted within the waste-emplacement rooms by the waste and backfill. However, the timing and extent of rehealing of relatively stiff marker beds, such as MB139, remain to be determined.

At the WIPP, the presence of a DRZ has been confirmed by geophysical studies, gas-flow tests, and direct observations. The origin of the DRZ is

complex; however, it is a function of dilation and rapid strain rates near the excavation. Several processes are apparently involved in forming the DRZ: strain-dependent brittle fracturing; dilatant microfracturing and increase in pore volume in response to fluid expansion or exsolution of contained gases; and partial brine desaturation. These processes lead to the development of a volume of disturbed rock that is partially detached within an "active opening" somewhat larger than the geometric opening. The active opening should reach a maximum size of no more than five times the effective radius of the original opening.

The presence of a significant DRZ is expected to have several potential effects. The presence of a DRZ may allow gas or brine to bypass emplaced panel seals and escape from waste-emplacement panels into adjacent portions of the WIPP underground workings. This would be an advantage from the point of view of decreasing internal gas pressures, but it could also increase the effective foot-print of the WIPP in performance-assessment considerations of human intrusion. Bypassing may occur unless the formation of a DRZ, especially within Marker Bed 139, is locally prevented (e.g., by emplacement of a rigid ring) or unless increased DRZ permeability is eliminated by such approaches as pressure grouting.

One long-term effect of the formation of a DRZ is slabbing of the roofs (backs) of rooms, entryways, and accessways. Such an event occurred in Room A-2 during the summer of 1990. Rock bolting of the roofs has begun at the WIPP for ground control; however, underground workings that must remain open for the entire WIPP operational period, such as the major accessways or haulage ways, will continue to age and creep closed. Floor trimming used to maintain opening clearance might also expose Marker Bed 139. The panel seals in the central haulage ways must be emplaced in openings that will be much older than openings for the normal waste-emplacement panels.

The presence of the DRZ may alter general fluid-flow behavior within the Salado Formation near the repository. First, a DRZ may allow increased flow of brine into the repository, due either to the local increases in permeability or to two-phase flow in response to gas evolution within the DRZ. However, fractures within the DRZ could also provide significant storage capacity for gases that may be generated as a result of brine inflow and reaction with waste materials.

In the long term, partial saturation of the matrix within the DRZ may result in a zone of relatively decreased brine permeability near the repository. With the possible exception of the marker beds, the connectivity of the DRZ is expected to be greatly reduced during the final stages of closure of the repository in response to far-field creep. In general, although the DRZ is important during the transient phases of repository behavior, it is not expected to affect the final state of the WIPP repository significantly.

Undisturbed Performance

Predictions of the undisturbed performance of the repository are revised in four ways from the work of Lappin et al. (1989). First, the porosity of MB139 and the cross-sectional area of the path through MB139 have been increased to more accurately reflect the geometry of the seals in the marker bed. Second, the geometry and location of the waste storage room and marker bed seal were changed to model the panel closest the shaft, presumably the one

from which waste would first reach the shaft. Third, separate simulations were made using lithostatic and hydrostatic driving pressures to produce lower- and upper-bound limits for the travel times. Finally, more-realistic threshold concentrations were used, 10^{-10} curies/day for radionuclides and 8 x 10^{-9} g/day for lead. The revised calculations, like the earlier calculations by Lappin et al. (1989), indicate that no radioactive materials will be released into the Culebra Dolomite within the regulatory time period of 10,000 years; release times range from 27,000 to >10,000,000 years depending of the parameters used. These times are longer than those calculated by Lappin et al. (1989).

Human-Intrusion Calculations

The human-intrusion calculations included here are analogous to those performed by Lappin et al. (1989) in support of the WIPP DSEIS (DOE, 1989a). Calculations assume a connection between the WIPP repository, an occurrence of pressurized brine within the underlying Castile Formation, and the overlying Culebra Dolomite. These new calculations differ in three important ways from the earlier calculations.

First, contaminant transport within the Culebra is modeled more realistically than in the previous work. For example, lateral dispersion of contaminants and the time-dependent widths of the contaminant plume resulting from variable rates of brine injection from the Castile Formation are modeled explicitly. In the earlier work, contaminant transport was calculated assuming constant, one-dimensional stream tubes. The more realistic modeling of contaminant transport in this report significantly decreases both doses and integrated radionuclide releases at the WIPP land-withdrawal boundary and at a hypothetical stock well approximately 5 km downstream along the Culebra flowpath.

Second, the new calculations use a revised Culebra transmissivity distribution (LaVenue et al., 1990). The revised transmissivity distribution is based on interpretation of all of the major hydrologic stresses that have been applied to the Culebra during site characterization, including the H-3 and H-11 multipad interference tests and construction of the WIPP shafts. The revised Culebra flow path indicates that contaminants injected to the Culebra from an intrusion well penetrating the southwest waste-emplacement panel (nearly identical to the location assumed in the earlier study) would follow a more easterly path than indicated by Lappin et al. (1989). Although the flow paths from the intrusion well to both the WIPP site boundary and the hypothetical stock well are longer than estimated previously, Darcy velocities are slightly higher, and the net result is that ground-water travel times along the two paths are similar.

Third, the calculations in this report explicitly compare results of single-porosity and double-porosity calculations. Even for the nominal or expected properties of the Culebra, contaminant transport over distances as great as 5 km is greatly affected by the presence of fracturing. This is in direct contrast to earlier conclusions (Reeves et al., 1987) that contaminant transport within the Culebra could be modeled reliably using a single-porosity formalism for transport distances of 5 km or more.

Estimates of direct exposure to a member of the drilling crew and indirect exposure to a hypothetical farm family living 500 m from the location of the

intrusion well remain unchanged from estimates contained in the DSEIS (DOE, 1989a). However, three other consequences of human intrusion into the WIPP are revised in this report. First, for expected conditions within the Castile brine occurrence, the WIPP repository, and the Culebra Dolomite (Case IIA'), integrated releases at the WIPP site boundary are several orders of magnitude below those allowed by the present form of 40 CFR 191. The normalized integrated release at 10,000 years (neglecting cuttings brought directly to the surface during drilling) is calculated to be 1.7×10^{-6} times the allowed release. Similarly, the integrated release at the distance of the hypothetical stock well (5 km) is 1.9×10^{-10} times the allowed amount. Second, for unlikely, degraded flow-and-transport conditions within both the WIPP repository and the Culebra Dolomite (Case IIC'), integrated releases at the WIPP site boundary at 10,000 years are calculated to be 3.2 times the limit presently set by 40 CFR 191 for releases with probability greater than 0.1. The calculated release at 5 km is only 0.7 times that limit for Case IIC'. Although it may be possible to estimate combinations of flow-and-transport properties within the Culebra and the repository for which compliance with 40 CFR 191 is not certain, these combinations have low probability. For releases with probability between 0.001 and 0.1, the normalized integrated release must be less than 10, as both results for Case IIC' are. These results indicate both that there is appreciable potential for radionuclide storage in the volume of the Culebra between the site boundary and the distance of the hypothetical stock well and that compliance with 40 CFR 191 is probably attainable. If additional assurance is desirable, the administratively controlled zone could be expanded.

Calculated individual 50-year dose commitments from daily ingestion of beef contaminated by drinking of contaminated Culebra ground waters directly downstream from the assumed intrusion well are less than those estimated by Lappin et al. (1989). For Case IIA', the maximum 50-year dose commitment from one year of beef ingestion is 7.9×10^{-7} mrem/50 years, as opposed to the 2.1×10^{-4} mrem/50 years estimated earlier. For Case IIC', the comparable estimates are 28 mrem/50 years versus 130 mrem/50 years. After cumulative effects from 50 years of beef ingestion, these values would be equivalent to the annual dose commitment. For comparison, the average national background radiation is about 100 mrem/year.

1.0 INTRODUCTION

The Waste Isolation Pilot Plant (WIPP) in southeastern New Mexico (Figure 1-1) is designed for the receipt, handling, storage, and disposal of defense-generated transuranic (TRU) wastes. The WIPP underground workings are currently being constructed at a depth of ~655 m in bedded halites in the lower portion of the Salado Formation (Fm.) (Figure 1-2). The U.S. Department of Energy (DOE) has published a number of reports describing the WIPP and its expected performance. One of these was the Final Environmental Impact Statement (FEIS, DOE, 1980). Following publication of the FEIS, the first shafts and drifts were excavated, and many data-collection programs were continued or instituted.

In 1988, before receiving the first waste at the WIPP, the DOE decided to prepare a Supplemental Environmental Impact Statement (SEIS) that would reassess the long-term performance of the WIPP in the light of improved understanding of the geology and hydrology of the site and of changes in both technical and regulatory requirements for the repository. The draft WIPP SEIS (DSEIS; DOE, 1989a) specifically addressed those areas in which the conceptual, numerical, and regulatory understanding of the expected behavior of the WIPP repository had significantly improved since the WIPP FEIS was prepared in 1980 (DOE, 1980). Both the overall conceptual model of repository behavior and the calculations of long-term repository performance in the draft SEIS were based, in part, on a study by Lappin et al. (1989). Because Lappin et al. performed a large number of calculations simultaneously, however, some are slightly inconsistent; for example, most calculations of ground-water flow within the Salado Formation were based on a preliminary estimate of 14.0 MPa for lithostatic pressure at the repository horizon; concurrent calculations determined 14.8 MPa to be the best estimate. In addition, some of the calculational techniques used by Lappin et al. (1989), e.g., the calculation of radionuclide concentration in a contaminant plume downstream of an intrusion well within the Culebra Dolomite, provided conservative upper bounds that were somewhat ambiguous when compared with the EPA standard (40 CFR 191).* Therefore, this study repeats the calculations of Lappin et al. (1989) using consistent parameter values throughout and, in some cases, improved calculational techniques. In general, the conceptual model of repository behavior is not revised here from that described by Lappin et al. (1989). The single exception is the description of the disturbed rock zone (DRZ) immediately surrounding the underground workings, which is updated.

Thus this report has two primary objectives. First, it briefly summarizes Sandia's current technical understanding of the DRZ (Chapter 2.0). This summary is consistent with the understanding presented by Lappin et al. (1989), but expands the discussion found in their report.

---

* The U.S. Environmental Protection Agency (EPA) has determined that the safe disposal of TRU wastes requires effective isolation of the waste from the accessible environment for thousands of years. The EPA has developed a standard for the performance of nuclear-waste repositories (40 CFR 191; EPA, 1985) that regulates the performance of a proposed repository on time scales that extend to 10,000 years. Although 40 CFR 191 Subpart B has been remanded to the EPA by the United States Court of Appeals for the First Circuit (Natural Resources Defense Council v. U.S. Environmental Protection Agency, 824 F.2d 1258 (1st Cir. 1987)), the WIPP Project will continue to respond to 40 CFR 191 as first promulgated until a new standard is in place (DOE and State of New Mexico, 1981, as modified 1987). Methods for applying 40 CFR 191 have been discussed by Rechard (1989).

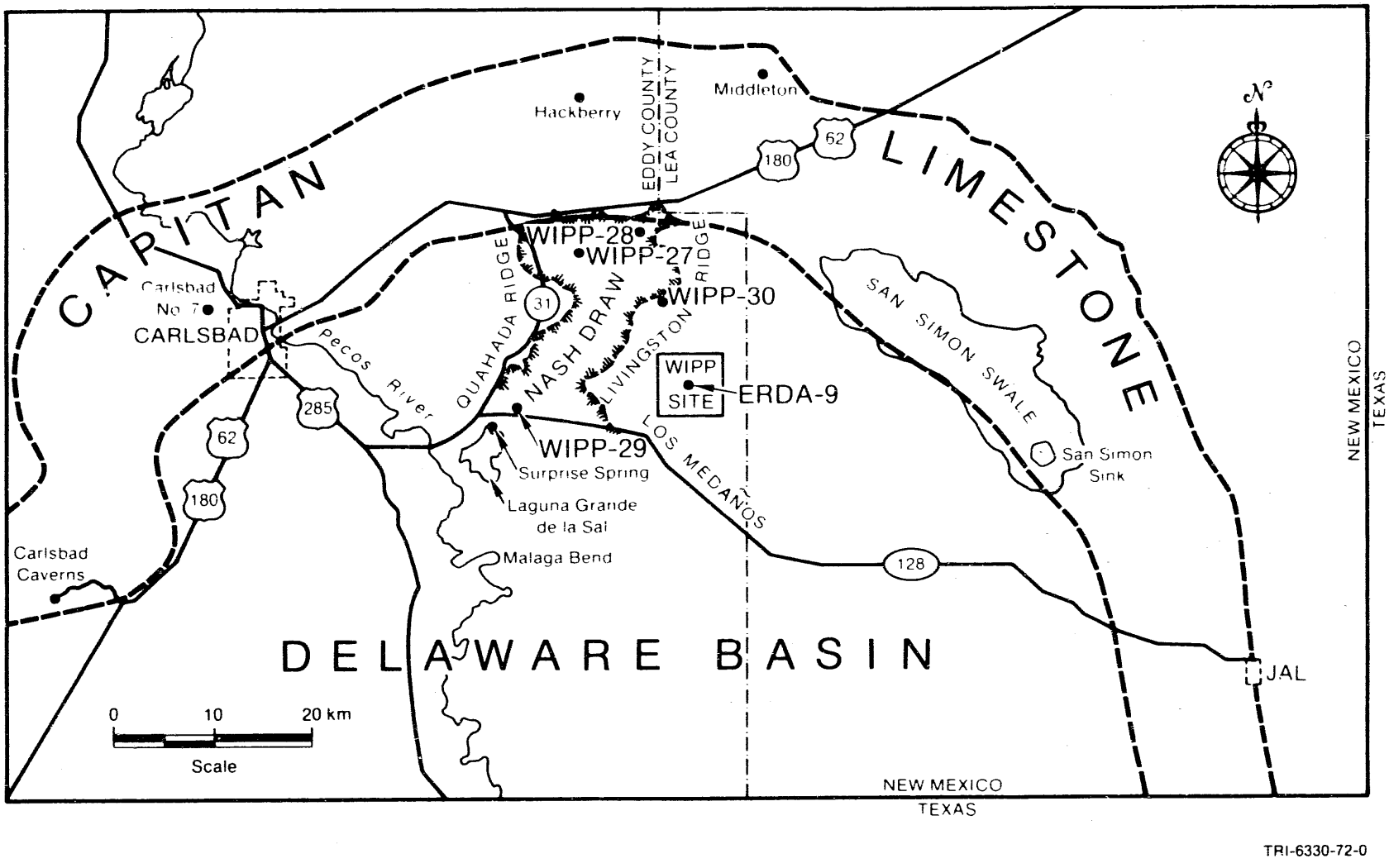

Figure 1-1. Setting of the WIPP site relative to the northern Delaware Basin, showing selected geomorphic features and some boreholes (after Lambert, 1983, Fig. VI-1).

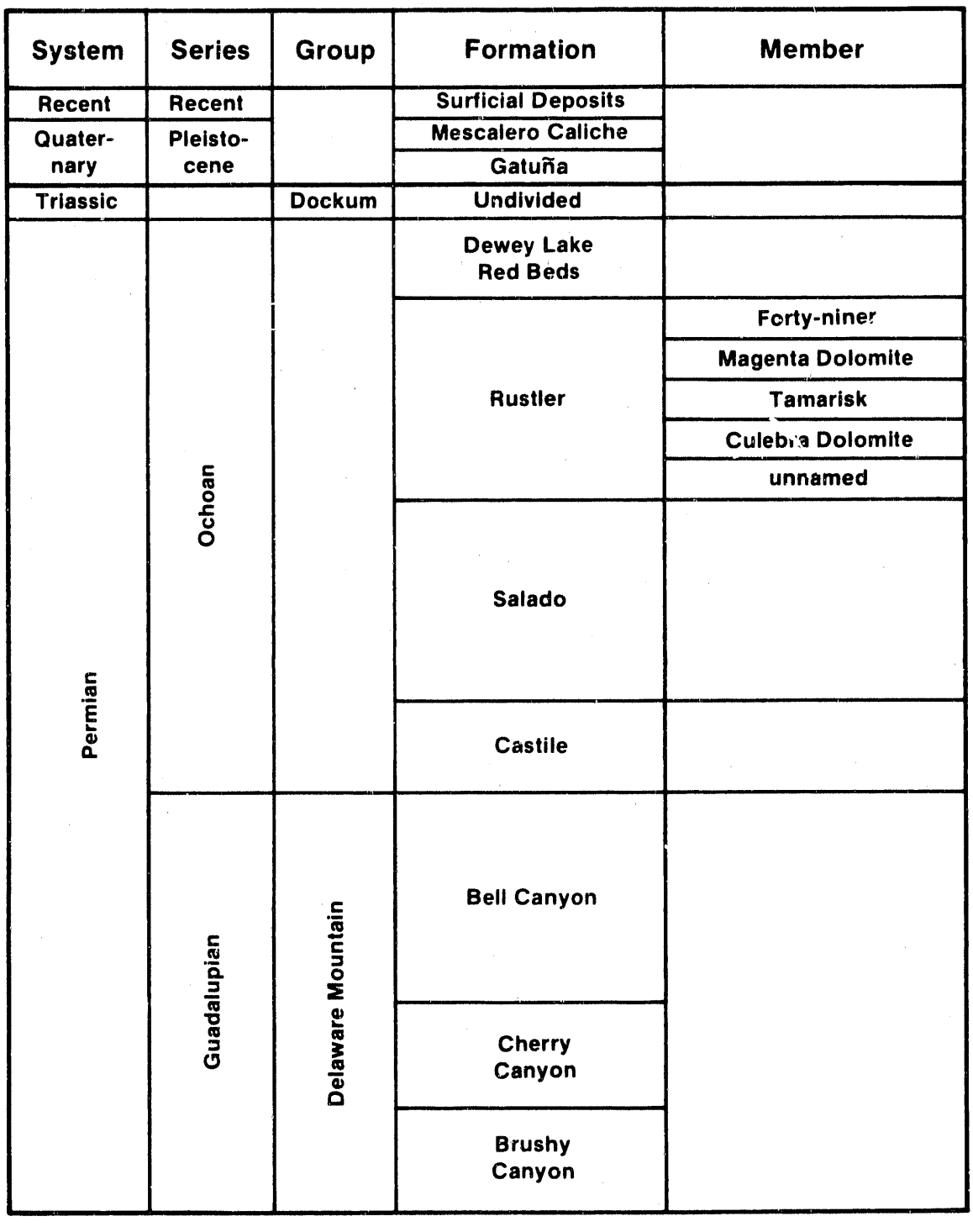

Figure 1-2. Generalized stratigraphic column of the Delaware Mountain Group and younger sedimentary rocks at and near the WIPP site (Beauheim, 1987, Fig. 2-1).

Second, it reexamines four of the six sets of calculations of potential health effects to individuals performed by Lappin et al. (1989). These health effects result from emplacement of TRU wastes in the WIPP, hydrologic saturation of the repository as a result of either natural processes or human intrusion, and ground-water transport of radionuclides. Cases IA′ and IB′ recalculate radionuclide migration resulting from undisturbed performance (Chapter 3.0). Case IA′ assumes the design-basis waste and backfill and expected waste solubilities and transport properties within the repository. Case IB′ assumes increased waste solubility and degraded flow-and-transport properties within the repository and in the geosphere. Cases IIA′ and IIC′ (Chapter 4.0) reexamine repository performance following drilling through the repository and an underlying Castile brine reservoir, using varying assumptions to examine the effects of uncertainties in transport properties of both waste and geosphere. As in the work of Lappin et al. (1989), Case II assumes that drilling of the borehole intruding the repository continues for at least 15 hours after the repository horizon is reached, that the Castile Fm. is penetrated, and that an occurrence of pressurized brine is encountered. Eventually, the borehole is plugged. After plug degradation, the pressurized brine drives the flow of radionuclide-contaminated brine up the borehole and into the Culebra Dolomite. Case IIA′ assumes expected properties within the repository, the intruding borehole, the underlying brine reservoir, and the overlying Culebra Dolomite. Flow and transport properties are degraded in three areas (all except the brine reservoir) for Case IIC′.

Appendix A is an unpublished memorandum initially prepared to examine the sensitivity of repository performance to several variables. These variables included initial void volume in the waste and backfill, room-closure rate, brine-inflow rate, and inventory. These scoping calculations influenced the research programs of the WIPP Project, particularly in the area of host-rock permeability, and ultimately led to the development of many of the data used in this report. Because of rapid advances in understanding the effects of these variables, the initial calculations were not published; they are included here for reference.

2.0 DISTURBED ROCK ZONE (DRZ)

The National Academy of Science's (NAS) original recommendation of salt as a storage medium for radioactive waste was based in part on the assumptions that salt surrounding underground excavations will creep to closure and that salt would provide sufficiently strong pillars to avoid failure and collapse (NAS, 1957). The WIPP FEIS (DOE, 1980) also assumed that the waste would reach some final compacted state, but its authors recognized that borehole and shaft walls may fracture and that such fractures required study. The initial design validation for the WIPP site (e.g., Weart, 1983) concluded that a minimum of ground control, such as rock-bolts, would be needed to maintain a stable opening during the operation of the WIPP.

Although the NAS's assumption of creep closure seems to be appropriate for the long term, especially in the far field, experience in salt and potash mines (e.g., Baar, 1977) indicates that fracturing is an expected behavior around underground excavations in salt. Fracturing and the effects of excavation have been studied at the WIPP since the first excavations were completed in 1983 (DOE, 1988; Borns and Stormont, 1988a, 1989). These studies indicate that fracturing is the expected behavior for some distance around the openings. Section 2.1.1 summarizes fracture observations at WIPP. Public awareness of these fractures increased during the spring of 1989, as acceleration of measured roof-to-floor convergence rates was observed in Rooms 1 and 2 of the SPDV panel (Figure 2-1). This acceleration, in conjunction with observations of fractures in excavation surfaces, fracturing within the roof beam, and bed separations occurring along Anhydrite "b," 2 m above the back (Figure 2-2), led to the decision to close both rooms. The generalized fracture pattern around a four-year-old SPDV room is shown in Figure 2-3.

In the spring of 1989, the room evacuation was well documented by the local and national press, which assumed that such fracturing is anomalous even though fractures are considered the expected behavior by much of the mining and scientific communities. The following sections describe the fracturing of halite in general, the present ground conditions around the WIPP excavations, and the potential impacts of the observed fracturing on long-term performance of the repository. This discussion of the disturbed rock zone (DRZ) and its specific development at WIPP expands the briefer discussion of the DRZ contained in Section 4.7 of Lappin et al. (1989).

Following the excavation of underground openings at the WIPP, a disturbed rock zone forms in the wall rock. The extent of the DRZ around workings at the WIPP is delineated by the zone of rock in which mechanical properties and intrinsic hydrologic properties of the rock have changed in response to excavation. For example, the development of two-phase flow in the hydrologic system around the opening, if it did not involve a change in intrinsic permeability, would not constitute formation of a DRZ. As used in this section, the term "near-field" describes the zone of rock within the DRZ, and the term "far-field" describes the rock outside the DRZ, where parameters such as porosity and intrinsic permeability are undisturbed from pre-excavation values. The processes involved in the development of a DRZ are complex, although basically related to stress relief and rapid strain rates. The redistribution of stress around an excavation drives coupled processes, such as changes in permeability in response to fracture growth. The DRZ is an important component of the repository system and should be considered in any

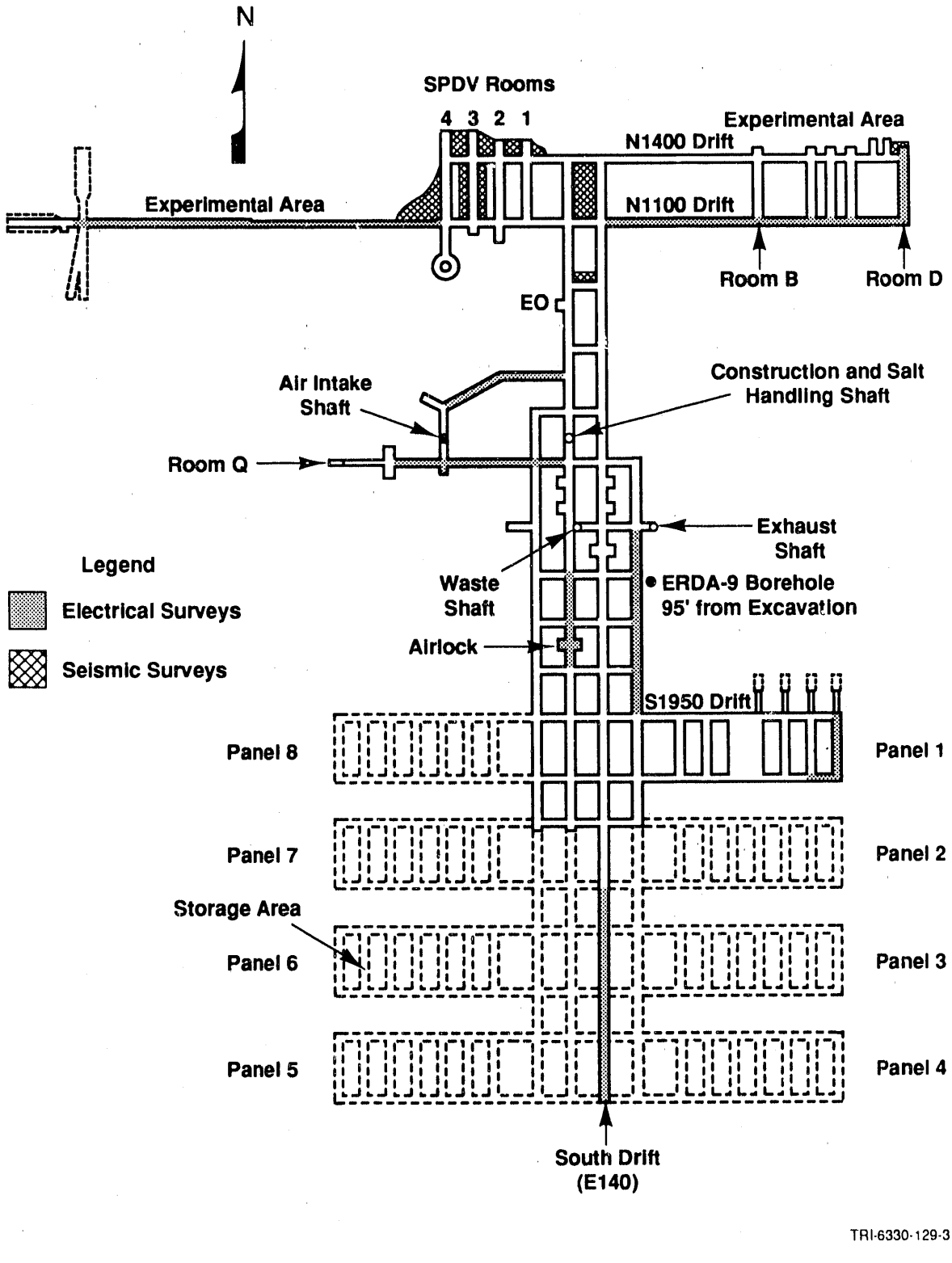

Figure 2-1. Map view of existing and planned underground workings.

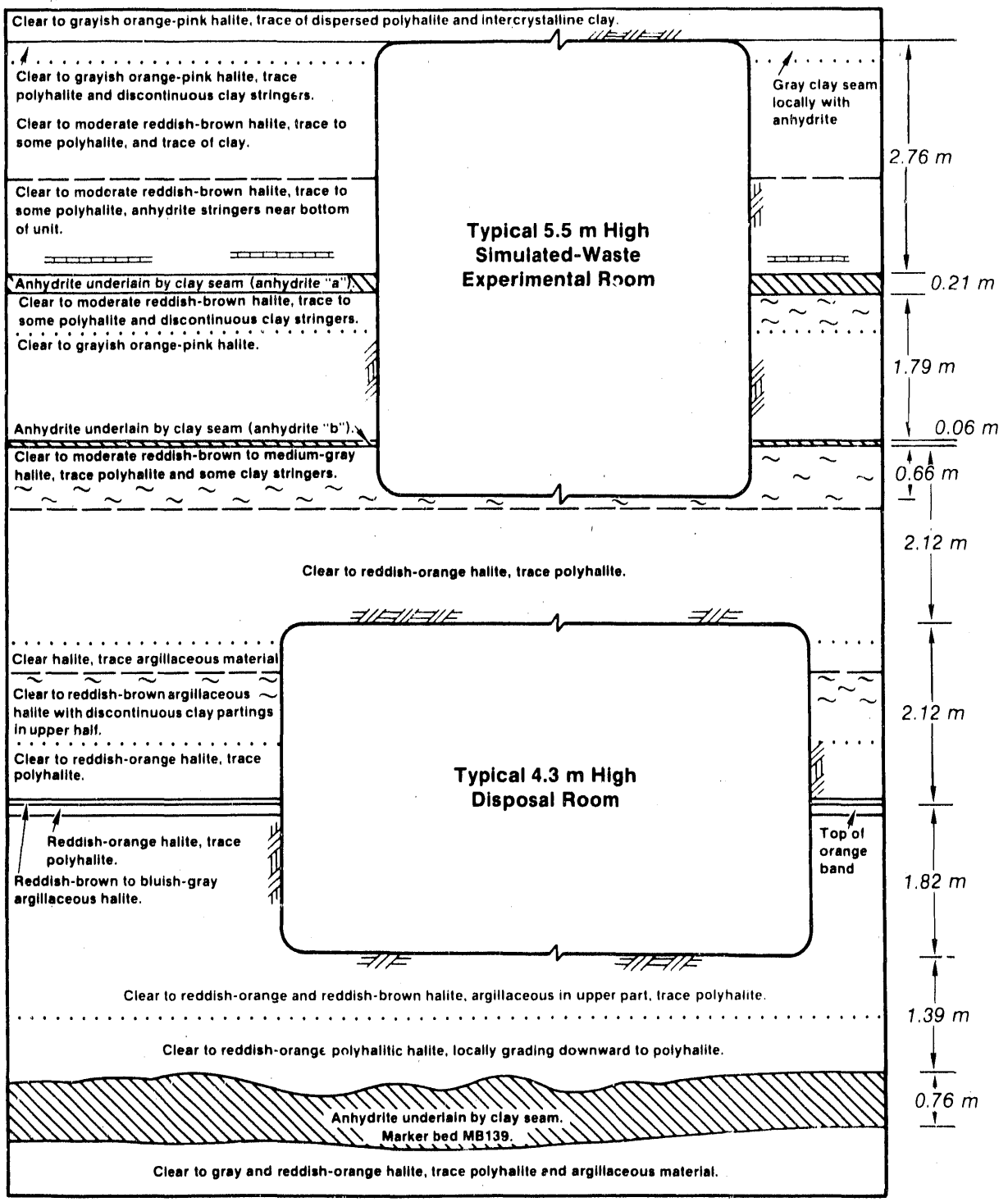

Figure 2-2. Geologic cross section at the repository horizon (Lappin et al., 1989, Figure 4-12).

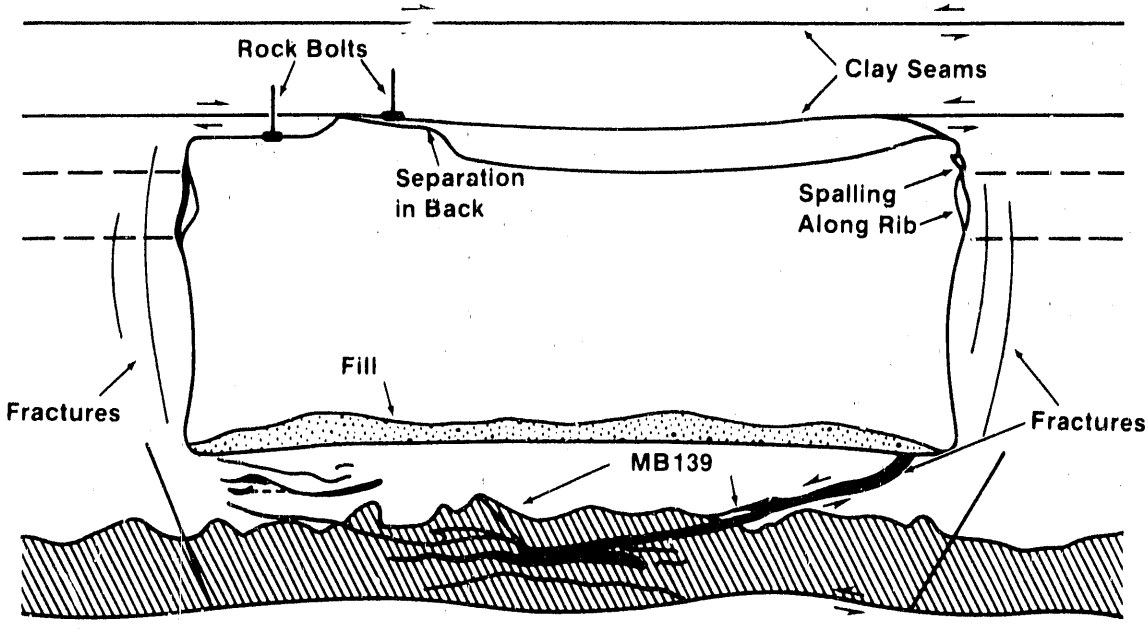

a. Observed fracture pattern around a 4-year-old SPDV Room (4 x 11 m) (Borns and Stormont, 1988a, Figure 3).

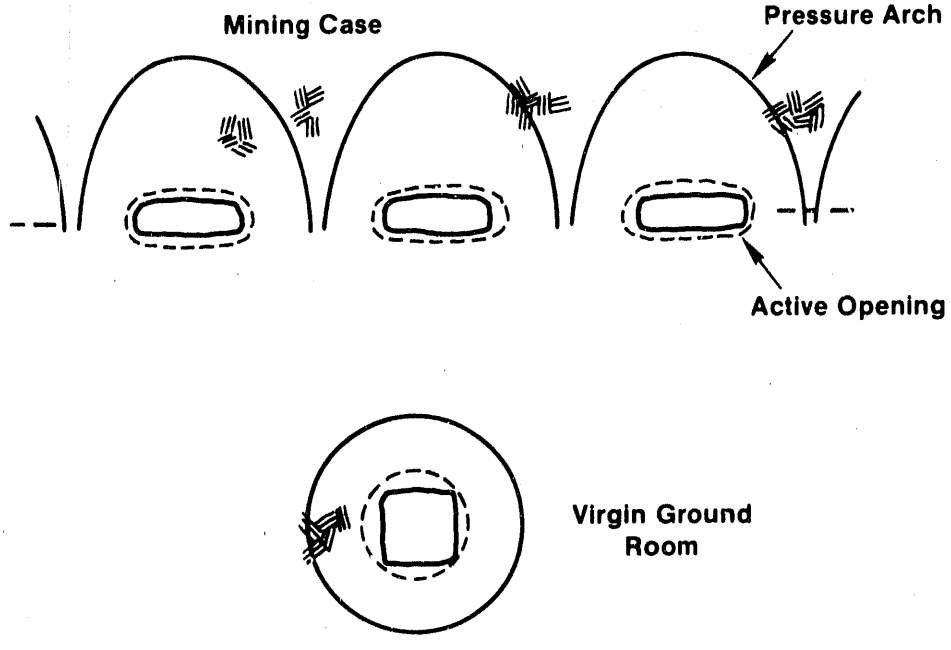

b. Mining and virgin conditions (after Dusseault et al., 1987, Figure 4).

Figure 2-3. Conditions around underground openings, shown in cross section.

analysis of it. Numerical methods to treat some aspects of the behavior of the DRZ do not exist at present, however.

2.1 Description of the DRZ

2.1.1 Fracture Observations at WIPP

In 1983, the exploratory drift, E140 (also known as the south drift, Figure 2-1), was mined 1000 m south of the site center to verify the stratigraphic continuity and suitability of the emplacement horizon in the waste-panel area. After this drift was completed, a separation was observed consistently 10 to 15 cm up into the back (Borns and Stormont, 1988a). This separation was within a massive halite unit and was not associated with a clay seam. Rather, the separation appears to be related to a marked change in halite grain size. In portions of the south drift, the rock salt below this separation has been scaled or rock-bolted to ensure a stable back. This treatment has been successful.

In the autumn of 1984, based in part on a recommendation by the New Mexico Environmental Evaluation Group (EEG), the structures of Marker Bed 139 (MB139, see Figure 2-2) were studied in several drillholes in the north end of SPDV Room 4 (Figure 2-1) (Borns, 1985). During this study, MB139 was found to be fractured. Many of these fractures, especially those parallel to bedding, were interpreted to have existed prior to excavation because they were partially healed or sealed with halite. These fractures also provided zones of weakness that reopened in response to the excavation. At the same time, several 36-inch diameter drillholes were completed in the south end of Room 4. In these holes, new fractures developed both in the halite above MB139 and within the marker bed.

In the summer and autumn of 1985, a set of 22 drillholes, 36 inches in diameter, was drilled in the south end of SPDV Room 3 (Figure 2-1) to provide the foundations for bulkheads. (Room 3 has since been divided, with the south end becoming Room T). These drillholes exposed fractures in MB139 and the halite between MB139 and the invert (floor), as seen the year before in Room 4. The fracture system in Room 3 was much more developed than that in Room 4, with fracture separations locally >10 cm. All the holes in Room 3 were interconnected by the fracture system. Exploratory drilling in the north end of Room 3 revealed that the fracture system extended throughout the floor beneath the room and that fracturing extended downward to the base of MB139.

In 1986, after the fracture systems in several of the SPDV rooms were documented, Bechtel National Inc. (1986) performed reconnaissance drilling throughout the excavations to gather more information for design validation. This study found areas of fracturing in the floor and back outside the SPDV rooms, notably in the shaft stations.

In 1987, Sandia National Laboratories began to evaluate whether the back in test rooms B and D (Figure 2-1) could support hoist equipment needed to retrieve cannisters of simulated waste from the floor. This study found areally extensive separations in the backs (roofs) in both rooms, and the rooms were rockbolted. However, the roof slab continued to fracture and was judged to be unstable in July 1987. The mining contractor informed DOE that similar fractures and separations would develop throughout the facility with

time and that, in fact, small rockfalls had occurred in Room 2 (Patrick, 1987). The rockfalls occurred along the west rib of Room 2, where several square feet of the roof fell. An Openings Maintenance Program was started to set the criteria and methods for control of these fractures and related features. The members of the Opening Maintenance Program discussed several points: (1) strategies to maintain working tolerances in tramways required for equipment movement; (2) control of slabbing in the waste acceptance room; (3) the significance of rockfalls in Room 2 (Figure 2-1) (the group recommended closing Room 2); and (4) the failure of 85% of the resin bolts installed (to that time) at WIPP. Subsequent meetings discussed retrieval in waste rooms and recommended pattern bolting in the first waste panel. Mining Operations stated the need to maintain the operational clearances in the tramways, such as E140, which will require periodic trimming and rock bolting to stabilize the back. Enlargement of the S1950 drift in the area of the panel plug for Panel 1 has been proposed (Figure 2-1).

In 1988, DOE published the results of the IT Excavation Effects Study, which described how the extent of macroscopic fracturing has increased since 1986. Seismic studies by the Colorado School of Mines and the University of Texas at Austin showed separations in the back of Room 3. Rock bolting is now complete in the first panel.

2.1.2 Fracture Pattern around Excavations

During the development of the underground workings at the WIPP, numerous holes were drilled for stratigraphic studies, areas for experiments, and construction of foundations. As the presence of a DRZ became apparent, Bechtel National Inc. (1986) drilled numerous holes specifically to investigate the DRZ. Therefore, direct observations of the DRZ are spread both spatially and in time. The history of these observations is summarized above. At the WIPP, the development of a DRZ has been confirmed by geophysical surveys and gas-flow tests in addition to borehole observations (DOE, 1988; Borns and Stormont, 1988a). The three approaches have defined a DRZ extending laterally throughout the excavation and varying in depth from 1 to 5 m, according to the size and age of the opening. Hydrologic desaturation and microfracturing have occurred to some degree within the zone. The dilation that results from microfracturing in the DRZ provides a component of the observed closure that is not accounted for in present creep models for closure in salt repositories. Visual observations using drillholes indicate that fractures are both preexisting and excavation-induced. Observations based on these various methods are summarized in an idealized cross section of a four-year-old or greater WIPP room (Figure 2-3). The basic features of these observations follow.

- An arcuate fracture system, concave toward the opening, develops in the floor and the back, locally crosscutting the stratigraphy.

- Separations may develop along stratigraphic markers, such as clay seams, both above and below the room, and also at more subtle discontinuities, such as changes in grain size within halite.

- Shear displacements occur along fractures and separations, especially near the corners of the rooms. Fracturing may or may not be locally symmetric about the room centerline.

- Vertical fractures and spalling are observed within the ribs.

Existing boreholes were reexamined in 1987 (Francke in DOE, 1988). This reexamination showed that the number of fractures per station (as a percentage of borehole array locations where fracturing was observed) in borehole arrays had increased from 48% of the array locations in 1986 to 73% in 1987. Locations without fractures are largely restricted to drifts with narrow spans (4.3 m or 14 ft). In the oldest test rooms (Rooms 1 through 4, Figure 2-1), macroscopic fractures were found at 100% of the locations. Work to date has concentrated on deformation around a single room or excavation.

Analysis by IT Corporation (Case, 1989, pers. comm.) of the SPDV room response suggests that fracture deformation may result from panel-scale interactions. However, as noted above, fracturing around individual rooms varies locally in symmetry.

2.1.3 Observation of Hydrologic Effects of the DRZ

Studies have also been undertaken to determine the effect of fracture-induced porosity increase and dilatancy within the DRZ on the hydrologic properties of the near-field Salado Formation. Tracer-gas studies were conducted from the floor of the N1400 (Figure 2-1) drift in 1986 (Stormont et al., 1987) and the N1100 drift in 1987 (Peterson et al., 1987). In these studies, a diluted tracer gas was injected into a packed-off region of the test borehole and sampled in surrounding boreholes. In most instances, plastic tarps were fixed to the drift floor to catch gas moving from the test interval into the drift. Gas samples were analyzed for evidence of the tracer, using electron-capture gas chromatography. The purpose of the N1400 testing was to estimate the degree and scale of fracture continuity and apertures in MB139 over distances >10 m. Tracer arrivals indicated that the flow-path aperture in MB139 increases as the span of the drift increases--from an estimated 0.002 cm in a 6.6-m-wide drift to 0.04 cm at the intersection of two 11-m-wide drifts. These tests also revealed that tracer gas was being transmitted from MB139 to the drift via the approximately 1-m-thick layer of salt between MB139 and the floor of the drifts. Consistent with the inferences about MB139, it was found that apparent vertical flow paths in the salt also increase in aperture with drift dimension--from 0.002 cm in a 6.6-m-wide drift to 0.02 cm at the intersection of two 11-m-wide drifts. These interpretations assume that the fractures are unsaturated.

In the 6.6-m-wide N1100 drift (3 to 4 years old at the time of the test, Figure 2-1), tracer-gas studies were conducted in three boreholes: one vertically up, one vertically down, and one horizontal. All test intervals were in the salt within 1 m of the drift face. Tests in the vertical boreholes indicated larger flow paths in the vertical direction (between the test interval and the drift) than parallel to bedding. The test in the horizontal borehole indicated flow paths parallel (essentially vertical) to the drift face appreciably larger than those between the test interval and the drift. The inferred aperture of the flow path in all tests was small, about 1×10^{-6} m, assuming that fractures are unsaturated.

Thus, there is direct evidence of the possibility of gas flow within portions of the DRZ where fracturing has occurred.

2.1.4 Mechanical Processes Active in the DRZ

In general, the composite time-dependent behavior of rock salt around an excavation results from several mechanisms, each of which dominates at different stress levels or regions around an excavation (Dusseault et al., 1987). Such regions, from the excavation outward, exhibit brittle, viscoplastic, and viscoelastic behavior. The time-dependent deformation that results from the interaction of these regions can be represented by a creep curve (Figure 2-4). The curve is often simplified by displaying measured closure of the excavation rather than strain (Figure 2-5). This approach does not, however, distinguish any variations in behavior within the rock mass, i.e., away from the excavation. A creep curve can be divided into three components: primary or transient creep, secondary or steady-state creep, and tertiary creep. For WIPP, primary and secondary creep have been extensively studied and modeled (e.g., Munson et al., 1989), but tertiary creep has received little attention. The accelerating closure of Room 1, for example, shows that tertiary creep or some new mechanism occurs (Figure 2-5), although tertiary-creep behavior primarily occurs in beams, slabs, and rock adjacent to the opening. The onset of tertiary creep can mark the point at which a critical strain has been achieved, after which the rock begins to fail by fracturing. As seen in the WIPP excavations, deformation has an early transient response and progresses toward steady-state creep, but steady state may not be an accurate assumption for long-term calculations in all cases, because tertiary creep may affect deformation at later times, especially adjacent to the walls (Figure 2-5).

The development of a DRZ, which consists of fractured and dilatant rock, is considered common in underground engineering (e.g., Baar, 1977; Peng, 1978; Brady and Brown, 1985). The origin of the DRZ is complex, with several processes competing or acting in concert. The local stress field and resultant DRZ also reflect any preexisting anisotropic features, such as fractures, bedding, and clay and anhydrite interbeds, as well as the effects of mining (Coates, 1981). For the WIPP, a general description of mechanical processes within the DRZ may include the following interpretations.

- Strain-rate-dependent brittle failure results in an elliptical zone of host rock immediately around the opening. Within this zone, the brittle failure envelope based on a strain-rate criterion is exceeded by the accelerated strain rate adjacent to the opening (Dusseault et al., 1987).

- Microfracturing develops in response to the release of in-situ fluid pressure. If an appreciable pore pressure exists and if salt obeys an effective stress law, then the redistribution of stresses in response to excavation combined with the low permeability and low tensile strength of salt will produce tensile failure in response to fluid expansion. Very small volume increases (dilatancy) will relieve the pore pressure and halt fracturing. Such failure may tend to create grain-boundary microfractures, which may heal after cessation of tensile failure.

- A volume of disturbed rock develops, bounded by the excavation face and the elliptical surface of "the active opening" (Mraz, 1980). This volume of rock can separate (decouple) from the host rock along a shear zone that follows the elliptical surface of the active opening. The extent of the active opening is largely controlled by the dimensions and shape of the excavation (Mraz, 1980), and hence, the active opening will reach its

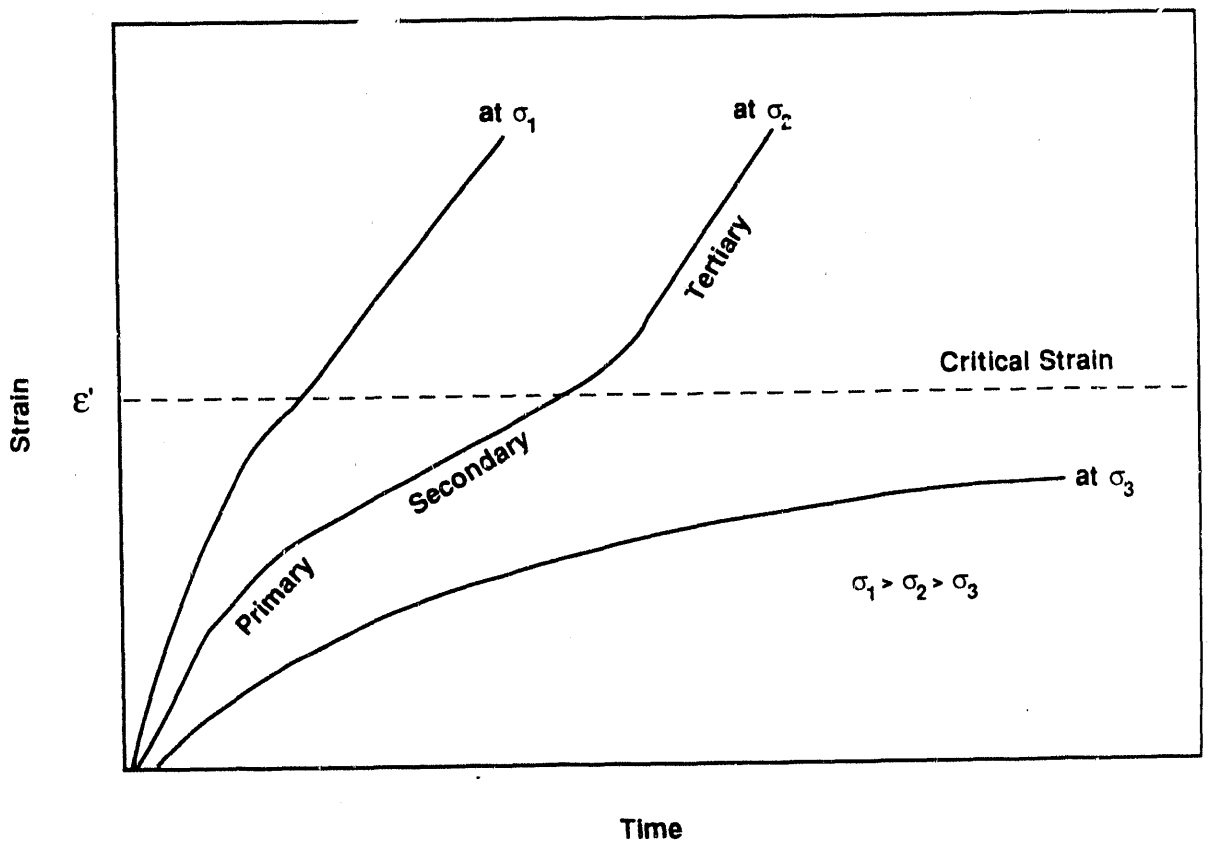

Figure 2-4. Generalized time-strain relationship for salt deformation, showing primary, secondary, and tertiary creep.

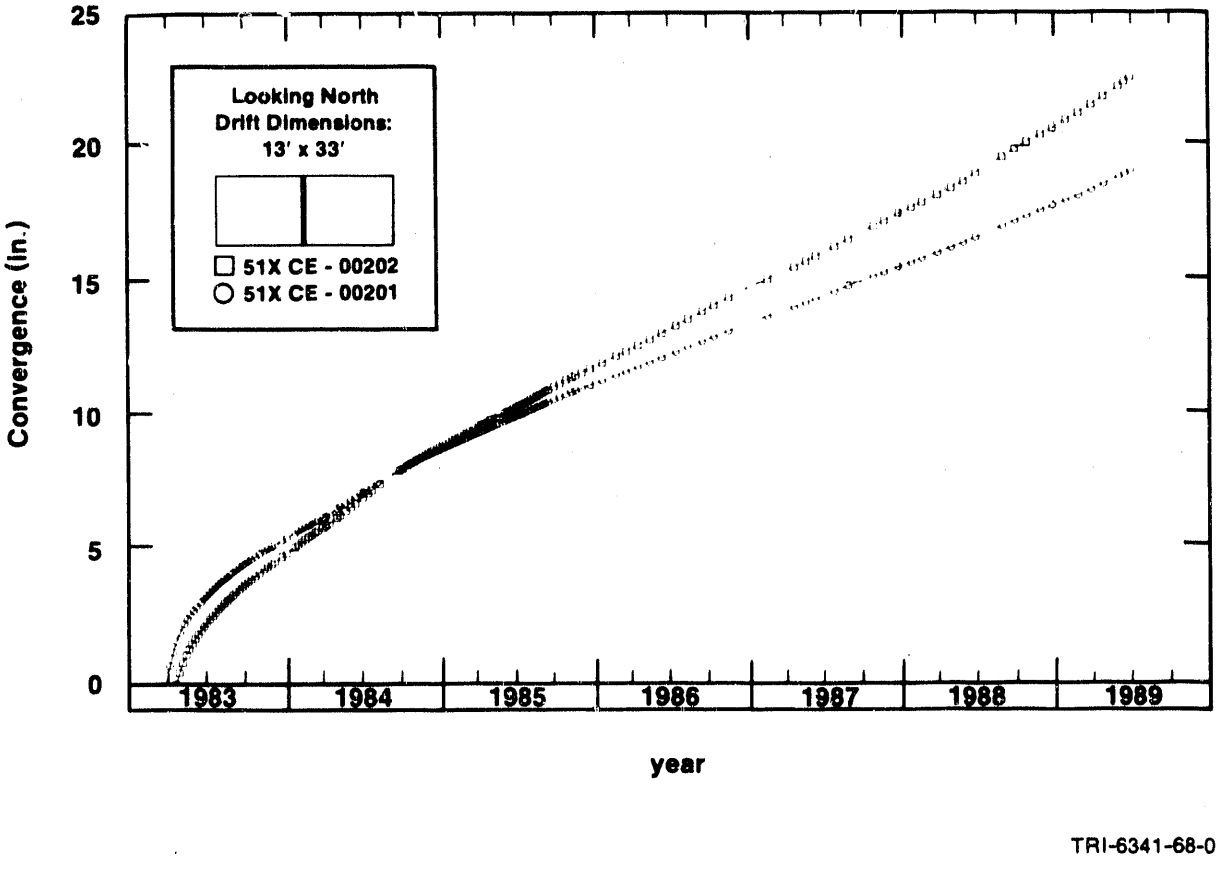

Figure 2-5. Wall convergence in SPDV Room 1, with rates beginning to increase in early 1989 (DOE, 1990b).

maximum extent soon after excavation. The active opening will reduce in extent when deformation around the opening has reached the point (e.g., consolidation of the backfill) that fractures begin to close and heal.

- Shear displacements along planes of weakness such as clay seams, both above and below the excavation, are induced by the excavation (Brady and Brown, 1985).

- Beam buckling and flexural slip folding develops within the active opening. The horizontal component of radial creep causes stress-relieved salt beds within the active opening to buckle, as observed immediately above and below excavations (Baar, 1977). These layers would continue to deform with time, in response to horizontal and vertical loading by creep of the adjacent intact salt mass.

- A pressure arch develops symmetrically above and below the opening, redistributing stresses and developing stress concentration about the opening (Coates, 1981). Within the pressure arch, zones that are in tension develop within the host rock.

2.1.5 Maximum Extent of the DRZ and Its Evolution Through Time

The extent of the DRZ depends on the definition used for the DRZ; this chapter defines the DRZ on the basis of changes in mechanical and hydrologic properties. Portions of the DRZ may not display mesoscopic fracturing, e.g., zones of grain boundary expansion, dilatancy, and microfracturing. Because the excavation is the only void volume added to the system, he maximum extent of the zone of microfracturing (porosity increase) can be estimated. Assume that the limit of stress redistribution around the excavation is five times the excavation radius (Brady and Brown, 1985), that the volume within the excavation is loaded to 60% of the original density of the rock salt, and that the void volume is redistributed uniformly out to a maximum extent of 22 m, the limit of stress perturbation. This rearrangement of void volume would increase the porosity from an undisturbed value of 0.02 to 0.04 within the affected zone. The elliptical zone of fractured rock that develops around an excavation (the active opening of Mraz, 1980) is a subset of the DRZ. The maximum extent of the active opening is largely set by the dimensions of the original excavation and is reached within 20 years after excavation. At the WIPP, the active opening component of the DRZ may currently extend to a depth of 2 to 4 m from the excavation surface.

The other major fracture component is shear along interbeds above and below the excavation. The extent of this shear displacement will decrease with distance from the excavation. At the WIPP, 2 years after excavation, shear displacements have been observed 12 m above the excavation surface (DOE, 1989b) and may extend at some time in the future to ~20 m (five times the excavation radius; Brady and Brown, 1985). These shear displacements will continue to form until both the excavation and its contents have consolidated or until gas pressure builds up sufficiently to prop the excavation, i.e., to prevent further closure.

Because of the complexity of the evolution of the disturbed rock zone, its behavior must be largely conjectured and split among its subsets: pore changes, volume development of an active opening, and shear displacements. The opening of pore space may be initially confined to a 1- to 2-m-wide zone

adjacent to the excavation as a zone of compression develops around the opening. With time, this zone of compression dissipates away from the opening. As this occurs, the zone in which the pore volume increases will expand. The fractures of the active opening develop relatively early in excavation history, but the shear-displacement fractures will continue to form until recompaction begins. The closure of both types of fractures will follow similar histories. They will begin to close when the waste and backfill have become partially consolidated and provide a back stress. The degree of closure within the DRZ in response to mechanical backpressure will depend on the material properties (halite versus anhydrite). For example, fractures in Marker Bed 139 have apparently remained partially unhealed for 70 million years (Borns, 1985). The availability of a fluid (gas or liquid) that can prop the fractures will affect the evolution of the DRZ. Calculations analyzing room response indicate that gas generated by the waste might prop the excavation. Although the distribution of compressive stress around the excavation will prevent new fractures from propagating, existing fractures and pore space, which were created within the DRZ since excavation, will remain propped until the gas or liquid is dissipated or the zone of compression migrates away from the excavation.

2.2 Possible Effects of the DRZ

2.2.1 Impacts on Seals

Unless their formation is prevented, fractures that develop in the DRZ, especially in the anhydrites of MB139, will initially provide interconnected flow paths parallel to but below the emplacement panels, bypassing seals and connecting individual waste-emplacement rooms, panels, or panels and shafts. These flow paths may close more slowly than the reconsolidation in the rooms, due to the presence of fluid in the fractures and the strength of anhydrite relative to the interbedded halite. Outside the DRZ, the marker bed appears to have permeabilities only one to three orders of magnitude higher than the host salt (Beauheim and Saulnier, 1990), i.e., 10^{-17} to 10^{-18} m^2 as opposed to 10^{-20} to 10^{-21} m^2. The fractures could provide preferential pathways around seals, sinks, or conduits for fluids originating in the formation and from the waste. In addition, the fractures may form a path of preferred gas flow from the WIPP excavations to ERDA-9, which is within 33 m of the excavation (Figure 2-1). Fracturing in MB139 may necessitate special attention to the design of underground seals, either to account for or to prevent the continued deformation of the marker bed after the initial emplacement of the composite seals.

2.2.2 Impacts on Shaft Stations, Tramways, and Access Drifts

Several excavations underground, such as the shaft station, tramways, and access drifts, will require maintenance (e.g., scaling) of opening dimensions to provide room for the conveyance equipment and ventilation for the entire operational phase. Such maintenance may require trimming the floor into or through the fractured anhydrite of MB139 in order to maintain the required thickness of salt in the back for stability. Especially where the back is rockbolted, fractured anhydrite in the floor may require further maintenance to permit travel. For some excavations, this maintenance will be required for more than 25 years. Ground control and mining can be used to maintain clearance.

Present planning also calls for areas of the access drifts and tramways to be used for waste storage. Current ground-control practices within tramways and mains (e.g., rock bolting only) do not conform to the practices for rock-bolting in the first waste panel (e.g., sealing around bolts to minimize brine inflow). Other panels, for which retrievability is not a criterion, are not projected to be rock-bolted. Finally, floor trimming is not expected to be required except in the major accessways. Fractures within the DRZ appear to increase in size and frequency with the size and age of the excavation (DOE, 1988; Borns and Stormont, 1988a). If this relationship is valid over periods greater than 5 years, fracturing of the DRZ will reach its greatest extent within the WIPP excavations in these older, and in many cases larger, access drifts and stations.

2.2.3 Impacts on General Structural Response of the Salado Formation

The DRZ affects deformation observed around underground openings. Such deformation affects mining operations at the WIPP. The studies described above and by Francke (in DOE, 1988) show that a DRZ will develop around all the underground workings that are allowed to close, given sufficient time. The development of the DRZ has already affected the maintenance of openings in several underground areas. A primary concern of mining operations is to maintain a safe back and rooms so that the retrieval of waste will not be impeded during the first 5 to 10 years by failure of the back. As experience underground increases at the WIPP, the magnitude of the effects on operations due to the DRZ will become known. We expect that the DRZ will develop throughout the excavation and will affect operations to some extent.

The dilatant component of deformation within the DRZ influences interpretation of in situ tests at WIPP, such as tests of structural interaction, brine inflow, and formation hydrology. Dilatancy refers to the volumetric strain that results from the opening of microfractures (Brace et al., 1966). Dilatancy around the WIPP excavations is observed or inferred from in-situ studies. Measurements of gas flow, apparent resistivity, and seismic velocity indicate that the porosity and gas content (degree of desaturation) of the host rock increases significantly within the DRZ. The 10^4 increase in gas-flow rates within the DRZ (Borns and Stormont, 1988a) indicates that hydrologic and geophysical properties change as a result of desaturation and increase in fracture porosity. The change in porosity (primarily dilatant volume increase) is accommodated by displacement of the excavation surface inward and contributes to the observed closure. Borns and Stormont (1988b) calculated the magnitude of this component of closure, using both the increase in gas porosity inferred from gas-flow tests (0.001 to 0.010, Stormont et al., 1987) and the increase in porosity inferred by analysis of seismic velocities (0.02 to 0.04, Skokan et al., 1988).

The calculation by Borns and Stormont assumed a uniform thickness for the zone of dilatancy (1 or 2 m from gas flow tests and seismic surveys) and a cylindrical, isotropic room configuration. The calculations indicated that dilatancy within the DRZ causes measurable closure within the adjacent opening. For both an experimental room (4-m equivalent radius) and an SPDV room (5-m equivalent radius), the apparent closure due to dilatancy alone is about 4.5 cm for a zone of dilatancy 2 m thick and 2.0 cm for a zone 1 m thick. These components are of same magnitude as the early-time closure (Munson et al., 1989, Figure 1). Microfracturing around an excavation in salt may develop as soon as excavation begins and continue as long as the

excavation remains open. The fractures that are observed around the openings could contribute approximately 2 cm of vertical closure and 1 cm of horizontal closure, in addition to the closure due to dilatancy.

Overall, deformation around the WIPP excavations is controlled by creep outside the DRZ, i.e., by far-field creep. This process drives the repository system, including the DRZ, toward reconsolidation approaching the virgin state. The DRZ, which plays a passive role in reconsolidation until significant backpressure is developed by the consolidating waste and backfill, affects the completeness to which and rate at which this virgin state is regained by the rock mass. Factors related to the DRZ that affect the rate of reconsolidation are the fracture-propping potential of pressurized fluids that may be present, the stiffer materials such as anhydrite in Marker Bed 139, and the interaction between blocks of salt and anhydrite that form during failure of the DRZ after a room is decommissioned. The prediction of long-term room behavior with detailed constitutive models and numerical methods requires that multiple mechanisms of deformation be accounted for, including the discontinuous behavior and tertiary creep or other new mechanism within the DRZ (Borns and Stormont, 1988b, 1989). These capabilities are not yet fully developed.

2.2.4 Impacts on the Hydrologic Response of the Salado Formation

Hydrologic and mechanical properties of the Salado host rock are interpreted here to have been altered around excavations at the WIPP site in response to excavation (Borns and Stormont, 1988a). The variation of both shear and compressional velocities with distance from the excavation surface (Ibrahim et al., 1989), combined with the 10^4 increase in gas-flow rates within the DRZ, indicates that the changes in rock properties within the DRZ are not due solely to desaturation; an increase in fracture porosity near the excavation is also required.

The development of the DRZ will have significant effect on the hydrologic environment around seals. The seal/rock interface and the flow properties in the DRZ near the seals are important to rock-mass sealing. Neither was explicitly considered in the undisturbed-performance calculations of Lappin et al. (1989), except for the evaluation of "degraded" performance, where seal permeability in the vicinity of MB139 was assumed to be two orders of magnitude greater than the design basis, i.e., 4×10^{-17} m^2 vs. 4×10^{-19} m^2. A substantial DRZ that persists in time could provide a path through which fluid could bypass the seals. If a DRZ is not healed with time, it could connect waste-disposal panels with other portions of the repository. Therefore, delineation of the DRZ is required to determine what, if any, remedial action is necessary to establish effective seals. Stress buildup in the vicinity of a relatively stiff inclusion (e.g., concrete or consolidated salt seals) may reverse the disturbance by forcing the rock back together, thereby decreasing its permeability. Preliminary numerical studies (Argüello and Torres, 1988), without incorporating fracture behavior or the material properties of anhydrite, suggest that stresses within the host rock around a seal build toward lithostatic. Qualitatively, the stress buildup should initiate healing, but the rates and amount of permeability reduction due to the healing process are not well known, especially in MB139. The behavior of anhydrite is important, because a major fracture system develops within MB139 in response to excavation, and fractures in anhydrite (with its increased strength and slow solution and reprecipitation relative to halite) will heal

at a different rate than halite. Lateral displacement (shear) occurs across fractures in the DRZ. This shear causes asperities on opposite walls of the fracture to fail to match. This mismatch will retard healing of the fracture.

If healing of the DRZ is expected to be incomplete over the 10,000-year performance period, excavation of the excessively transmissive portion of the DRZ at strategic locations, such as the panel-seal locations, is an option. However, it must be demonstrated that mechanical interactions such as new fracturing, without incorporating fracture behavior or the material properties of anhydrite, have not occurred at the margin of the rock removed prior to emplacement of the seal. To demonstrate this, detailed studies of the effects of excavation, such as the extent of newly fractured rock around the excavation and the extent of new fracturing that occurs between the time of seal emplacement and the reconsolidation of the seal system, are required. Alternatively, it may be possible to grout fractures within MB139 with a grout that deforms plastically, thereby reducing the time required for reduction of permeability in MB139. Finally, if a rigid ring sufficiently strong to withstand lithostatic load were emplaced "instantaneously" upon excavation at proposed seal locations, the time-dependent development of any significant DRZ might be locally prevented.

2.2.5 Impacts on Gas and Brine Storage

The fracture porosity of the DRZ has been studied primarily for its effects on brine influx. However, the DRZ may also provide a sink or reservoir for gas and brine in the repository system. As long as the land surface above the repository remains level or subsides, the maximum volume of void space within the DRZ can not be greater than the volume of void in the original excavation. The void space in the DRZ will begin to decrease when the backfill, rigid inclusions, and waste in the excavation have at least partially consolidated to a state at which they begin to supply a back stress (Argüello and Torres, 1988). Hence, the DRZ may be the last component of the system to approach its final porosity. Gradients for fluid flow would cause gas or brine to collect in the DRZ. This gas or brine in turn would retard closure of a finite fracture system. Fracture porosities within the zone of rock from the excavation wall to a depth of 2 m may be greater than 0.15. Borns and Stormont (1988a, 1989) have demonstrated that, in response to microfracturing and mine ventilation, the pore space within the DRZ has already become unsaturated, thus creating a two-phase region (gas and liquid). Within this two-phase region, the permeability to gas may increase and the permeability to brine may decrease relative to those within the far-field. Hence, the capacity of the DRZ to accept available gas is enhanced relative to the far-field rock salt. However, the relative permeability to gas and to brine within the DRZ will be a complex time-dependent function of the degree of fracturing and degree of saturation.

In summary, a sink for both gas and brine is provided by a network of fractures and zones of higher permeability that develop in the DRZ. This sink can accept fluids introduced during construction (e.g., water-jet cutter and the brine spread from the shaft sumps), during post-decommissioning brine inflow, and by degradation of the waste. The DRZ, especially the anhydrite beds, can also be a source of fluid at late times. As the room and its contents approach the final state (i.e., as the porosity in the backfill-waste system reduces), the open fractures in the anhydrite, which had been collecting fluids, will close at a slower rate than room compaction. As they close, they may inject fluids into the room.

2.2.6 Impacts of Ground Control Methods, Including Rock Bolting

Currently, the ground-control practices of WIPP mining operations include pattern rockbolting of the first waste panel, to insure a stable back during the retrieval period, and scaling and rock bolting in other excavated areas, as needed following continuous monitoring of the excavation. As an example of the as-needed program, over 5000 rock bolts were installed during a one-year period (June 1987 to July 1988) in areas other than the first waste panel (DOE, 1989b). No commitment has been made to pattern rock bolt the waste panels remaining to be mined, because these panels are not subject to a formal retrievability period. The rock bolts in the first waste panel were installed in 1988 following the design and pattern shown in Figures 2-6 and 2-7. The ten-foot length of these rock bolts penetrates through the beam of rock salt between the excavation and anhydrite "b" (2 m above the excavation, Figure 2-2). In SPDV Rooms 1 and 2, this beam has begun to separate along this anhydrite layer, leading to the acceleration in closure rates. The role of the mechanical rock bolts is to suspend the lower beam on the anchors above the anhydrite "b" layer. Because the overall closure of the excavation is a response to creep in the far field, the addition of rock bolts will not stop closure, but may delay the onset of tertiary creep or other new mechanism. The anchors are actually moving toward the center of the excavation. For example, in the experimental Room B, the back continued to fail after it was rock bolted. Other apparent impacts of rock bolting follow.

- Rock bolts will eventually fail in response to corrosion, shear along the clay seams, deterioration of the anchor, or deterioration of the face plate.

- The suspended beam will eventually fail, as seen in Room B, although the onset of tertiary creep and fracture separation will be delayed by rock-bolting.

- Rock bolts may connect brine accumulations, resulting in a larger hydrologically effective room size and an increase in brine-inflow rate, as seen in Room D after rockbolting of the roof (Deal et al., 1989). This increase in brine inflow may, however, be transient. Alternatively, in the event of repository pressurization as a result of internal gas generation, these same rockbolts may provide increased access to marker beds above the repository horizon (especially anhydrites "a" and "b").

- The rock bolts will contribute a negligible mass of steel to the waste rooms. Assuming ~300 bolts/room, steel density of 7.8 g/cm^3, and bolt dimensions of 0.75 inch by 10 feet, the mass of steel added is about 2000 kg/room. This is the equivalent of about 75 drums, about 1% of the expected number of drum equivalents per room.

2.2.7 Summary of Previous and Current Assumptions About the DRZ

The development of a disturbed rock zone around the WIPP workings was not considered in the WIPP FEIS (DOE, 1980), although the possible formation of a dilatant zone was recognized. It was assumed at that time that salt would behave as an isotropic, homogeneous material and that underground excavation could be accomplished with only a minimum of ground control to mitigate fracturing. One exception to these assumptions was the effort to reconcile the three-fold difference between modeled and observed room closure. Morgan

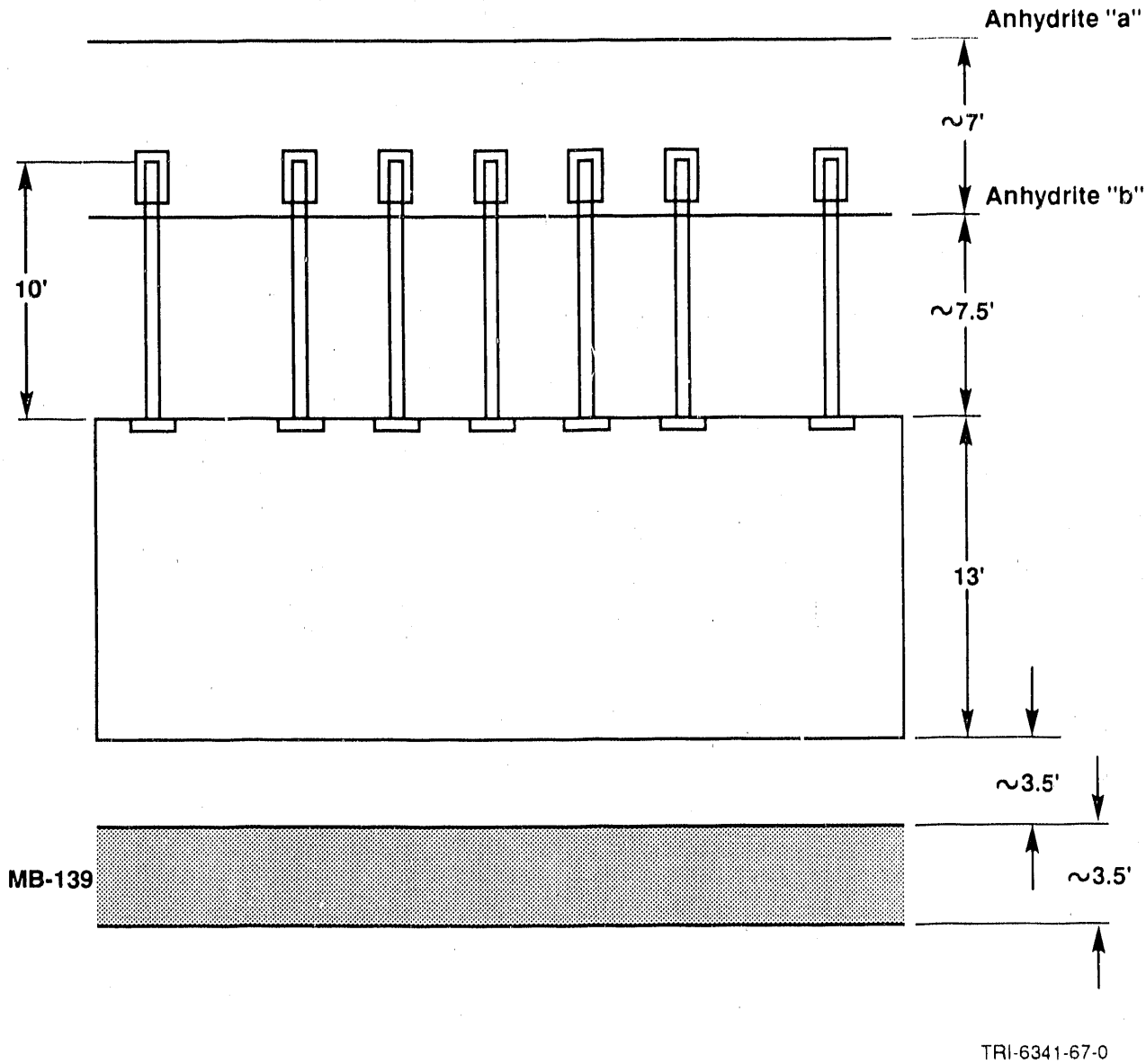

Figure 2-6. Cross section of rock-bolt installation in Panel 1 (courtesy of Westinghouse Corporation).

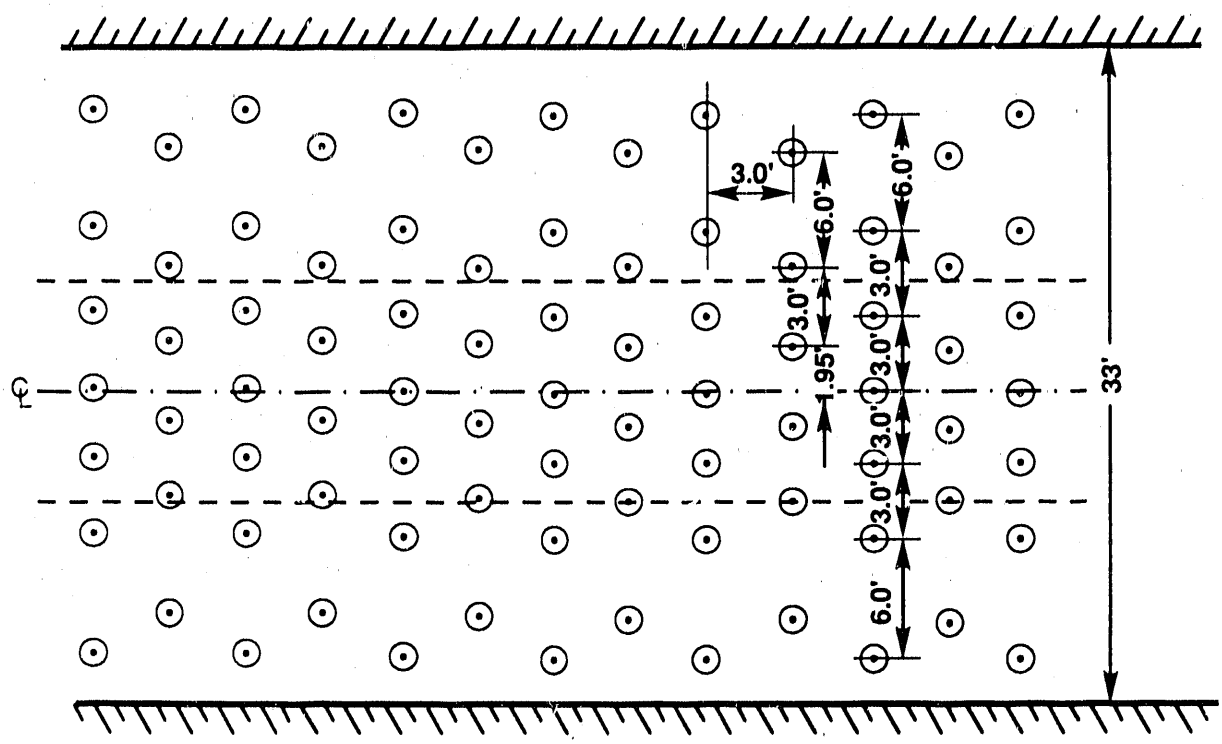

Figure 2-7. Horizontal plan of vertical rock-bolt pattern in roof of Panel 1 (courtesy of Westinghouse Corporation).

(1987), as part of a numerical modeling study, found that weakening the anhydrite marker bed (MB139), as it may be weakened within the DRZ by fracturing, increased the calculated closure and hence decreased the discrepancy between measured and calculated closure rates. Lappin et al. (1989), in support of the draft SEIS (DOE, 1989a) described the DRZ, including fractures around the excavation, as seen in Rooms 1 and 2 (Lappin et al., 1989, Figs. 4-5 and 4-6). In regard to the DRZ, they generally assumed the following, for the purpose of calculating steady-state structural and hydrologic conditions within the repository.

- Closure times and the resulting room "final state" can be accounted for by non-dilatant (no fractures nor microfractures) closure mechanisms. However, Lappin et al. (1989) consider a possible role of the DRZ in storing gases generated within the repository.

- With the exception of anhydrite, rock around the excavation within the DRZ will return, at the "final" state of closure, to its original in situ properties (strength, porosity and permeability). The role of the DRZ was not explicitly considered, with the exception of potential gas storage.

- Anhydrite within the DRZ can be effectively sealed with as-yet undetermined grout. Lappin et al. (1989), in Case IB, examined the effects of degraded transport properties on undisturbed performance, considering the possibility that the seals of anhydrite might only be within two orders of magnitude of design-basis values.

- Final room configuration is not influenced by the extent or mode of rock-mass failure, such as roof collapse and rib spalling. It was recognized, however, that the DRZ might alter the time at which steady state was reached.

If, however, the presence of the DRZ affects structural room-closure times, Lappin et al. (1989) may have underestimated closure times, because their estimates were based on extrapolation of wall-closure rates only. In addition, the DRZ, including MB139, may form a relatively high-permeability pathway around emplaced seals under some conditions. Table 2-1 compares the assumptions made by Lappin et al. (1989) concerning the DRZ with the present understanding of DRZ behavior.

Table 2-1. Current understanding of the DRZ, contrasted with the assumptions in the calculations of Lappin et al. (1989)

Lappin et al.'s Assumptions	Current Understanding
Closure mechanism has no dilatant component.	Borns and Stormont (1988b, 1989) demonstrated that dilatancy can account for a significant portion of the observed closure, especially at early times. Lappin et al. (1989) neglected dilatancy to simplify calculations.
Rock within DRZ will regain in-situ properties with time.	The assumption of rock healing simplifies long-term or steady-state calculations. Rock will approach in-situ properties with time, but studies are needed to demonstrate the extent and rate of approach. Laboratory studies of permeability of fractured and healed specimens (Sutherland and Cave, 1978; Holcomb and Shields, 1987; and Case et al. 1987) used gas injection to measure permeabilities. At lower porosities, if the rock is partially saturated or saturated, this method for determining permeability is not applicable unless the relative saturation is well known. Other studies have used elevated temperatures and pressures, relative to WIPP underground conditions, to facilitate rock healing (Costin and Wawersik, 1980). The one sample tested by Costin and Wawersik at repository conditions did not heal. Studies have not yet examined the effect of fluids in fractures and microfractures of the DRZ. These fluids, if contained, would eventually lower the effective stress, thus enhancing fracturing and maintaining fracture openings.
Sealing of Marker Bed 139 is effective to within an order of magnitude of the properties of the country-rock and compacted salt backfill in the drifts.	This assumption depends greatly on the effectiveness of the composite seal-backfill-formation grout system and the time-dependent deformation around a rigid seal component. Extensive research is underway on seal-material selection and design and small-scale testing of seal systems (Bertram-Howery and Hunter, 1989). Final design and materials are not yet determined. Grout designs must accommodate deformation around composite seals. Recent studies (Beauheim and Saulnier, 1990) suggest that far-field anhydrite may have permeabilities one to three orders of magnitude higher than the host salt, as a result of the presence of fractures. Hence, the marker bed, even outside the DRZ and the seal area, may provide a short-circuit between panels and between the waste emplacement area and the

Table 2-1. Current understanding of the DRZ contrasted with the assumptions in the calculations of Lappin et al. (1989) (concluded)

Lappin et al.'s Assumptions	Current Understanding
	access drifts, <u>if</u> a pathway is established through the intact salt between the repository and marker beds.
Final room configuration is not affected by closure mechanism.	Previous models did not incorporate DRZ effects, in part because final decisions on backfill and rock bolting have not been made. DRZ effects cannot be modeled efficiently by current methods, but the effects may be significant. For example, SPDV Rooms 1 and 2 show that roof failure can occur. Because the DOE does not expect to rockbolt panels other than Panel 1, roof failure and possibly rib spalling is expected in a decommissioned room. It is not well understood how this affects room models in detail, e.g., timing of drum breach and intermingling of contents or the storage volumes created for gas. Finally, effects of fluid-filled fractures on closure mechanisms and rates are not understood; the presence of fluids may accelerate closure while maintaining fracture openings.

3.0 RADIONUCLIDE TRANSPORT IN THE ABSENCE OF HUMAN INTRUSION

Case I of Lappin et al. (1989, Chapter 6 and Appendix D) examined the performance of the repository under undisturbed conditions by analyzing the potential migration of radionuclides from the repository through engineered sealing systems and geologic media to the biosphere. They found that for a period of 10,000 years after repository decommissioning, no radionuclides were released to a stock well located ~4800 m from the repository in the Culebra Dolomite.

Lappin et al. (1989) defined a conceptual model of the system and used a generalized network model (NEFTRAN; Longsine et al., 1987) to simulate radionuclide transport. The analyzed system comprised the wastes, the engineered barriers, and the surrounding geologic media, including Marker Bed 139. Case I was divided into two parts. Case IA simulated expected performance using representative values for all input parameters. This simulation represented the most realistic evaluation of expected long-term repository behavior without modifications of the existing designs of engineered barriers or wastes, assuming that the repository has reached steady state after a period of relatively high gas-generation rates. Case IB simulated degraded performance using parameter values that assumed less than expected performance. This provided a measure of performance under unfavorable and less probable conditions.

The work of Lappin et al. (1989) is revised here in four ways. First, the porosity of MB139 and the cross-sectional area of the path through MB139 have been increased to more accurately reflect the geometry of the seals in the marker bed (Table 3-1, Figure 3-1). The retardation factors used in Cases IA' and IB' (Table 3-2) are unchanged from Cases IA and IB. Second, in these calculations, the geometry and location of the waste storage room and marker bed seal were changed to model the northern equivalent panel, not Panel 1; the northern equivalent panel is the one closest to the shaft, and presumably would be the one from which waste would first reach the shaft. Third, Lappin et al. (1989) chose the value of pressure in the repository to be lithostatic (14.8 MPa). In fact, the pressure driving the flow out of the repository varies spatially between roughly lithostatic (14.8 MPa) and roughly brine hydrostatic (7.0 MPa). Because NEFTRAN accepts only a constant driving pressure, separate simulations were made for Cases IA' and IB' using lithostatic and brine hydrostatic driving pressure. Lithostatic pressure produces a lower-bound limit for the travel times, and hydrostatic pressure produces an upper-bound limit for the travel times (Table 3-3). Finally, Lappin et al. used an unrealistically low threshold concentration, 10^{-18} curies/day, for describing the radionuclide front. The arrival times presented in Table 3-3 use a threshold value of 10^{-10} curies/day for radionuclides or 8×10^{-9} g/day for lead.

3.1 Description of Cases IA' and IB'

With the exceptions noted above, the assumptions and calculations for Cases IA' and IB' were identical to those for Cases IA and IB of Lappin et al. (1989, Chapter 6 and Appendix D). At the time of repository decommissioning, the panels are filled with waste and backfill, with no free water present. New fractures have been formed in MB139, as a result of earlier excavation of the drifts and panels, and in response to later salt creep into these

Table 3-1. Numerical parameters used by NEFTRAN for Cases IA′ and IB′ (cf. Lappin et al., 1989, Tables D-2 and D-3)

	Permeability (m^2)		Porosity		Path-Length (m)	Cross-Sectional Area of Path (m^2)
	IA′	IB′	IA′	IB′		
MB139 Seal Leg 2	4×10^{-19}	4×10^{-17}	0.05	0.05	20	6.13
MB139 Leg 3	3×10^{-7}	3×10^{-7}	0.10	0.10	366	5.57
Lower Shaft Leg 4	10^{-20}	10^{-18}	0.05	0.05	200	29.2
Upper Shaft Leg 5	10^{-12}	10^{-12}	0.20	0.20	200	29.2
Culebra Leg 6	5×10^{-15}	5×10^{-15}	0.16	0.07	430	800
Culebra Leg 8	5×10^{-14}	5×10^{-14}	0.16	0.07	1030	800
Culebra Leg 9	5×10^{-13}	5×10^{-13}	0.16	0.07	3450	800
Salado host rock Leg 7	3×10^{-21}	3×10^{-21}	0.001	0.001	400	45,500

Dispersivity (m)	15.2
Pressure at Repository (MPa)	14.8
Pressure at Culebra above the shaft (MPa)	1.0
Solubility Limit of Radionuclides [M]	Case IA′: 10^{-6}; Case IB′: 10^{-4}

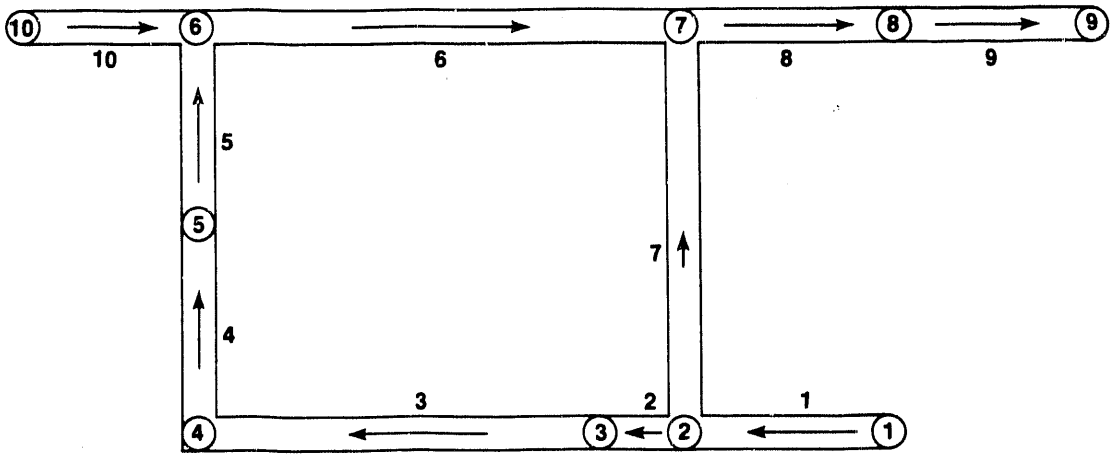

TRI-6330-67-0

Figure 3-1. Numerical flow-network input for simulation of Cases IA′ and IB′. Legs (uncircled numbers) are keyed to Table 3-1. Nodes (circled numbers) are points at which radionuclide concentrations are calculated.

Table 3-2. Retardation factors for use in Cases IA' and IB' (Lappin et al. (1989, Table D-4)

Path	Retardation Factor		Grain Density Assumed ρ_R (g/cm^3)
MB139 Seal	1.0	All Radionuclides	--
MB139[a]	4.7	Pu, Th	--
	1.93	Am	
	1.04	U, Np, Ra, Pb	
Lower Shaft[b]	5.16	Pu, Am, Th	2.19
	1.42	Np	
	1.04	U, Ra, Pb	
Upper Shaft[b]	1.74	Pu, Am, Th	1.84
	1.07	Np	
	1.007	U, Ra, Pb	
Salado Host Rock[b]	231.0	Pu, Am, Th	2.30
	24.0	Np	
	3.3	U, Ra, Pb	
Culebra[c] (Case IA)	1497.0	Pu, Th	2.85
	2994.0	Am	
	16.0	U, Np, Pb, Ra	
Culebra[c] (Case IB)	3787.0	Pu, Th	2.85
	7574.0	Am	
	39.0	U, Np, Pb, Ra	

a. Using the K_a values of anhydrite in MB139 of Lappin et al. (1989, Table D-5). The retardation factor is calculated as $R_a = 1 + aK_a$, where a, the surface-area-to-volume ratio of the parallel fractures, is 10 cm^{-1}.

b. Using the K_d values of crushed salt of Lappin et al. (1989, Table D-5). The retardation factor is calculated as $R = 1 + 0.001\ \rho_R K_d(1-\phi)/\phi$.

c. Using the K_d values of Lappin et al. (1989, Table E-1).

Table 3-3. Arrival times at intermediate points between waste-disposal rooms and the Culebra Dolomite (years after repository resaturation)

	To Bottom of Shaft	To Top of Lower Shaft Seal	To Culebra Aquifer
Lithostatic Pressure at Repository (14.8 MPa)			
Case IA′			
Radionuclides	5×10^5	1.3×10^6	4.8×10^6
Stable Lead	nc	nc	3.5×10^6
Case IB′			
Radionuclides	3500	8500	27,000
Stable Lead	nc	nc	28,500
Direct Route			
Radionuclides	na	na	3.8×10^5
Hydrostatic Pressure at Repository (7.0 MPa)			
Case IA′			
Radionuclides	3.5×10^6	$>1.0\times10^7$	$>1.0\times10^7$
Stable Lead	nc	nc	$>1.0\times10^7$
Case IB′			
Radionuclides	17,000	44,000	160,000
Stable Lead	nc	nc	155,000
Direct Route			
Radionuclides	na	na	$>1.0\times10^7$
Calculations of Lappin et al. (1989, Chapter 6)			
Case IA			
Radionuclides	5×10^5	9×10^5	2.8×10^6
Stable Lead	nc	nc	3.8×10^6
Case IB	nc	8000	25,000
Direct Route	na	na	4×10^5

na = not applicable
nc = not calculated

excavations prior to closure. These new fractures in MB139 only occur directly under excavations, including the experimental area to the north of the access shafts. Seals have been emplaced in MB139 only directly under panel and drift seals. All access drifts and the experimental area have been backfilled. Shaft seals have been emplaced. However, the system is not at steady state. Gas generation by microbial degradation of organic material in waste containers begins prior to final repository closure and continues after closure, because it does not require free brine. As rooms and drifts creep closed, waste containers rupture. Gas from microbial activity and corrosion fills the rooms, migrates through the fractured rock to MB139, and fills the fractures under all previous excavations, regardless of other possible storage mechanisms. Gas pressure rises to lithostatic pressure at some time later than 60 years after decommissioning, slowing brine inflow and helping to maintain open fractures in MB139. Gas generation is assumed to continue for ~2000 years, although this time period is uncertain. As gas generation slows and gas pressures decrease below that required to prevent brine inflow, brine begins to saturate both the repository and MB139. The interaction of closure, gas generation and dispersion, and saturation with host-rock brines is complex and depends strongly on room chemistry and waste types.

As in the work of Lappin et al., the NEFTRAN transport calculations for Cases IA′ and IB′ assume complete resaturation of all media along the flow paths. The repository and MB139 are assumed to be gas-filled for 2000 years and then to be instantaneously resaturated with brine. Radionuclides from the entire repository are assumed to be available for dissolution in the brine according to the solubility limits. Transport calculations are started at 2000 years after waste emplacement, and credit is taken for 2000 years of radioactive decay. Because the time required for repository saturation may exceed 2000 years, Cases IA′ and IB′ may be very conservative; however, all the calculated travel times are much longer than the 10,000-year regulatory period. Even if transport calculations had begun at the time of closure, the change would not have led to violations of 40 CFR 191.

The preferred transport path in Cases IA′ and IB′ is unchanged from Cases IA and IB, i.e, from the waste panels into MB139, through the MB139 seal, along fractures in MB139 to the base of the shafts, through the lower and upper seal systems of the shaft to the Culebra Dolomite, and through the Culebra Dolomite to the stock well. The lower seal system is assumed to be well consolidated, while the upper seal system is less consolidated. Flow is driven by a pressure gradient between the panels and Culebra Dolomite and eventually follows a path within the Culebra Dolomite to the stock well.

Although the pathway described above is a more likely path because each leg has a higher permeability than the host rock, a flow path from the repository through the host rock directly to the Culebra Dolomite also must be considered because of the large cross-sectional area of the repository. Darcy flow may not occur in the Salado Fm., but such flow must be assumed in the NEFTRAN network model.

3.2 Results of NEFTRAN Calculations

The results of the Case-IA and -IIB calculations of Lappin et al. (1989) and the results of the revised Cases IA′ and IB′ are summarized in Table 3-3. The new calculations for Case IA′ (lithostatic) use representative conditions

and properties to estimate first arrival times for the least retarded radionuclides (U, Np, Pb, and Ra) at the top of the Culebra Dolomite in the shaft to be 4,800,000 years, at the middle of the shaft at the top of the reconsolidated salt to be 1,300,000 years, and at the bottom of the shaft to be 500,000 years. These values are similar to the results for Case IA of Lappin et al. Case IA' also calculated a travel time for stable lead; it reaches the Culebra Dolomite in 3,500,000 years. The travel times for radionuclides for Case IA' (hydrostatic) are much longer: 3,500,000 years to reach the bottom of the shaft, and more than 10,000,000 years to reach to top of the lower shaft seal or the Culebra Dolomite. Stable lead also does not reach the Culebra Dolomite for more than 10,000,000 years. In Case IA' (lithostatic) the least retarded radionuclide was estimated to have travelled less than 10 m beyond the seal in MB139 in 10,000 years. Case IB (lithostatic) calculations use degraded conditions in the MB139 seal and lower shaft-seal system to estimate that the same least-retarded radionuclides travel less than 20 m above the lower shaft seal in 10,000 years. For hydrostatic driving pressure, in 10,000 years, the least retarded radionuclides travel about 1 m beyond the MB139 seal in Case IA' and about 200 m beyond the MB139 seal in Case IB'. Thus, assuming that drift and shaft permeabilities after repository saturation are within two orders of magnitude of design-basis values, there should be no release to the Culebra Dolomite or above the top of the Salado Fm. within 10,000 years.

Calculations for transport, applicable to both Case IA' and Case IB', were also performed for the path through the host rock, assuming a cross-sectional area of 45,500 m^2 for this leg (Table 3-1). For lithostatic pressure, the arrival time for the least retarded radionuclide at the Culebra Dolomite is estimated to be at least 380,000 years, and for hydrostatic pressure, more than 10^7 years. The least retarded radionuclide travels about 10 m from the repository in 10,000 years. The calculated travel time through the host rock is much shorter than the 4,800,000 years calculated for travel through the shaft for Case IA'. This difference results from Darcy's Law and the extremely low effective porosity (0.001) of the Salado Fm. The validity of using Darcy's Law in such a low-permeability medium is questionable.

In summary, based on these calculations for representative conditions and degraded conditions, there are no releases of radionuclides to the Culebra Dolomite in Case I, and therefore, no releases to either the surface or the hypothetical stock well in 10,000 years. Because radionuclides are not available for transport through exposure pathways to humans, dose calculations are not warranted in either Case IA' or IB'.

4.0 CONTAMINANT TRANSPORT AND DOSES ARISING FROM HUMAN INTRUSION

This chapter reports three types of calculations, all of which examine the response to human intrusion through the repository into an assumed underlying brine reservoir within the Castile Fm.: (1) detailed calculations of contaminant transport within the Culebra Dolomite; (2) integrated release of contaminants to two boundaries around the repository; and (3) doses that arise from the ingestion of contaminated beef from cattle watered at a stock well located approximately 5 km from the surface projection of the waste panels. The calculations of contaminant transport reported here are revised in three ways from similar calculations by Lappin et al. (1989). First, they use a revised Culebra transmissivity distribution resulting from model calibration that incorporates transient hydraulic stresses at and near the WIPP site, especially those resulting from the H-11 multipad interference test. The revised transmissivity distribution has resulted in some change in expected flow directions and rates within the Culebra Dolomite. In addition, the location of the hypothetical stock well in this report differs slightly from that used by Lappin et al. (1989). Second, the calculations here incorporate more realistic, two-dimensional contaminant transport, as opposed to the one-dimensional stream-tube approach used by Lappin et al. (1989). Finally, these calculations explicitly compare the results of single- and double-porosity calculations. Only two of the four human-intrusion cases examined by Lappin et al. (1989) are recalculated here; the revised calculations are designated Case IIA′ and Cases IIC′. The calculations of dose have been performed identically to similar calculations presented by Lappin et al. (1989). The more realistic, two-dimensional implementation of contaminant transport provides a more accurate calculation of integrated release than the rough estimates contained in the WIPP DSEIS (DOE, 1989a), which were based on one-dimensional, constant-plume-width assumptions.

Incorporating a more realistic, two-dimensional contaminant-transport analysis has significantly reduced centerline concentrations of radionuclides and lead in the waste plume, relative to those estimated by Lappin et al. (1989). These reduced concentrations, in turn, have resulted in smaller estimated integrated releases of contaminants to the accessible environment and in lower doses to persons exposed to beef contaminated by radionuclides in the stock well.

The calculations described in this chapter lead to three major conclusions:

1. For expected conditions and properties (Case IIA′), individual doses at the hypothetical Culebra stock well are extremely small. Integrated releases over 10,000 years at the distances of the stock well and the projected land-withdrawal boundary are several orders of magnitude below the limits set in 40 CFR 191 (currently remanded).

2. For degraded waste and contaminant-transport properties (Case IIC′), the expected 50-year dose commitment at the Culebra stock well, from one year's ingestion of contaminated beef, is 27.8 mrem.

3. For Case IIC′, the calculated integrated radionuclide release at the distance of the stock well (5.04 km) is ~0.7 of that allowed by the remanded

version of 40 CFR 191 for releases with probabilities >0.1 and much less than that allowed for releases with probabilities <0.1. In contrast, the estimated integrated release at the land-withdrawal boundary is ~3 times that currently allowed for releases at these probabilities. Thus, there seems to be considerable contaminant-storage potential between the present WIPP land-withdrawal boundary and the maximum distance allowed for a controlled zone by 40 CFR 191 (EPA, 1985).

4.1 Numerical Implementation of Post-Plugging Analysis

4.1.1 Modeling Approach

The updated analysis of Case II uses the SWIFT II computer code (Reeves et al., 1986a, 1986b) to simulate the time-dependent release of fluid from a hypothetical brine reservoir within the Castile Formation connected to the Culebra Dolomite by a borehole penetrating the repository; ground-water flow within the Culebra; and two-dimensional transport of radionuclides and stable lead in the Culebra. Figure 4-1 is a schematic diagram of the brine-reservoir breach simulation. It shows a borehole passing through the repository and connecting a Castile brine reservoir to the Culebra Dolomite. Figure 4-2 shows the location of the breach borehole and the Culebra flow path to the hypothetical stock well. As discussed below, the Culebra flow path used in the calculations reported here is updated from that estimated by LaVenue et al. (1988), which was used by Lappin et al. (1989). The method used here to assign the stock-well location remains the same as described in the earlier report, i.e., the position is fixed by the intersection of the fastest flow path and the estimated contour of 10,000 mg/L solute concentration in Culebra waters. The change in flow paths due to the revised transmissivity distribution results in a slightly different stock-well location, however. Consistent with hydraulic- and tracer-test interpretations for the H-3 and H-11 hydropad locations (Beauheim, 1987, 1989; Kelley and Pickens, 1986) and with the work of Lappin et al. (1989), the Culebra is assumed here to be a fractured porous medium everywhere along the travel path between the intrusion borehole and the stock well.

The theoretical aspects of implementing the coupling of the brine reservoir to the Culebra Dolomite used here were presented by Lappin et al. (1989). The calculations consider time-dependent release of fluid from the brine reservoir and assume steady-state brine inflow from the Salado Fm. to the intrusion borehole. They simulate time-dependent contaminant injection (radionuclides and stable lead) into the Culebra Dolomite, while assuming that the scale of disturbance of the Culebra flow field due to brine injection from below is small compared with the scale of off-site transport. Therefore, these calculations assume steady-state flow in the Culebra. Section 4.1.2 describes the confirmation of this assumption.

Revised Case-II transport simulations were performed only for Cases IIA and IIC of Lappin et al. (1989). In Cases IIA′ and IIC′, the Castile brine moving up the borehole is conservatively assumed to enter, mix with, and dissolve the waste within the breached waste panel to the solubility limit of each waste constituent (Lappin et al., 1989; DOE, 1989a), unless concentrations are inventory limited. Steady-state brine seepage from the Salado Fm. provides a second source of waste-dissolving fluid to the borehole. The principal difference between Case IIA′ and Case IIC′ entails the selection

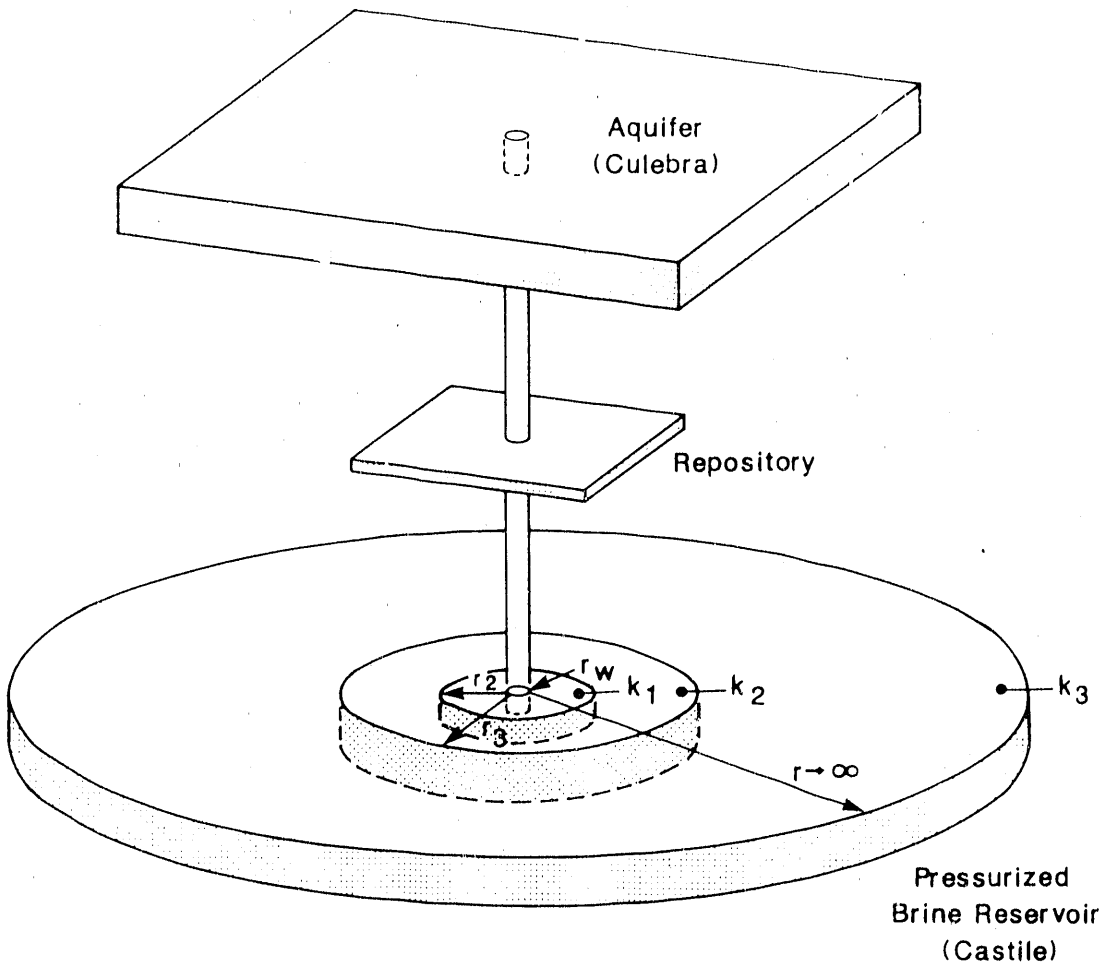

Figure 4-1. Schematic diagram of the brine-reservoir-breach release simulation (Lappin et al., 1989, Figure E-1).

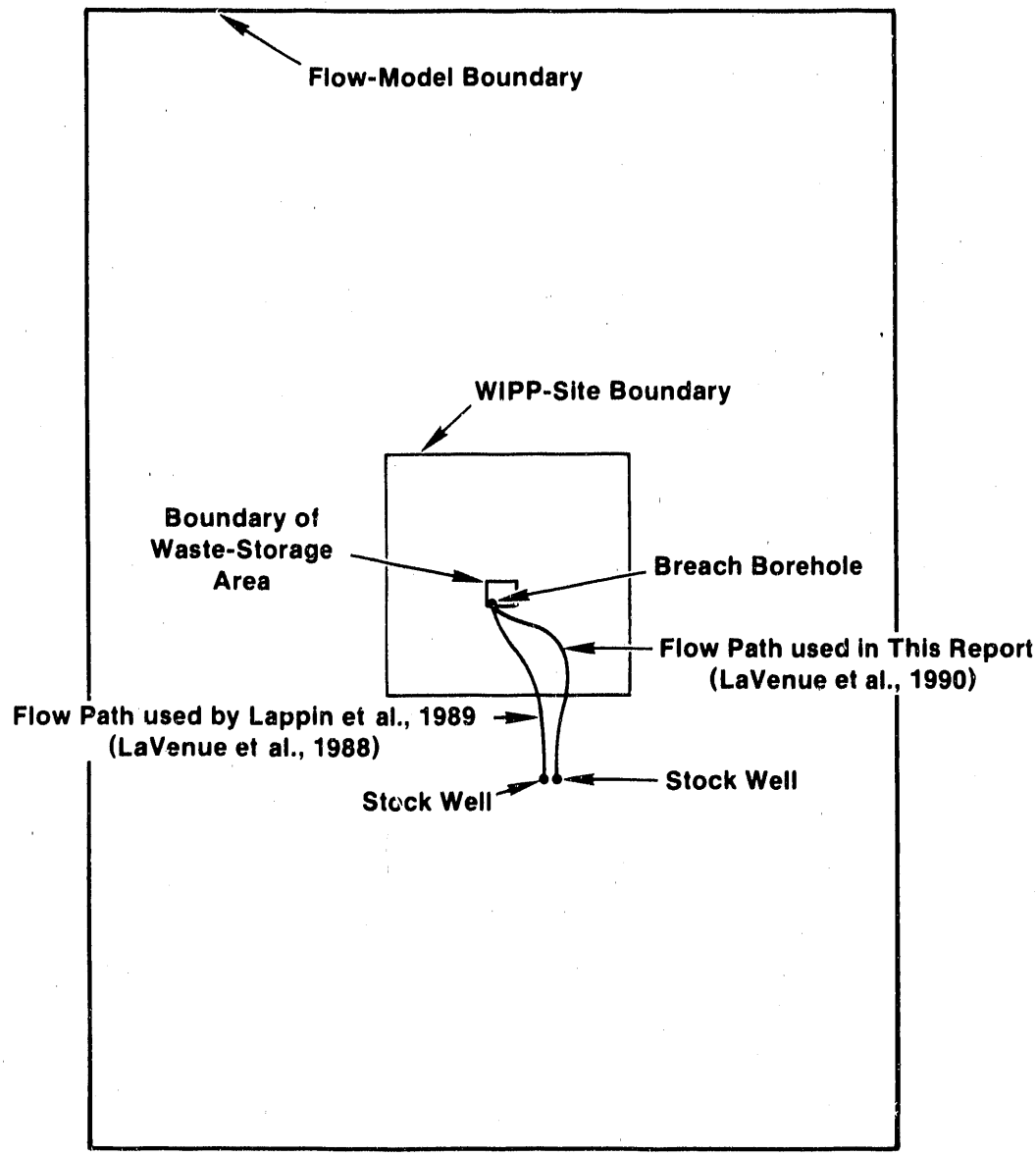

Figure 4-2. Model area, site boundary (projected land-withdrawal boundary), waste-panel layout, breach-borehole and stock-well locations, and transport pathways from the ground-water flow models of LaVenue et al. (1988) and LaVenue et al. (1990) (cf. Lappin et al., 1989, Figure E-2).

of parameter values for the borehole, properties of waste in the repository, and properties of the Culebra Dolomite. Case IIA′ uses expected or representative properties for each of these system components, and Case IIC′ uses degraded properties, i.e., properties selected to increase flow through the borehole and the extent of contaminant transport in the Culebra Dolomite. The assumed properties of the Castile brine reservoir are the same for Cases IIA′ and IIC′.

The Case-II simulations of Lappin et al. (1989) used a one-dimensional stream-tube approach to simulate contaminant transport in the Culebra Dolomite. The revised Case-II transport simulations use a two-dimensional system within the Culebra to meet two objectives: (1) to estimate breakthrough-curve concentrations for contaminants at the stock well, incorporating lateral dispersion and species-specific diffusion effects that were not accounted for in the calculations of Lappin et al. (1989); and (2) to quantitatively estimate cumulative releases of radionuclides at two distances from the waste panel, coincident with the projected land-withdrawal boundary and with the hypothetical stock-well location about 5 km from the surface projection of the waste panels (Figure 4-2). Lappin et al. (1989) calculated only the concentration of contaminants at the stock well; the DSEIS (DOE, 1989a) presented Lappin et al.'s results and also calculated integrated release at the distance of the stock well. This report revises both calculations.

Figure 4-3 illustrates the differences between the assumptions in the models of Lappin et al. (1989) and this report and the situation after an actual intrusion. After an intrusion (Figure 4-3a), the plume source width varies as a function of time, as pressure in the brine reservoir is depleted. Down-gradient from the source, the contaminant-plume width varies due to lateral contaminant dispersion and to variation in source width. Lateral dispersion will reduce contaminant concentrations at the plume centerline. If the plume centerline coincides with the fastest flow pathways, then lateral dispersion may move some contaminants into slower pathways, reducing the integrated release for a given time at a given boundary. The contaminant-concentration calculations of Lappin et al. (1989) and the integrated-release calculations of the DSEIS (DOE, 1989a) made several conservative simplifying assumptions (Figure 4-3b). Although transport calculations incorporated a variable source width, they assumed no lateral dispersion, and therefore no associated reduction in centerline contaminant transport. The calculation of upper bound for integrated release assumed a constant plume width at all times equal to the maximum plume width, corresponding to maximum flow from the brine reservoir. In addition, the maximum flow velocity was assumed to be the flow velocity over the entire width of the plume.

The calculations in this report incorporate a more realistic, two-dimensional model for contaminant transport (Figure 4-3c). In this model, plume width varies not only as a function of source width, but also as a function of lateral dispersion. This simulates the reduction of centerline concentration by lateral dispersion more realistically. The integrated release calculations in this report fully incorporate lateral variations in plume width, rather than using the constant, maximum plume width assumed in the draft SEIS. Like the DSEIS calculations, the new calculations assume a uniform flow velocity across the plume width. Therefore, lateral dispersion does not move contaminants into slower flow paths, which still makes the calculations of integrated release conservative. Finally, the new calculations incorporate a revised Culebra flow field and species-specific diffusion coefficients (see below).

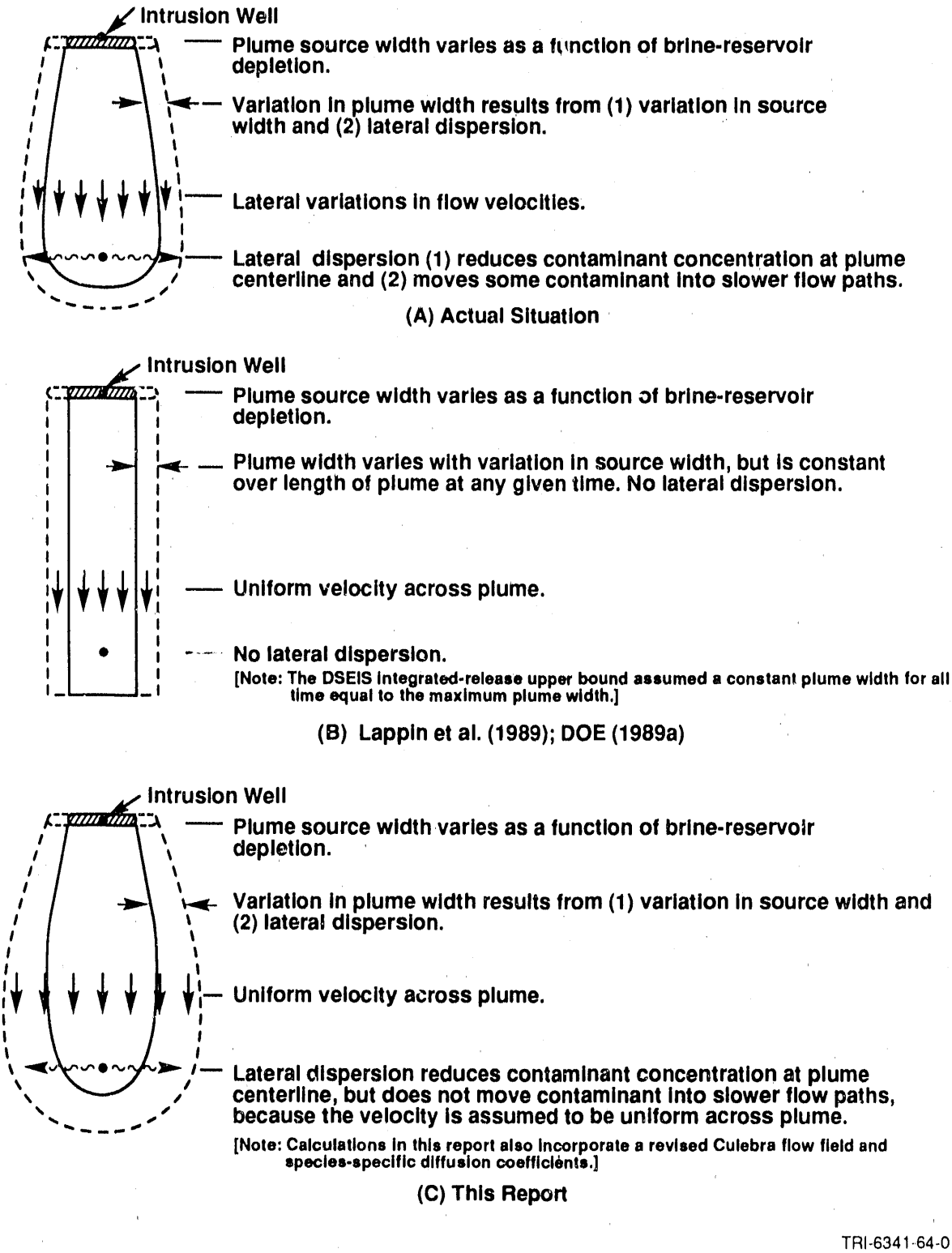

Figure 4-3. Comparison of modeling assumptions and actual intrusion well. (a) Schematic diagram of actual response to intrusion. (b) Simplifying modeling assumptions used by Lappin et al. (1989). (c) Modeling assumptions used in this report.

Section 4.1.2 presents the approach for implementing the two-dimensional contaminant-transport calculations. Revised transport parameters and the model results are discussed in Sections 4.2 and 4.3.

4.1.2 Two-Dimensional Calculations of Flow and Transport

The solution strategy for two-dimensional calculations of flow and transport after a brine-reservoir breach consists of three steps. The first step dynamically couples the brine-reservoir and borehole submodels to the calibrated Culebra ground-water-flow model. This coupling results in estimates of the rate of fluid and contaminant release into the Culebra Dolomite, considering the time-varying degradation of the borehole plugs (Section 4.2.2) and depressurization of the brine reservoir. The calculational approach used here for the brine-reservoir coupling step was described by Lappin et al. (1989, Section E.1.3). The second step calculates the transport pathway within the Culebra Dolomite, using a particle-tracking code (Reeves et al., 1987, Appendix A). The approach is used with an updated transmissivity distribution (LaVenue et al., 1990), as discussed in Section 4.2.4. The third step, described in this section, simulates the transport of radionuclide chains and stable lead (Pb) in the Culebra Dolomite, assuming double-porosity behavior. To simplify the transport calculations, it was assumed that the steady-state flow field is insignificantly disturbed by fluid release from the breach borehole.

Ground-water travel time is defined as the time required for a unit volume of water to travel between two locations, and it is calculated by dividing average ground-water flux (i.e., Darcy velocity) by the hydraulically effective porosity. Although a carefully calibrated flow model provides good estimates of average ground-water flux, determining an appropriate effective porosity in a fractured, double-porosity flow system like the Culebra Dolomite is difficult. In a double-porosity system, some water flows through the fractures, and some water flows through the matrix. Therefore, one can consider the extreme cases of all water flowing through the fractures (and calculate a fracture-only ground-water travel time by dividing average ground-water flux by fracture porosity) or of all water flowing through the porous matrix (and calculate a porous-medium ground-water travel time by dividing average ground-water flux by the matrix porosity). Computing fracture-only and porous-medium travel times is useful here for comparing some aspects of flow-system behavior, e.g., comparing the impact on flow rates of the revised transmissivity distribution of LaVenue et al. (1990) with the impact of the earlier one of LaVenue et al. (1988). Ground-water travel-time estimates do not provide a meaningful characterization of the overall transport behavior of the Culebra Dolomite flow system, however, because contaminant transport in a fractured, double-porosity system is strongly influenced by the degree of fracture/matrix interactions of the contaminant, and because the ground-water travel time extremes for this study are so far apart, 151 years for fracture-only flow versus 16,140 years for porous-medium flow. Only actual contaminant transport calculations can provide information on overall transport behavior.

To justify the use of a steady-state flow field in Step 3, particle travel times in the Culebra Dolomite from the release point (breach well) to the revised stock-well location (Section 4.3.2) were calculated for steady-state conditions and for transient conditions calculated for Case IIA′ and Case IIC′. Particle travel times are calculated using Darcy velocities and an estimated effective porosity. Longitudinal or lateral dispersion, matrix

diffusion, and sorption (retardation) are not included. The calculated particle travel times all assumed fracture-only transport, with a fracture porosity of 1.5×10^{-3}, to assess the maximum transport impact of the transient brine-reservoir perturbations on the undisturbed Culebra flow field. The calculated particle travel time for the undisturbed, steady-state flow simulation (151 years) differs by only ~2.9% from the Case IIA' particle travel time (147 years) and ~5.1% from the Case IIC' travel time (144 years) assuming transient flow conditions. In addition, the transport pathway for the three flow fields discussed above varied insignificantly. In contrast, the calculated matrix-porosity ground-water travel times assuming steady-state flow to the land-withdrawal boundary and stock well are 10,480 and 16,140 years respectively, assuming a hydraulically effective matrix porosity of 0.16. Travel times and travel path are discussed further in Section 4.3.2.

The possibility that karstic hydrology is present within the Rustler Fm. at the WIPP site has been considered repeatedly (e.g., Barrows et al., 1983; Lappin, 1988). A common inference is that the presence of a fractured karstic system would increase radionuclide migration. Isotopic evidence, however (e.g., Lambert, 1987; Lambert and Carter, 1987), indicates isolation times of confined Rustler waters (from surface exposure) of more than 10,000 years. Therefore, there is good evidence that actual ground-water travel times near the WIPP site are on the order of at least several thousand years.

Figure 4-4 illustrates an idealized contaminant plume formed as the result of a point-source injection, at time-dependent rate Q, into a undirectional flow field, with undisturbed Darcy velocity u_o, and aquifer thickness b. The figure is a schematic illustration of the streamlines as they emanate from the borehole in response to a release of brine-reservoir and Salado fluids to the Culebra Dolomite. The streamlines diverge from the point of release, but become parallel to the direction of the natural, undisturbed, ground-water flow at some distance downstream.

The streamlines of the injected fluids thus form a plume of contaminated water of theoretical width 2w, from flow divide to flow divide (Figure 4-4), defined by the relation

$$2w = Q_{(t)}/bu_o \qquad (4\text{-}1)$$

The flux within the plume asymptotically equals that of the natural ground water system, u_o. The distance s that separates the points of release and the stagnation point, at which the local flow velocity is zero, is defined by the relation

$$s = Q/2\pi bu_o \qquad (4\text{-}2)$$

The stagnation-point distance provides a measure of the spatial extent of the region in which fluid velocities differ significantly from u_o. The maximum rate of fluid release Q_{max} calculated for the borehole in Cases IIA' and IIC' and the local, natural ground-water velocity u_o calculated for the Culebra flow model at the point of release (i.e., the borehole) can be used to calculate maximum stagnation-point distances. As discussed in Section 4.3.1, a comparison of the maximum stagnation-point distances and maximum plume widths to the travel-path distance, from the point of release to the stock

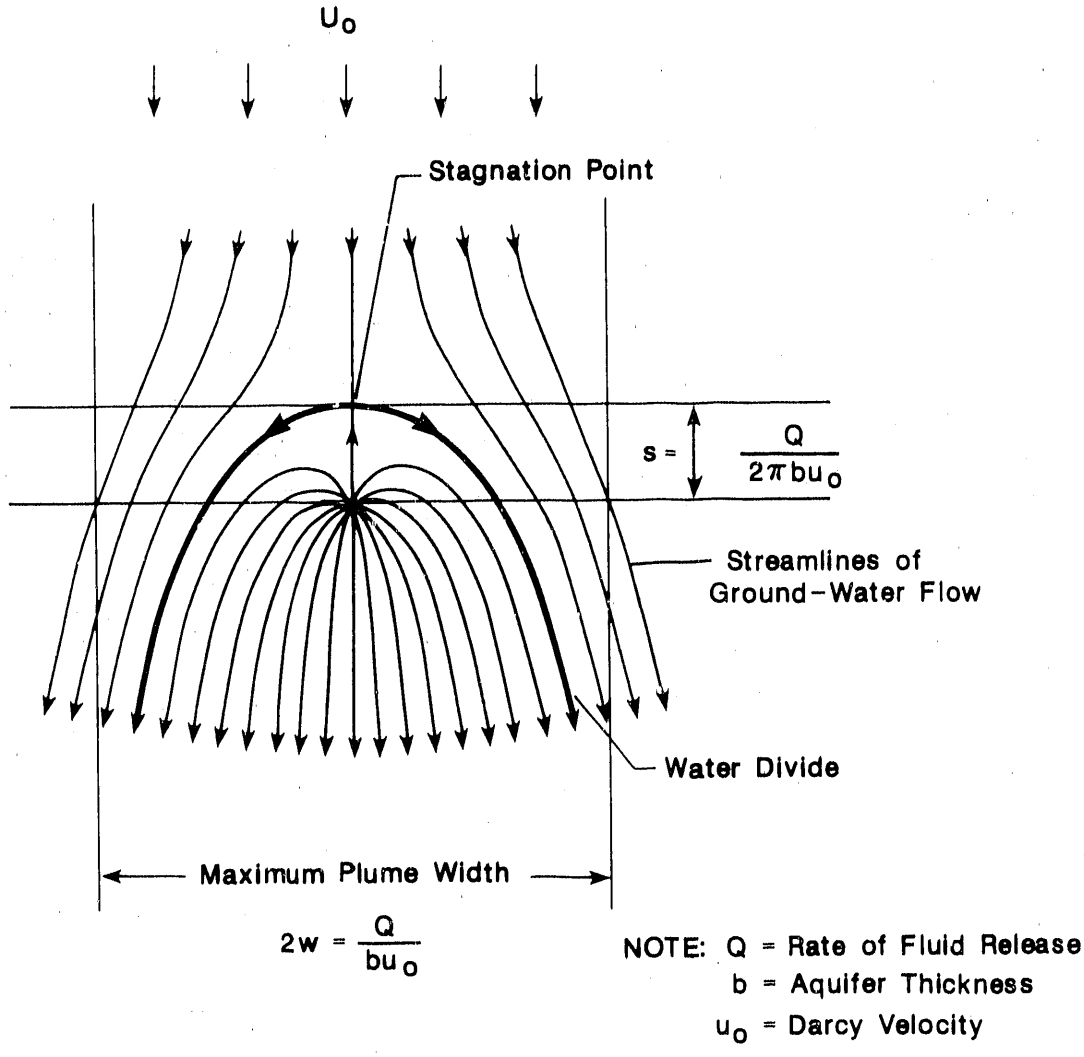

Figure 4-4. Schematic illustration of streamlines in a unidirectional flow field perturbed by an injection well (after Bear, 1972). For the calculations in this report, the rate of brine injection ($Q_{(t)}$) is time dependent.

well, indicates that the region of disturbed velocities is small relative to the overall scale for solute transport, supporting the assumption of a negligibly disturbed steady-state flow field. The plume width reaches a maximum when the borehole plugs have first fully degraded to the permeability of a rubble-filled borehole (Section 4.2.2) and decreases monotonically with time from the time of complete degradation of the borehole plugs to 10,000 years, as a result of depletion of pressure in the underlying Castile brine reservoir.

Several other assumptions were used in implementing the two-dimensional approach for simulating contaminant transport in the Culebra Dolomite. Equation 4-1 was used to estimate the variation in plume width at the release point, based on the estimated time-dependent injection rate into the Culebra ($Q_{(t)}$). Because the region of disturbed flow was relatively small compared with the transport distances to the WIPP-site boundary and the stock well, the mass flux at any time was assumed to be uniformly distributed laterally from the point of release across the plume, i.e., the concentration was uniform across the plume in the injection zone. The time-varying width of the input zone (Figure 4-3) was modeled by specifying the number of blocks with mass input at various times, e.g., times t_1, t_2, etc., in Figure 4-5. An assumption of symmetry about the plume centerline allows the simulation grid to include only one half of the Culebra system. Concentration was assigned a uniform value only at the injection zone (Figure 4-5). Downstream from this zone, longitudinal and lateral dispersion were treated numerically.

The calculated Darcy-velocity distribution was relatively uniform along the transport pathway, from point of release to stock well, i.e., the Darcy velocity at the point-of-release, WIPP-site-boundary, and stock-well locations varied by only about 13%. Therefore, an average Darcy velocity was used in the transport simulations.

4.2 Input Parameters for Post-Plugging Analysis

4.2.1 Brine-Reservoir Parameters

A Castile brine reservoir is assumed to extend beneath the WIPP repository. The estimates of the reservoir parameter values used by Lappin et al. (1989) to characterize a hypothetical brine reservoir beneath the repository for the initial Case-II simulations were also used for the revised Case-II' simulations reported here (Table 4-1). In both studies, only the base-case parameter values for the brine reservoir were used in simulating the release of fluid from the brine reservoir.

4.2.2 Intrusion-Borehole Parameters

The intrusion borehole (Figure 4-6) is assumed to be drilled through the center of the southwestern waste panel, because this waste panel has the shortest particle travel time to the hypothetical stock well. The UTM (Universal Transverse Mercator) coordinates for the center of the southwestern waste panel are estimated to be 3581141 m N and 613331 m E. These coordinates were estimated based on the UTM coordinates for the construction and salt-handling shaft (Gonzales, 1989) and distances to the center of the southwestern waste panel (Bechtel drawing 51-R-401, Underground Excavation General Arrangement). These UTM coordinates differ by several meters from those of

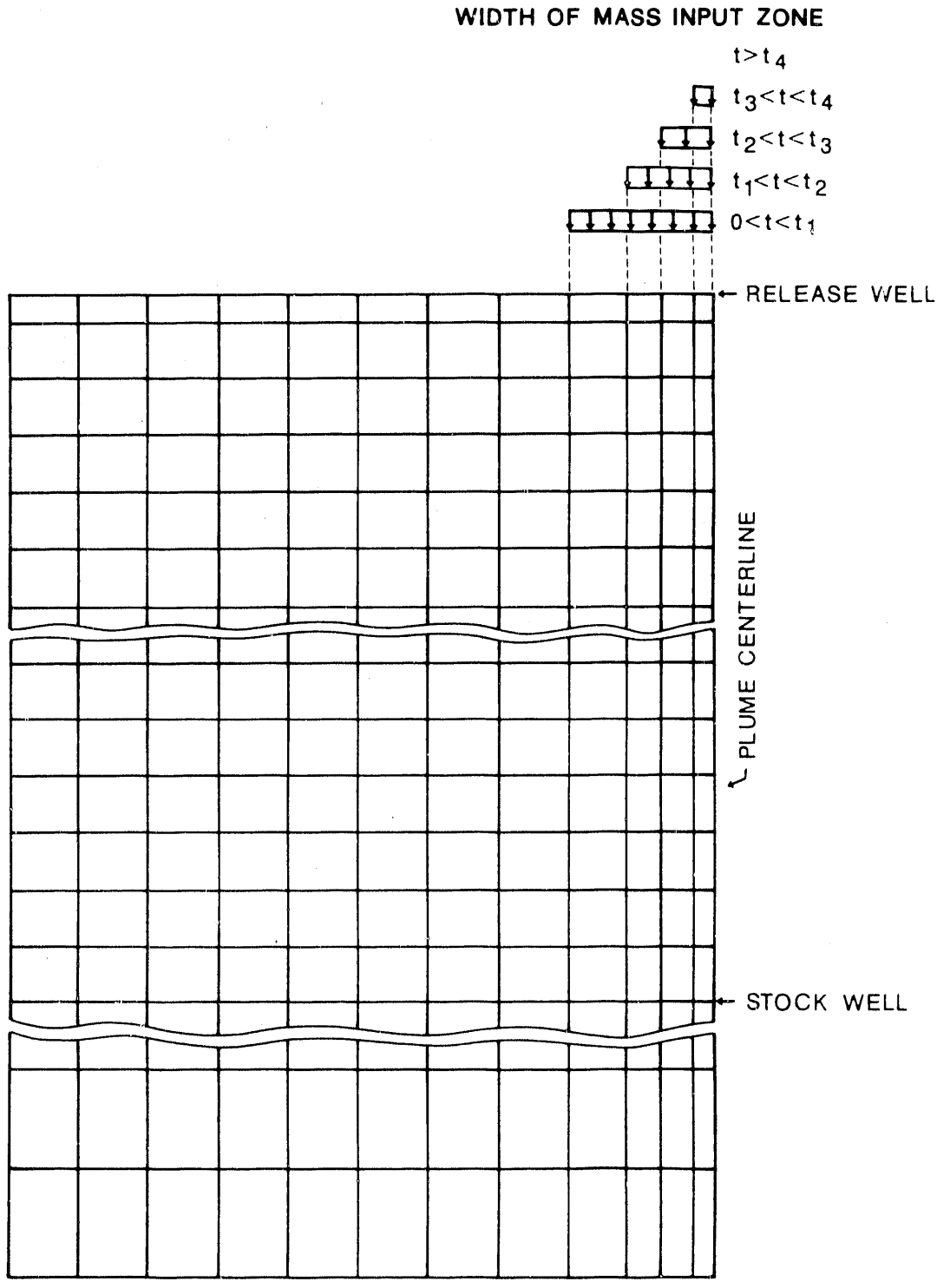

Figure 4-5. Schematic illustration of the two-dimensional grid for the Culebra Dolomite used for Case-II simulations using SWIFT II.

Table 4-1. Parameter base-case and range values selected for the hypothetical brine reservoir, Case II (Lappin et al., 1989, Table E-4)

Parameter	Symbol	Base Case	Range	Units
Initial pressure	P_i	12.7	7.0 to 17.4	MPa
Effective thickness	b	7.0	7.0 to 24.0	m
Transmissivity of inner zone	T_i	7×10^{-4}	7×10^{-6} to 7×10^{-2}	m^2/s
Distance to inner/ intermediate zone contact	r_2	300	100 to 900	m
Transmissivity of intermediate zone	T_o	7×10^{-6}	7×10^{-8} to 7×10^{-4}	m^2/s
Distance to intermediate/ outer zone contact	r_3	2000	30 to 8600	m
Transmissivity of outer zone or intact castile	T_m	1×10^{-11}	constant	m^2/s
Fluid density	ρ_f	1240	constant	kg/m^3
Porosity	ϕ	0.005	0.001 to 0.01	
Compressibility of medium	α	1×10^{-9}	1×10^{-10} to 1×10^{-8}	1/Pa

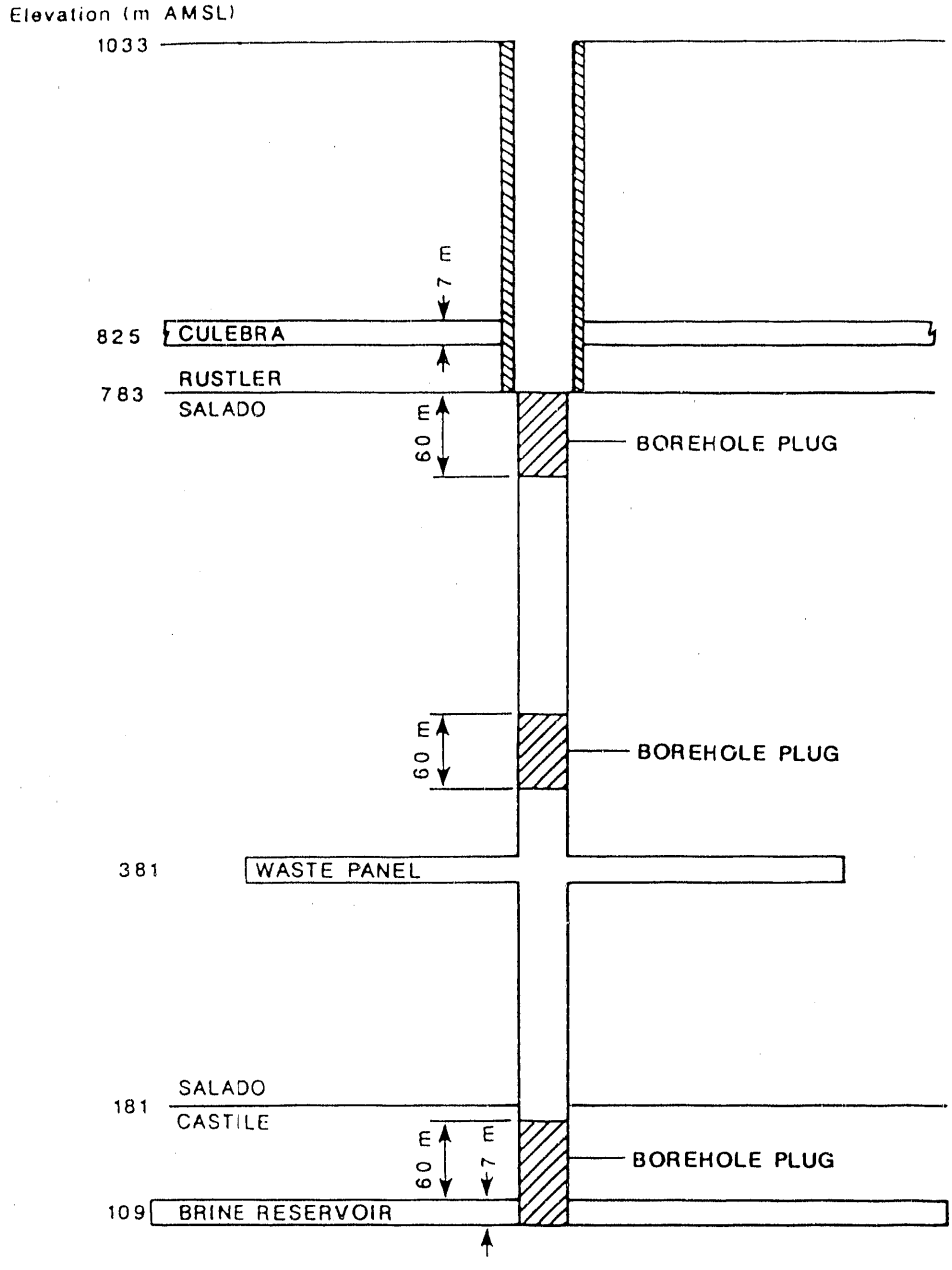

Figure 4-6. Schematic illustration of intrusion borehole after plug emplacement (Lappin et al., 1989, Figure E-5).

Lappin et al. (1989) as a result of minor scaling differences. All other borehole specifications (elevations of Castile Fm. and Culebra Dolomite, average borehole diameters, borehole-plug lengths, and effective borehole permeabilities at various times) used in the revised Case II simulations (Table 4-2) are the same as those used by Lappin et al. (1989).

An effective borehole transmissibility between the brine reservoir and the Culebra Dolomite was used in modeling the hydraulic coupling of the Castile brine reservoir and the Culebra. The effective borehole transmissibility was calculated as a harmonic average of the borehole hydraulic conductances using the appropriate borehole or plug lengths with specific permeabilities and cross-sectional areas (Table 4-2). The effective borehole transmissibility is given by the relation

$$T = 1/\Sigma[1/(\rho g k_i A_i/\mu L_i)] \qquad (4\text{-}3)$$

where i refers to the zones between the center of the Culebra and the base of the Rustler and between the base of the Rustler and the center of the brine reservoir; k_i is the effective borehole permeability; A_i is the borehole cross-sectional area; L_i is the length of the plugs or rubble-filled borehole zones; ρ and μ are the fluid density and viscosity of the Castile fluid; and g is the gravitational constant. The assumed length of plugs and open or rubble-filled zones within the boreholes are shown in Figure 4-6. Constant fluid density and viscosity values of 1240 kg/m^3 and 1.6×10^{-3} Pa-s, respectively, considered representative of the Castile fluid, were specified for the borehole-fluid properties. Thus, any variation in density of the borehole fluids in response to variable mixing of Castile and Salado brines was ignored. The effect is expected to be minimal.

For modeling, the repository is assumed to remain unbreached during 100 years of institutional control following decommissioning. During this time, radioactive decay of the waste occurs. A borehole through the repository is assumed to be drilled immediately following this 100-year period. The borehole is assumed to be plugged immediately, and the borehole plugs are assumed to remain intact for 75 years after emplacement. The borehole transmissibility was assumed to increase linearly in magnitude during the next 75 years, at the end of which time (t=250 years) the effective borehole permeability along the full length of the borehole was equal to 10^{-12} m^2 for Case IIA' and 10^{-11} m^2 for Case IIC'. The time-varying transmissibility was implemented in a step-wise manner with equal logarithmic increments to the transmissibility at 75, 100, 125, and 150 years after plug emplacement.

4.2.3 Repository Source-Term Parameters

For Cases IIA' and IIC', the permeability of the waste panel is conservatively assumed to be high enough to allow circulation of Castile brine through the waste prior to continuing up the borehole. During this circulation, the brine is assumed to dissolve waste to the assigned solubility limit for the radionuclide constituents and stable lead, unless the concentration is inventory-limited, i.e., unless there is insufficient inventory to maintain saturation within the waste panel. The inventory-depletion model implemented in this event assumes uniform contaminant concentration in the panel. The assumptions and numerical approach used here are the same as described by Lappin et al. (1989). Steady-state brine inflow from the Salado Fm. provides an additional source of fluid passing through the repository and dissolving

Table 4-2. Specifications for the intrusion borehole, Case II'. All parameter values for the intrusion borehole are the same as those of Lappin et al. (1989, Table E-2), with the exception of the borehole UTM coordinates

Parameter	Value	Units
Borehole UTM location at center of southwestern waste panel	613331 3581141	m E m N
Altitudes		
- ground surface	1033	m
- center of Culebra	825	m
- Rustler/Salado contact	783	m
- center of waste panel	381	m
- Salado/Castile contact	181	m
- center of brine reservoir	109	m
Drilled diameter		
- in Rustler Fm. (oil well)	0.413	m
(gas well)	0.457	m
- in Salado and Castile Fms. (oil well)	0.311	m
(gas well)	0.356	m
Hole diameters used in numerical analysis		
- Cased inside diameter of average hole in Rustler	0.326	m
- diameter of average borehole in Salado and Castile Fms.	0.334	m
Borehole plugs		
- lengths	60	m
- locations: (i) above brine reservoir (ii) below potash zone (iii) below Rustler		
Effective borehole permeability		
- open-borehole period		infinite
- plug in Castile Fm.	10^{-15}	m^2
- plugs in Salado Fm.	10^{-18}	m^2
- for times greater than 150 years		
- Case IIA'	10^{-12}	m^2
- Case IIC'	10^{-11}	m^2

waste prior to flowing up the borehole. The Salado brine inflow to an entire waste-emplacement panel is assumed to have access to the borehole. Thus, the time-dependent mass loading of each radionuclide constituent and stable lead to the Culebra Dolomite is controlled by the combination of time-varying flow rate from the Castile Fm., assumed steady-state brine-flow rate from the Salado Fm., solubilities of the waste constituents, and the masses emplaced or generated by decay in the waste panel.

Parameter values quantifying the source term for the Case-II' simulations reported here are presented in Tables 4-3 and 4-4. Simulations were performed for four simplified radioactive-decay chains (^{240}Pu, ^{239}Pu, ^{238}Pu, and ^{241}Am) and for stable lead for 10,000 years after repository decommissioning, beginning after the 100-year period of institutional control. The initial waste inventory for the repository and the waste inventory after 175 years (corresponding to 100 years of institutional control and 75 years of undegraded plug performance) (Table 4-3) differ somewhat from those used by Lappin et al. (1989). The mass inventory of the radioactive species is larger here than specified by Lappin et al. (1989), because it has been scaled upward to fill the entire repository design volume (DOE, 1990a). The SWIFT II simulations consider transport in the Culebra Dolomite beginning at the latter time (175 years), which also corresponds to the start of plug degradation, using the aged inventory. With the exception of ^{241}Am, the numerical treatment of radionuclides used here is the same as used by Lappin et al., (1989). They did not model ^{241}Am explicitly, because of its relatively short half life (432 years), but instead assumed that all ^{241}Am had decayed to ^{237}Np before the beginning of radionuclide transport. They obtained the interesting result that, for cases involving extreme fracture flow, migration of ^{241}Am appeared to be significant. Therefore, this report models ^{241}Am explicitly.

The repository parameter values for the revised Case-II simulations are given in Table 4-4. The solubilities are the same as those used by Lappin et al. (1989). Assuming uniform waste-emplacement density at the scale of waste panel, the mass of each waste species in the southwestern waste panel was calculated based on the excavation volumes of actual and equivalent panels as follows:

$$M_i^P = M_i [A/(8A)+B+C] \qquad (4\text{-}4)$$

where M_i^P is mass of waste species i in the southwestern waste panel, M_i is the total mass of waste species i in the repository, A is the excavation volume of each of the eight waste panels, and B and C are the excavation volumes of the northern and southern equivalent panels in the central portion of the waste-panel layout. Based on the excavation volumes of these panels (Lappin et al., 1989, Table 4-7), Equation 4-4 reduces to

$$M_i^P = 4.6\ M_i/43.5 \qquad (4\text{-}5)$$

The final-state pore volume of one room reported by Lappin et al. (1989), 106 m^3, was not used in their Case-II simulations, because it was not available when the simulations were performed. The revised simulations presented here use the estimated final-state pore volume of 1330 m^3 for one panel, based on a room pore volume of 106 m^3 and the ratio of initial excavated panel volume to initial excavated room volume (45,700 m^3/3640 m^3 = 12.55). The assumed steady-state Salado-fluid loading has also been slightly changed from

Table 4-3. Mass inventory of radionuclide species and stable lead in the repository, Case II'

Decay Chain or Waste Species	Radio-nuclide	Half Life (years)	Ci/g	Initial Inventory* (g)	Inventory at 175 Years(1) (g)
$^{240}Pu \rightarrow {}^{236}U$	^{240}Pu	6.54×10^{3}	2.28×10^{-1}	5.27×10^{5}	5.17×10^{5}
	^{236}U	2.34×10^{7}	6.47×10^{-5}	0	9.52×10^{3}
^{239}Pu	^{239}Pu	2.41×10^{4}	6.21×10^{-2}	7.88×10^{6}	7.84×10^{6}
$^{238}Pu \rightarrow {}^{234}U$	^{238}Pu	8.77×10^{1}	1.71×10^{1}	3.06×10^{5}	0(2)
$\rightarrow {}^{230}Th \rightarrow {}^{226}Ra$	^{234}U	2.44×10^{5}	6.26×10^{-3}	0	3.01×10^{5}
$\rightarrow {}^{210}Pb$	^{230}Th	7.70×10^{4}	2.02×10^{-2}	0	0(3)
	^{226}Ra	1.60×10^{3}	9.89×10^{-1}	0	0(4)
	^{210}Pb	2.23×10^{1}	7.64×10^{1}	0	0(4)
^{241}Pu	^{241}Pu	1.44×10^{1}	1.03×10^{2}	4.56×10^{4}	0(2)
$\downarrow$	^{241}Am	4.32×10^{2}	3.43×10^{0}	2.25×10^{5}	2.06×10^{5}
$^{241}Am \rightarrow {}^{237}Np$	^{237}Np	2.14×10^{6}	7.05×10^{-4}	1.53×10^{4}	7.93×10^{4}
$\rightarrow {}^{233}U \rightarrow {}^{229}Th$	^{233}U	1.59×10^{5}	9.65×10^{-3}	9.82×10^{5}	9.81×10^{5}
	^{229}Th	7.43×10^{3}	2.10×10^{-1}	0	0(3)
Stable Pb	-	-	-	1.33×10^{9}	1.33×10^{9}

* Initial inventory at the time of decommissioning (in Ci) is from DOE (1990a, Table B.2.13, except stable Pb, from Lappin et al. (1989, Table E-5). The inventory of stable Pb is not scaled up, because stable Pb is not depleted in any of the cases.

(1) Transport calculations start 175 years after institutional control begins, i.e., after 100 years of institutional control and an effective plug life of 75 years.

(2) Because ^{238}Pu and ^{241}Pu have short half-lives and large retardation factors, their migration from the source is minimal. Therefore, the conservative approach taken here converts all ^{238}Pu and ^{241}Pu to daughter products at simulation beginning.

(3) Because of large retardation factors relative to their parents, ^{230}Th and ^{229}Th migration is controlled by their parents. In addition, both radionuclides have very little mass in place at 175 years. Therefore they are not considered to be present at 175 years.

(4) These nuclides are not present in quantities large enough at 175 years to warrant source inclusion.

Table 4-4. Repository parameters, Case II' (after Lappin et al., 1989, Table 3-4)

Parameter	Symbol	Base Case	Units
Soluble radionuclide concentration for each decay-chain member i			
- Case IIA'	C_s	1×10^{-6}	molar
	C_s*	2.4×10^{-7}	kg/kg
- Case IIC'	C_s	1×10^{-4}	molar
	C_s	2.4×10^{-5}	kg/kg
Soluble stable-Pb concentration			
- in repository	C_s	1.16×10^{2}	mg/L
	C_s	1.16×10^{-4}	kg/kg
- in Culebra	C_s	5.4×10^{1}	mg/L
	C_s	5.4×10^{-5}	kg/kg
Mass of waste in southwestern waste panel in contact with circulating fluids after borehole is plugged	-	$4.6\ M_i/43.5$	g
Pore volume in southwestern waste panel	-	1330	m^3
Salado-fluid loading (Q_s) from repository to the borehole in Cases IIA' and IIC'	-	1.4	m^3/yr

* Based on the specified radionuclide solubilities expressed as molarity, solubility values expressed as kg/kg have about a 6% range. Because of the large uncertainty in molarity values, however, a single solubility value for all radionuclides was used in numerical simulations, i.e., the 6% range resulting from the change in units is ignored.

the earlier report, from 1.3 m^3/yr to 1.4 m^3/yr, as a result of a modification of the estimated Salado lithostatic pressure value (from 14 MPa to 14.8 MPa) used in estimating long-term brine-inflow rates.

4.2.4 Culebra Parameters

The Culebra Dolomite is assumed to behave as a fractured porous medium along the travel path between the intrusion borehole and the stock well. Lappin et al. (1989) discussed the selection of contaminant-transport parameter values for the Culebra Dolomite. The base-case and range parameter values for the revised Case-II simulations reported here are presented in Table 4-5. Changes in parameters from those presented by Lappin et al. (1989) are briefly discussed below.

4.2.4.1 Regional Flow Field. The Case-II simulations by Lappin et al. (1989) used LaVenue et al.'s (1988) Culebra ground-water-flow model calibrated to the undisturbed head distribution determined from data collected through about October 1987. The Culebra transmissivity distribution and regional Darcy velocity field estimated by LaVenue et al. (1988) are shown in Figures 4-7 and 4-8. A newly revised Culebra model, used in this report, includes calibration to undisturbed- and transient-head data collected through June 16, 1989 (LaVenue et al., 1990). This modeling study included an expanded model domain (21.3 km x 30.6 km) and an expanded and revised data base of Culebra transmissivities and heads. This study also quantified the estimation errors in the available transmissivity data, mapping the distribution of transmissivity measurement uncertainty over the model region (Figure 4-9). Major transient hydraulic stresses included in the recent calibration include the responses to construction of the four WIPP shafts; the H-3, WIPP-13, and H-11 multipad pumping tests; and the H-3 and H-4 conservative-tracer tests. LaVenue et al.'s (1990) model differed from the model presented by LaVenue et al. (1988) in that it included calibration to all significant transient events (shaft construction and H-3 and H-11 multipad tests) in the vicinity of the off-site transport pathway between the southwestern waste panel and the stock well (Figure 4-2). The simulated Culebra transmissivity distribution and regional Darcy velocities resulting from the recent calibration for the new Culebra model are shown in Figures 4-10 and 4-11.

Comparison of the transmissivity distributions shown in Figures 4-7 and 4-10 indicates that results of the H-11 multipad interference test and inclusion of major transient hydraulic stresses has not changed the calibrated Culebra transmissivity distribution in a major way. The primary effect of the updated testing and calibration has been to generally broaden the embayment of the transmissivity contour of 10^{-6} m^2/s (Figures 4-7 and 4-10) in the southeastern portion of the WIPP site. As briefly discussed by Lappin et al. (1989) and by Beauheim (1987b), fracturing effects are generally evident in which local-scale hydraulic testing if the local transmissivity is ~10^{-6} m^2/s or greater. Thus the updated model calibration indicates an increased role of fracturing in the southeastern portion of the WIPP site, as well as south of the site.

The effect of the revised transmissivity distribution on the undisturbed Darcy-velocity field can be seen by comparing Figures 4-8 and 4-11. The two off-site flows paths from the intrusion borehole to the stock well are compared graphically in Figure 4-2. While the regional flow direction is

Table 4-5. Parameter base-case and range values selected for the Culebra Dolomite, Case II' (after Lappin et al., 1989, Table E-6)

Parameter		Symbol	Base Case	Range	Units
UTM location of stock well		-	615115	-	mE
			3576367	-	mN
Matrix tortuosity		θ'	0.15	0.03 to 0.5	
- Case IIA'		θ'	0.15	-	
- Case IIC'		θ'	0.03	-	
Matrix-block length		2L'	2.0	0.25 to 7.0	m
- Case IIA'		2L'	2.0	-	m
- Case IIC'		2L'	7.0	-	m
Matrix porosity		ϕ'	0.16	0.07 - 0.30	
- Case IIA'		ϕ'	0.16	-	
- Case IIC'		ϕ'	0.07	-	
Fracture porosity		ϕ	1.5×10^{-3}	1.5×10^{-4} to 1.5×10^{-2}	
Longitudinal dispersivity		α	100	50 - 300	m
Fracture flux		u	1.87×10^{-9}	-	m/s
Grain density		ρ_R	2.82	2.78 - 2.86	g/cm^3
Matrix distribution coefficient					
- Case IIA':	Pu	K_d	50	-	mL/g
	Am	K_d	200	-	mL/g
	U	K_d	1	-	mL/g
	N_p	K_d	1	-	mL/g
	Th	K_d	50	-	mL/g
	Ra	K_d	0.1	-	mL/g
	Pb	K_d	0.1	-	mL/g
- Case IIC':	Pu	K_d	25	-	mL/g
	Am	K_d	100	-	mL/g
	U	K_d	1	-	mL/g
	N_p	K_d	1	-	mL/g
	Th	K_d	25	-	mL/g
	Ra	K_d	0.05	-	mL/g
	Pb	K_d	0.05	-	mL/g

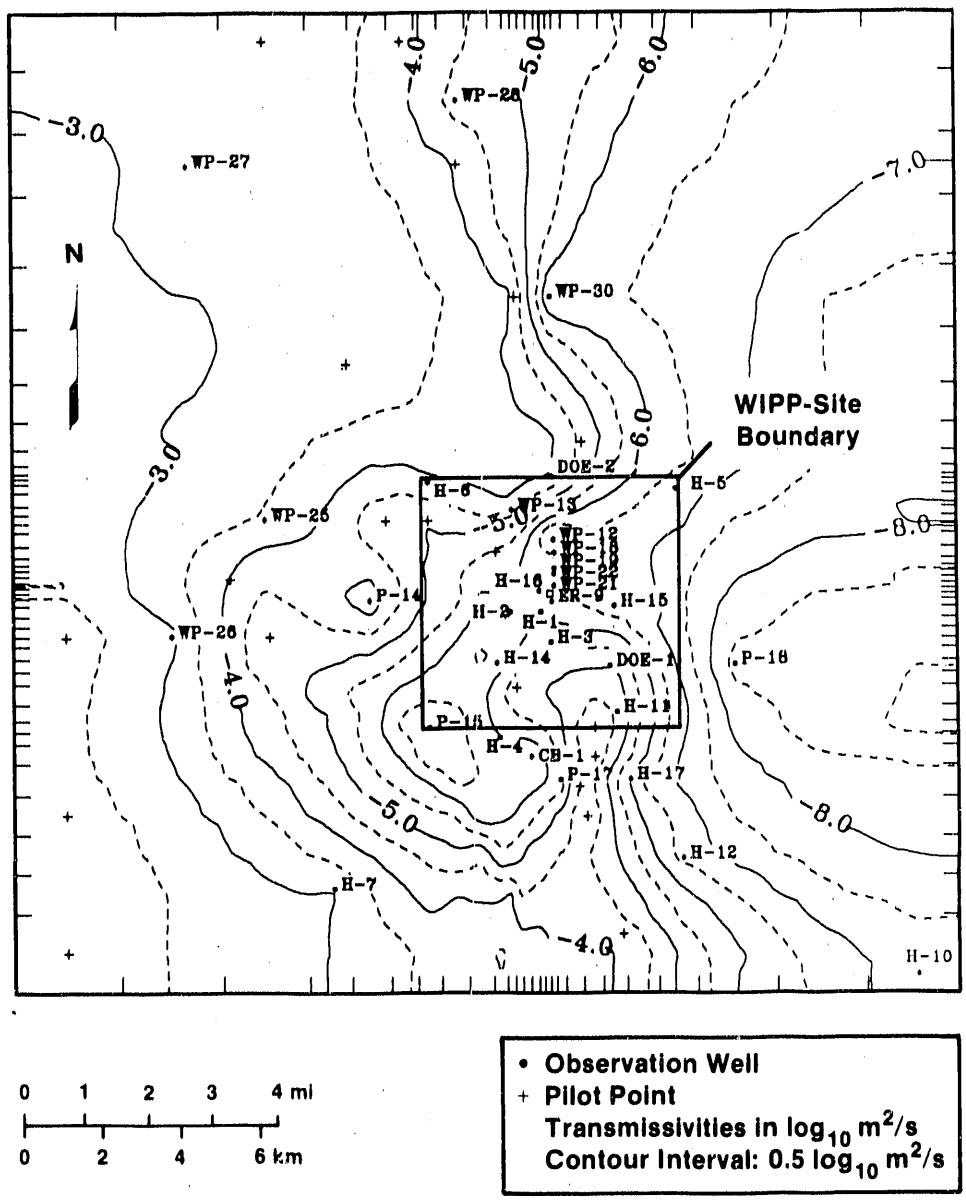

Figure 4-7. Distribution of Culebra transmissivities, as estimated by LaVenue et al. (1988) and used by Lappin et al. (1989).

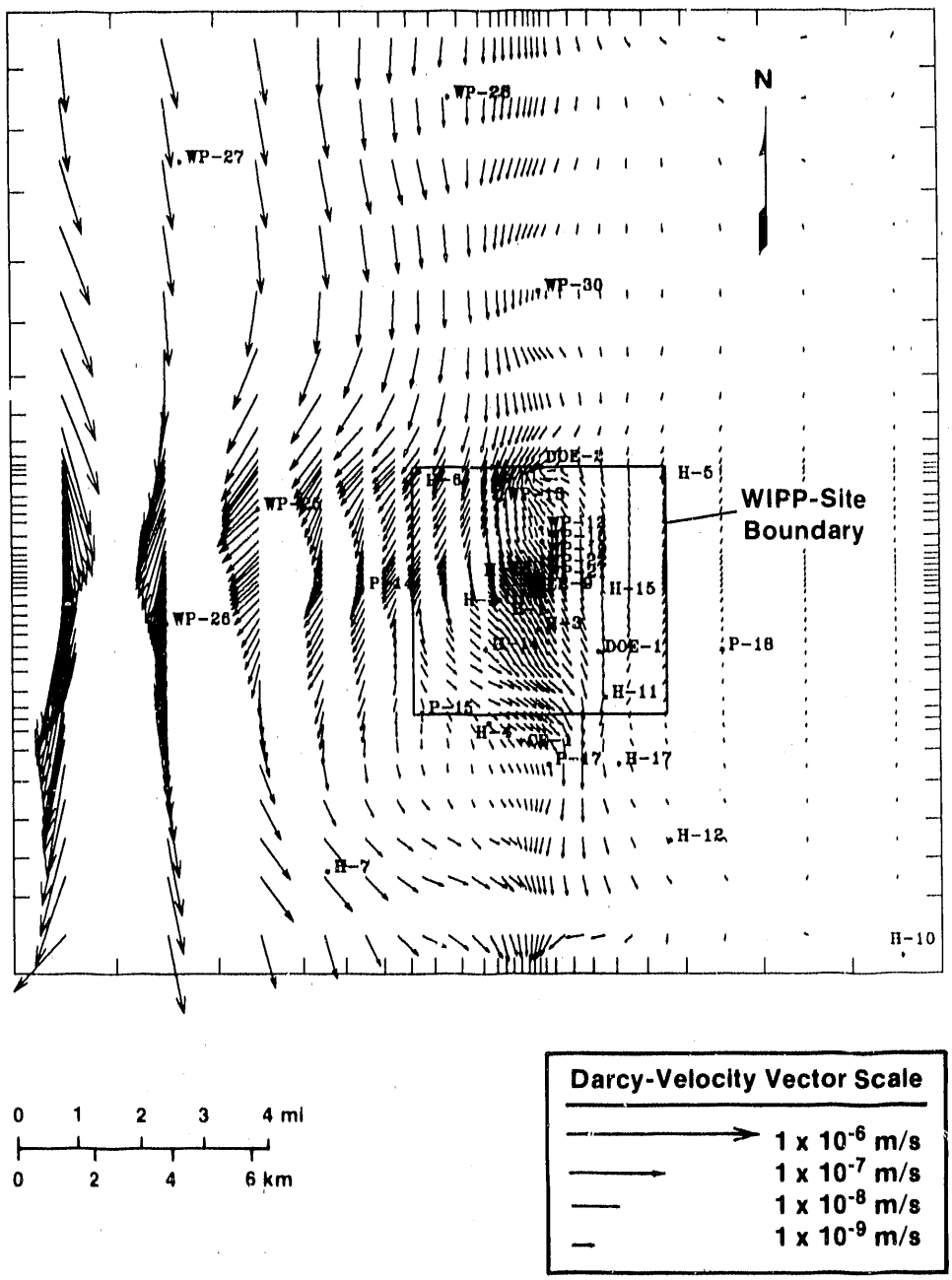

Figure 4-8. Simulated flow field (Darcy velocities) for the Culebra Dolomite under undisturbed conditions, as estimated by LaVenue et al. (1988) and used by Lappin et al. (1989).

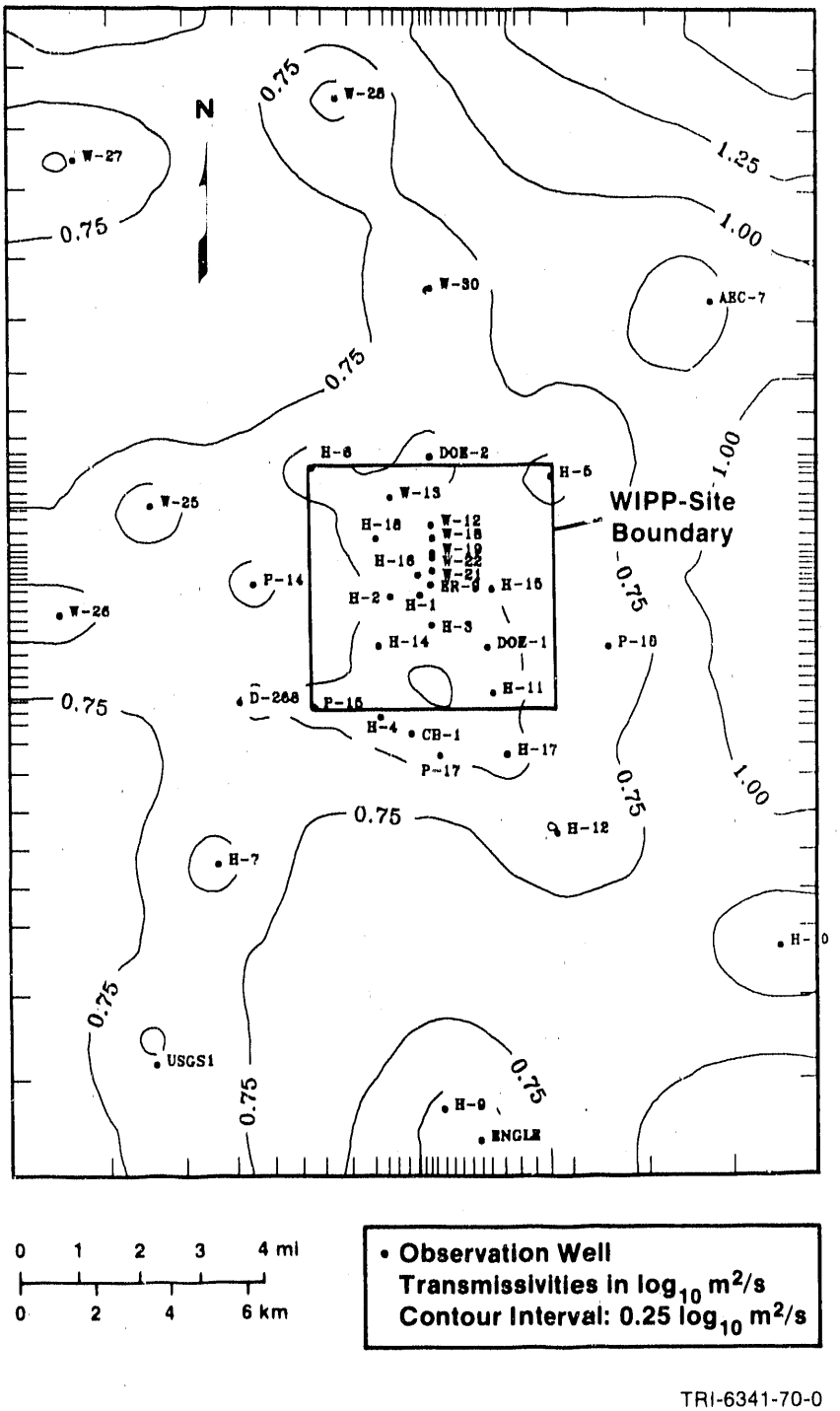

Figure 4-9. Initial kriged transmissivity estimation errors in Culebra transmissivity distribution used in this report (after LaVenue et al. (1990).

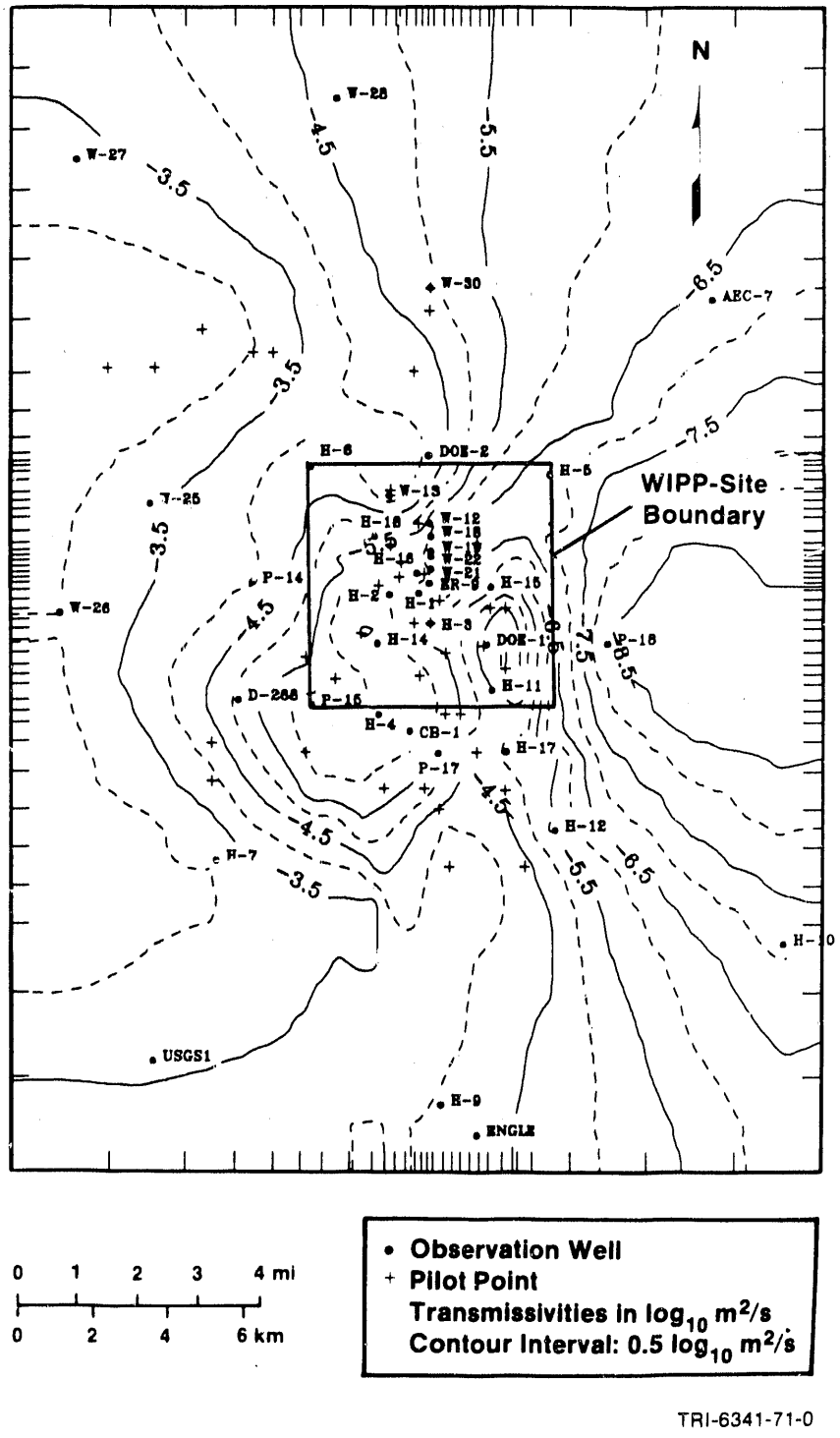

Figure 4-10. Distribution of Culebra transmissivities, as estimated by LaVenue et al. (1990) and used in this report (cf. Figure 4-7).

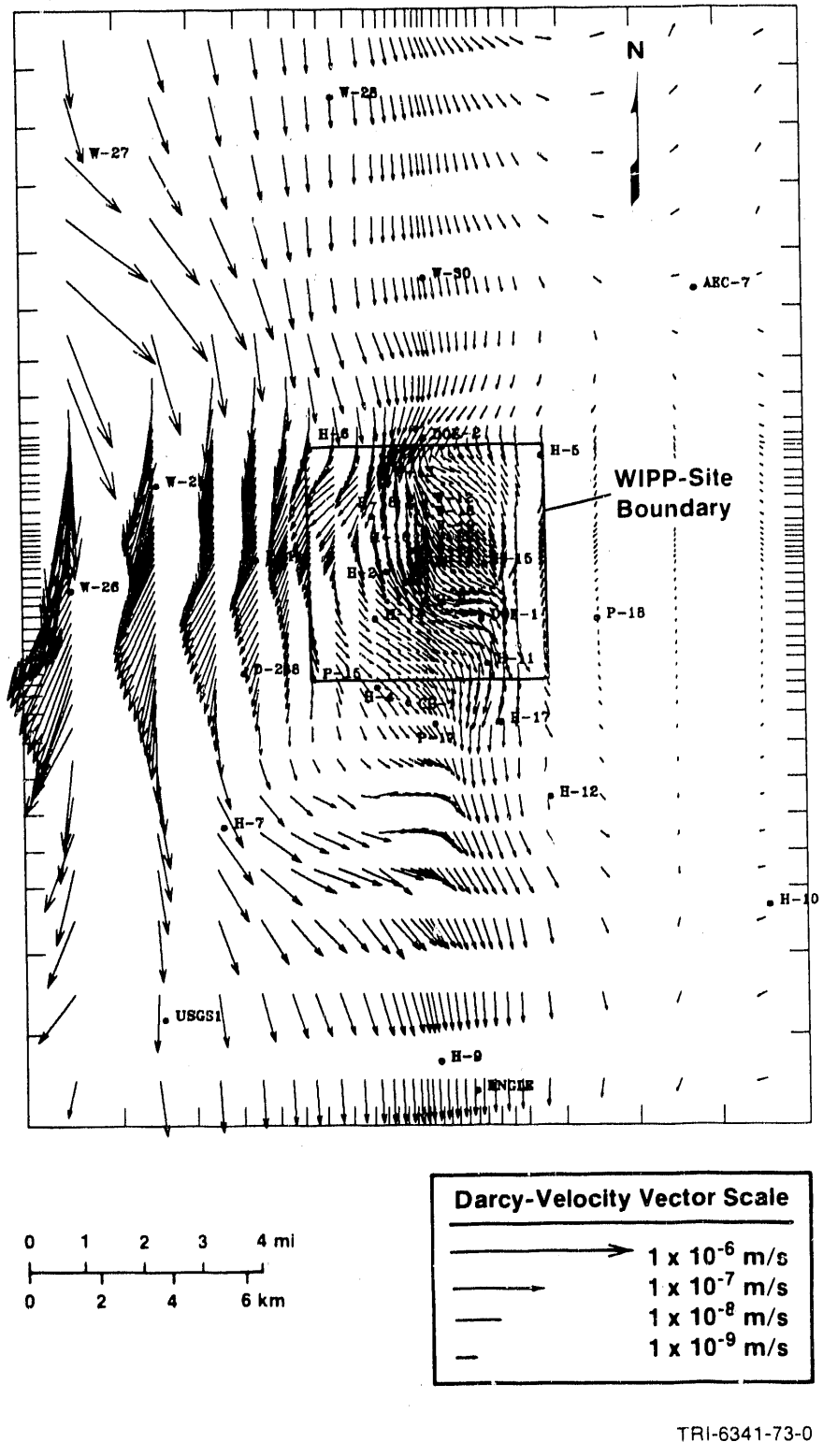

Figure 4-11. Simulated flow field (Darcy velocities) for the Culebra Dolomite under undisturbed conditions, as estimated by LaVenue et al. (1990) and used in this report (cf. Figure 4-8).

generally north to south, flow directions near the center of the site are more easterly in the revised model (Figures 4-2 and 4-11) than in the model calibration of LaVenue et al. (1988) (Figures 4-2 and 4-8). In addition, the magnitudes of the Darcy velocities differ slightly at the intrusion borehole and stock well in the two series of calculations. Culebra Darcy velocities in the calculations reported here are 1.97×10^{-9} m/s at the intrusion well and 2.06×10^{-9} m/s at the stock well (Table 4-6). Analogous velocities in the calibration of LaVenue et al. (1988) were 9.36×10^{-10} m/s at the intrusion well and 2.18×10^{-9} m/s at the stock well.

4.2.4.2 Culebra Transport Parameters. All Culebra transport parameters presented by Lappin et al. (1989) remained unchanged, with the exception of the stock-well location, the Darcy velocity, and the free-water diffusivities of the contaminants. Travel-path and stock-well locations are discussed in Section 4.3.2. As noted above, the new calibrated ground-water-flow model of the Culebra Dolomite (LaVenue et al., 1990) has resulted in a revised Darcy-velocity distribution. Based on this revised distribution, an average Darcy-velocity of 1.87×10^{-9} m/s (Table 4-6) is used for the transport simulations.

The revised Case-II transport simulations use species-specific diffusion coefficients for each member of a radionuclide chain (Table 4-7). Lappin et al. (1989, Table E-6) used uniform radionuclide free-water diffusion coefficients of 1×10^{-6} cm^2/s for Case IIA and 5×10^{-7} cm^2/s for Case IIC. A single diffusion coefficient was necessary in their calculations, because SWIFT II could not handle species-specific diffusion coefficients at that time. Lappin et al. (1989) discussed the range of diffusion-coefficient values reported in the literature for each radionuclide. An arithmetic mean of the reported range was selected as the base-case value (Table 4-7). For Ra and Pb, which have only a single value, the lower end of the range was assumed to be zero in order to compute a mean or base-case value. These estimates of base-case values for Case IIA' are assumed to include some salinity effects. For the degraded transport properties for Case IIC', the base-case value is reduced by a factor of two to account for greater salinity effects and other uncertainties in estimating the diffusion coefficient. In general, the species-specific coefficients used here are slightly higher than those used by Lappin et al. (1989).

4.3 Post-Plugging Release to the Culebra Dolomite

4.3.1 Fluid and Waste Release to the Culebra Dolomite

Figure 4-12 contrasts the flow rates to the Culebra Dolomite for Cases IIA' and IIC'. These flow rates are strongly influenced by the permeability of the degraded borehole plug. In both cases, the borehole plugs are assumed to hold their initial permeabilities for 75 years after emplacement, and then to degrade continuously during the next 75 years to a higher permeability appropriate for a rubble-filled borehole (Section 4.2.2). For Case IIA' this permeability is assumed to be 10^{-12} m^2, for Case IIC', 10^{-11} m^2 (Table 4-2). The flow rate during the first 75 years is more than five orders of magnitude less than the flow rate corresponding to the end of plug degradation. Because fluid release during the undegraded lifetime of the plugs is insignificant (~2 L), calculations using SWIFT II begin at a time corresponding to 75 years after plug emplacement, i.e., at the beginning of plug degradation. However, the time axis in the flow-rate and breakthrough-concentration plots is labeled

Table 4-6. Characteristics of the waste plume within the Culebra Dolomite from point of release to stock well (cf. Lappin et al., 1989, Table E-3)

	Case IIA'	Case IIC'
Distance from release to stagnation point		
- at end of borehole plug degradation	2.9 m	24.6 m
- at 10,000 years	2.3 m	2.7 m
Theoretical plume width at end of borehole plug degradation		
- near release point	18.2 m	154 m
- at WIPP-site boundary	19.7 m	167 m
- at stock well	17.4 m	148 m
Theoretical plume width at 10,000 years		
- near release point	14.3 m	17.1 m
- at WIPP-site boundary	15.5 m	18.5 m
- at stock well	13.7 m	16.3 m
Brine-reservoir discharge rate [Q_b]		
- at end of borehole plug degradation	7.31 m^3/yr	72.6 m^3/yr
- at 10,000 years	5.44 m^3/yr	6.78 m^3/yr
Salado brine-inflow rate [Q_s]	1.4 m^3/yr	1.4 m^3/yr
Total brine-injection rate to Culebra [Q_b+Q_s]		
- at end of borehole plug degradation	8.71 m^3/yr	74.0 m^3/yr
- at 10,000 years	6.84 m^3/yr	8.18 m^3/yr
Darcy velocity in Culebra		
- at release point	1.97×10^{-9} m/s	1.97×10^{-9} m/s
- at WIPP-site boundary	1.82×10^{-9} m/s	1.82×10^{-9} m/s
- at stock well	2.06×10^{-9} m/s	2.06×10^{-9} m/s
Average Darcy velocity in Culebra along transport pathway to stock well	1.87×10^{-9} m/s	1.87×10^{-9} m/s

Table 4-7. Free-water diffusion coefficients (cm^2/s) for radionuclides and stable lead, Case II (after Lappin et al., 1989, Table E-7)

Element	Case IIA'	Case IIC'	Range of Values in Literature(1)
Pu	1.7×10^{-6}	8.5×10^{-7}	4.8×10^{-7} - (3×10^{-6})
Am	1.8×10^{-6}	9.0×10^{-7}	5.3×10^{-7} - (3×10^{-6})
U	2.7×10^{-6}	1.4×10^{-6}	1.1×10^{-6} - $\underline{4.3 \times 10^{-6}}$
Np	1.8×10^{-6}	9.0×10^{-7}	5.2×10^{-7} - (3×10^{-6})
Ra	3.8×10^{-6}	1.9×10^{-6}	$\underline{7.5 \times 10^{-6}}$
Pb	4.0×10^{-6}	2.0×10^{-6}	$\underline{8 \times 10^{-6}}$
Th	1.0×10^{-6}	5.0×10^{-7}	5×10^{-7} - $\underline{1.53 \times 10^{-6}}$

(1) Data from estimated values of Brush (1988) and Higgo et al. (1987) (indicated by parentheses); values calculated from the Nernst expression by Li and Gregory (1974) (underlined); and measurements by Torstenfelt et al. (1982) (all others). Temperature dependence has not been considered for the recommended values. Literature values were further discussed by Lappin et al. (1989).

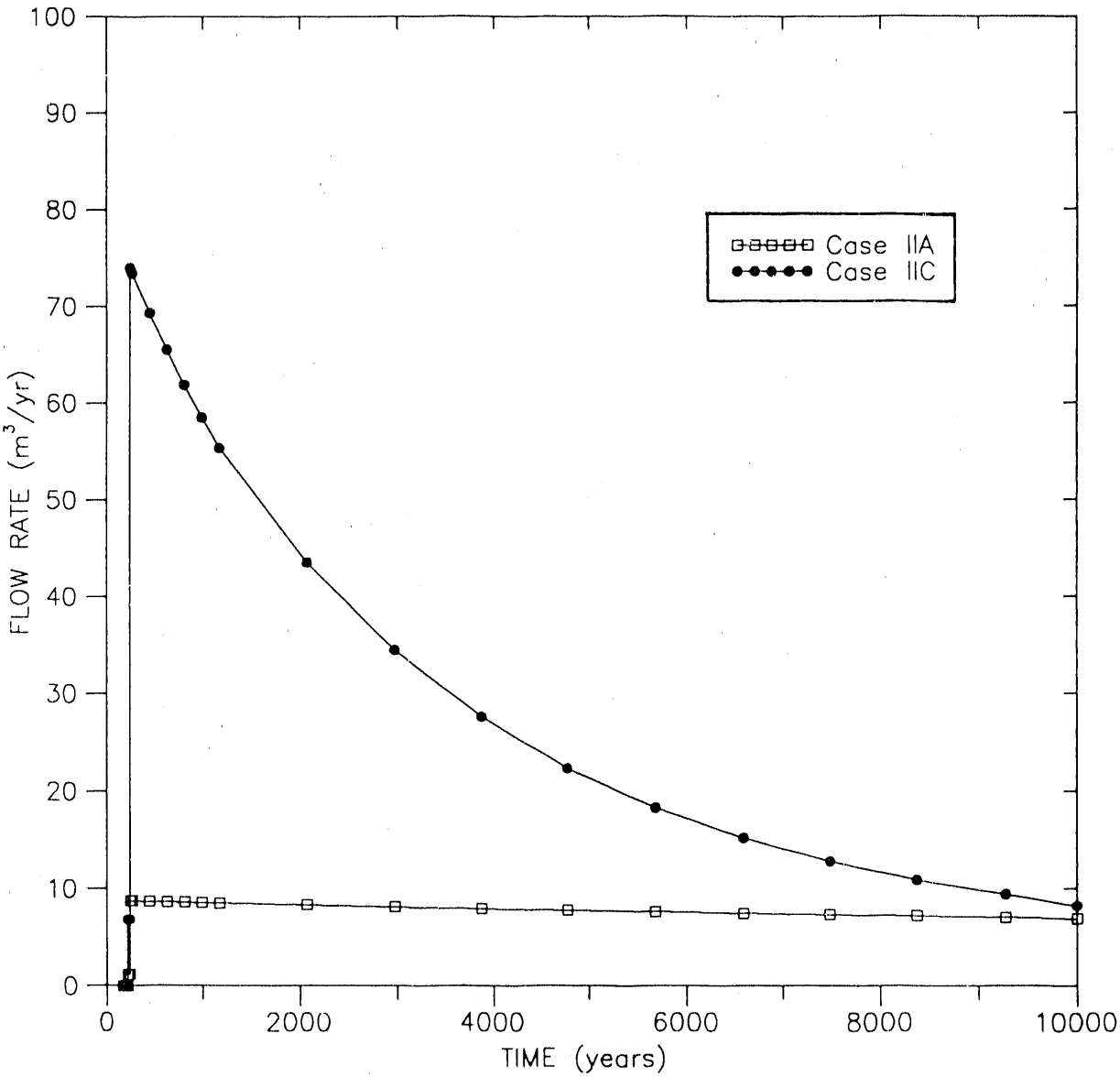

Figure 4-12. Flow rates to the Culebra Dolomite from the intrusion borehole, Cases IIA′ and IIC′.

with t = 0 corresponding to the repository decommissioning and the beginning of the 100-yr institutional-control period, i.e., 175 years prior to the beginning of the SWIFT II transport simulation.

The flow rate from the Castile Fm. increases during the period of borehole degradation and reaches a maximum at about the same time that the borehole permeability reaches its maximum value characterizing the final rubble-filled state of the borehole (Table 4-2). The maximum borehole permeability for Case IIC' bears a 10:1 ratio to the Case IIA' permeability, and the Case-IIC' maximum Castile flow rate bears a similar ratio (~9.9:1) to the Case-IIA' flow rate (Table 4-6). No decrease in borehole permeability is assumed during the 10,000-year period, although salt creep and precipitation may decrease this permeability with time. The rate of flow from the Castile Fm. (the brine-reservoir discharge rate), Q_b, decreases slightly with time in Case IIA', from a high of 7.31 m^3/yr at 250 years (150 years after plug emplacement) to a low of 5.44 m^3/yr at 10,000 years (Table 4-6). The Castile brine-flow rate for Case IIC' decreases from 72.6 m^3/yr at 250 years to 6.78 m^3/yr at 10,000 years. The total fluid discharge rate from the intrusion borehole to the Culebra Dolomite is the sum of the flow rate from the brine reservoir, Q_b, and the flow rate from the Salado brine inflow, Q_s. For both cases, the flow rate from the Salado Fm. is constant at 1.4 m^3/yr (Section 4.2.3).

Stagnation-point distance and plume width near the release point are greatest when the brine-reservoir discharge rate reaches its maximum, 150 years after plug emplacement (Table 4-6). Even for the high Case-IIC' discharge rates, stagnation-point distance, 24.6 m, and plume width near the release point, 154 m, are small compared with the transport distances of interest, 3610 m to the site boundary and 5960 m to the stock well. This supports the assumption (Section 4.1.2) that the disturbance of the steady-state Culebra flow field caused by brine injection at the release point can be considered negligible for the present calculations.

For Case IIC', brine-reservoir depressurization becomes evident 150 years after plug emplacement (250 years in Figure 4-12). For Case IIA', depressurization is minimal, and at 10,000 years, the total brine-injection rate ($Q_b + Q_s$) into the Culebra Dolomite has only decreased to 79% of its maximum value. For Case IIC', however, depressurization effects are more substantial, and at 10,000 years, the rate is only 11% of its maximum value (Table 4-6).

The numerical implementation of the coupling of the brine reservoir and the Culebra Dolomite assumes that all flow enters the Culebra and that no fluid is released to the ground surface. The maximum pressure-build-up values simulated at the borehole location in the Culebra Dolomite are 0.003 MPa for Case IIA' and 0.019 MPa for Case IIC'. This pressure increase, which is small relative to the 1.5-MPa pressure increase at Culebra depth that that would be required to drive brine to the surface, confirms that there would be no flow to the ground surface for the brine-reservoir, Culebra, and borehole properties used in the Case-II' simulations.

In Case IIA', brine flowing up the borehole from the Castile Fm. and brine inflow from the Salado Fm. are assumed to mix within the waste panel, bringing the concentration of dissolved radionuclides up to the assigned solubility limit of 2.4×10^{-7} kg/kg, with the exception of ^{241}Am (cf. Table 4-4). Radionuclides at these concentrations in concentrated brines are then released

through the intrusion borehole to the Culebra Dolomite. Lead is estimated to be less soluble in Culebra ground waters (5.4×10^{-5} kg/kg) than in concentrated brines (1.16×10^{-4} kg/kg) (Table 4-4). Therefore, input concentrations of lead to the two-dimensional model grid are controlled by the solubility of lead in Culebra ground waters. The main factor keeping source concentrations constant in Case IIA' is the lack of inventory depletion; i.e., neither radionuclides nor stable Pb are depleted from the panel inventory after 10,000 years of flow, except ^{241}Am. Table 4-8 presents the times of source depletion for Cases IIA' and IIC'. Decay reduces source concentration at the release point for some of the radionuclides during the 10,000-year period.

Like Case IIA', Case IIC' assumes that Castile brines penetrate into and mix within the waste panel. However, radionuclide solubilities in Case IIC' are assumed to be two orders of magnitude higher than in Case IIA' (Table 4-4). For waste constituents having sufficient mass to saturate the total fluid volume contained in one panel, the initial concentration of dissolved waste in the brine is the specified degraded solubility limit of 2.4×10^{-5} kg/kg (10^{-4} M) for radionuclides and 1.16×10^{-4} kg/kg for stable lead. For waste constituents not having sufficient mass to reach saturation, the initial concentration of dissolved radionuclide is the available radionuclide mass divided by the fluid volume contained in one panel. Subsequent concentrations in the waste panel, which are assumed to be laterally uniform, are reduced by mass discharge to the borehole and by radioactive decay. The input concentration to the Culebra Dolomite for stable lead is controlled by its solubility in Culebra ground waters (5.4×10^{-5} kg/kg). The use here of a solubility based on the relatively fresh Culebra formation fluids recognizes the dilution of brine that occurs in the Culebra Dolomite. Dissolved solids in the brine are subject to the same lateral-dispersion processes that affect contaminants. Therefore, lateral dispersion will reduce brine concentrations by about an order of magnitude near the borehole, with the effect increasing with distance down the transport pathway, in a manner similar to the contaminant behavior discussed in Section 4.3.3.

In summary, in Case IIA', contaminated brine enters the Culebra Dolomite at a rate $Q_b + Q_s$ that varies slightly over 10,000-year simulation time (from 8.71 to 6.84 m^3/yr; see Table 4-6), and the concentration of most of the radionuclides near the intrusion well remains constant for 10,000 years at the "expected" solubility limit of 2.4×10^{-7} kg/kg (10^{-6} M). In Case IIC', contaminated brine from the breach borehole enters the Culebra Dolomite at a rate $Q_b + Q_s$ that varies significantly over the 10,000 year simulation time (from 74.0 to 8.18 m^3/yr). In Case IIC', the concentration of contaminants entering the Culebra Dolomite varies greatly with time for some species, as a result of source depletion and radioactive decay.

4.3.2 Transport Pathways and Particle Travel Times in the Culebra

With the Darcy-velocity distribution presented in Figure 4-11, a particle-tracking code was used to define the flow path between the release point in the center of the southwestern waste panel and the stock well. The location of the stock well was selected based on two constraints: the well was assumed to be on the flow path from the breach borehole and to be located in an area where the water is potentially stock-potable. Lappin et al. (1989) discussed the method used to define the stock-well location. The intrusion-borehole and stock-well locations (Tables 4-2 and 4-5) are illustrated, along with the

Table 4-8. Times of source depletion, times to reach peak concentrations, and calculated peak concentrations, all at site boundary and stock well

Species	CASE IIA' Site Boundary			CASE IIC' Site Boundary			CASE IIC' Stock Well	
	t_{sd} (yr)	t_p (yr)	C_p (kg/kg)	t_{sd} (yr)	t_p (yr)	C_p (kg/kg)	t_p (yr)	C_p (kg/kg)
^{241}Am	1.85×10^{3}	na	na	0	3.53×10^{3}	5.82×10^{-16}	na	na
^{237}Np	$>1 \times 10^{4}$	1×10^{4}	2.09x10-14	0	1.49×10^{3}	1.57×10^{-8}	2.91×10^{3}	5.47×10^{-9}
^{210}Pb	na	na	na	na	1×10^{4}	9.60×10^{-14}	1×10^{4}	7.80×10^{-14}
^{239}Pu	$>1 \times 10^{4}$	na	na	818	1×10^{4}	1.51×10^{-8}	1×10^{4}	6.54×10^{-10}
^{240}Pu	$>1 \times 10^{4}$	na	na	266	8.29×10^{3}	5.30×10^{-10}	1×10^{4}	2.34×10^{-11}
^{226}Ra	na	1×10^{4}	1.58×10^{-15}	na	1×10^{4}	7.66×10^{-12}	1×10^{4}	6.12×10^{-12}
^{229}Th	na	na	na	na	5.52×10^{3}	2.69×10^{-11}	1×10^{4}	1.33×10^{-11}
^{230}Th	na	na	na	na	9.74×10^{3}	8.11×10^{-12}	1×10^{4}	4.37×10^{-12}
^{233}U	$>1 \times 10^{4}$	1×10^{4}	1.05×10^{-15}	198	1.41×10^{3}	4.29×10^{-8}	3.39×10^{3}	1.24×10^{-8}
^{234}U	$>1 \times 10^{4}$	1×10^{4}	1.01×10^{-15}	250	1.40×10^{3}	1.39×10^{-8}	3.38×10^{3}	4.00×10^{-9}
^{236}U	$>1 \times 10^{4}$	1×10^{4}	1.19×10^{-15}	0	6.08×10^{3}	6.86×10^{-9}	1×10^{4}	3.47×10^{-9}
Stable Pb	1×10^{4}	1×10^{4}	1.32×10^{-8}	4.52×10^{-12}	2.08×10^{3}	5.81×10^{-6}	2.40×10^{3}	3.31×10^{-6}

t_{sd} = Time of source depletion, at which there is insufficient mass to keep the concentration at the solubility limit. If t_{sd} is zero, the solubility limit could not be attained because of inadequate initial mass.

t_p = Time to reach maximum calculated concentration. In most cases, $t_p = 10^4$ years, and this is not a true peak concentration.

C_p = Concentration observed at t_p.

na Not applicable. When used for a parent nuclide, the parent was not simulated. When used for a daughter nuclide, the nuclide was not originally present in the repository. When used for t_p and C_p, the concentrations were insignificant (i.e., $<10^{-16}$ kg/kg).

transport path in the Culebra Dolomite, in Figure 4-2. The travel-path lengths from the breach borehole to the WIPP-site boundary and the stock well are 3610 m and 5960 m. (These distances were 2860 m and 4840 m in the work of Lappin et al. (1989).) The straight-line distance between the stock well and the southern boundary of the southwestern waste panel where intersected by the travel path is 5040 m. The calculated particle travel times from the intrusion borehole to the WIPP-site boundary is 10,480 years; to the stock well, 16,140 years, assuming a porous-medium equivalent transport porosity of 0.16. Travel time has been discussed in more detail in Section 4.1.2.

The travel path to the stock well is longer than that of Lappin et al. (1989) as a result of the revised calibrated ground-water-flow model. In particular, model calibration to the H-11 multipad pumping test has moved the travel path eastward and the location of the stock well eastward and southward (Figure 4-2). However, calculated particle travel times from the center of the southwestern waste panel to the stock well, assuming porous-medium behavior, have remained about the same (15,400 years in Lappin et al. (1989) versus 16,140 years here). The combination of longer travel-path length and higher Darcy velocities has resulted in similar particle travel times.

4.3.3 Contaminant Transport for Case IIA'

The parameter values selected for Case IIA' are considered to be most representative of the expected behavior of the repository-geosphere system under breach conditions. No new information about the properties of Castile brine reservoirs, hydraulic properties of WIPP waste, plugged boreholes, or the Culebra Dolomite has become available since the work of Lappin et al. (1989). The Case-IIA' analysis has been updated, however, by directly including lateral dispersion, species-specific diffusion, and a revised Culebra flow field from the recently recalibrated model of LaVenue et al. (1990). The results of this updated analysis show that contaminant transport to the stock well is minimal in Case IIA', with the most mobile species showing only minor concentrations there at 10,000 years.

Figure 4-13 shows a spatial profile for stable Pb concentrations at the centerline of the contaminant plume. As a result of lateral dispersion, this plot shows reduced centerline concentrations relative to the analogous results of Lappin et al. (1989). Near the point of release, the centerline profile evidences a concentration reduction by a factor of 10, relative to the solubility-limited concentration (5.4×10^{-5} kg/kg) present at the intrusion well. Lappin et al. (1989, Figure 7-3) reported that concentrations near the point of release were approximately equal to the solubility limit.

For the range of matrix-diffusion parameters they chose, Reeves et al. (1987) found that single-porosity behavior approximately characterizes contaminant transport in the Culebra Dolomite for transport distances of more than a few kilometers, with the total effective porosity chosen as the sum of fracture and matrix porosities. If this point were generally valid, it would represent a considerable simplification in numerical modeling of far-field transport, because it would allow use of a single-porosity formalism. However, based on the updated information presented in Table 4-7, the present analysis for Pb uses a free-water diffusivity that is a factor of twenty lower than that used by Reeves et al. (1987). Therefore, it is of interest to see whether the present representative-parameter case, Case IIA', preserves the single-porosity behavior observed by Reeves et al. Figure 4-13 displays

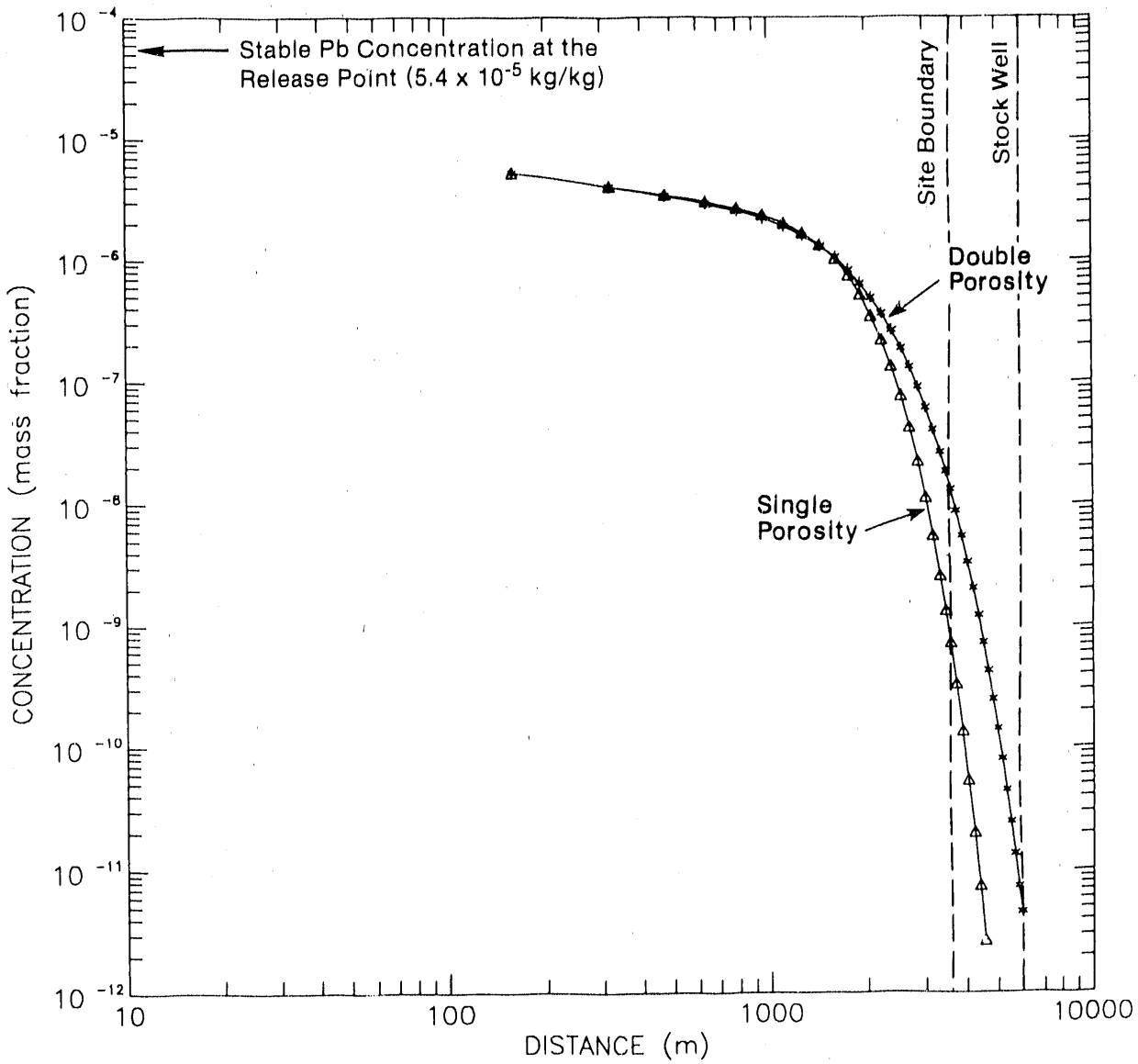

Figure 4-13. Concentration profiles along the plume centerline for stable Pb at 10,000 Years, Case IIA' (cf. Lappin et al., 1989, Figure 7-3). Dashed vertical lines show the distance to the projected site boundary and the hypothetical stock well.

profiles for stable Pb calculated using single-porosity (i.e., transport porosity equal to the sum of fracture and matrix porosities) and double-porosity assumptions and values (Table 4-5). The single-porosity analysis shows relatively good agreement with the double-porosity analysis in the first segment of the travel path, roughly 2000 m, where the rock has been exposed to contaminants for a sufficiently long period that the matrix is fully participating, i.e., radionuclide concentration within the matrix blocks is nearly uniform and similar to concentrations within the fractures. Along the second segment of the travel path, contaminated fluid containing radionuclides at relatively high concentrations is present in the fractures. There has not yet been enough time for matrix diffusion to occur to the same extent as in the first segment. Therefore, although concentrations decrease downstream, contaminant transport is dominated by the fractures, resulting in higher concentrations than in the single-porosity simulation. At the WIPP-site boundary, the double-porosity calculation yields ~10^{-8} kg/kg at 10,000 years, whereas the single-porosity prediction is nonconservatively low by about one order of magnitude, ~10^{-9} kg/kg). Thus, at the site boundary and using expected Culebra properties, use of a-porosity formalism increases estimated Pb concentrations at 10,000 years by about one order of magnitude.

Figures 4-14 through 4-17 show spatial profiles of centerline concentrations for the ^{240}Pu, ^{239}Pu, ^{238}Pu, and ^{241}Am chains for the Case-IIA' simulations. Because of its short half life (87.7 years), the parent ^{238}Pu rapidly converts to ^{234}U and is not present in concentrations greater than the minimum 10^{-16} kg/kg shown in Figure 4-16. As in the case of stable Pb, centerline concentrations show the effect of lateral dispersion. Typical of many of the radionuclide concentrations near the point of release, the spatial profile of ^{234}U shows a reduction factor of 15 relative to the solubility-limited concentration (2.4 x 10^{-7} kg/kg) of the injected fluid, within approximately 150 m of the intrusion well (Figure 4-16). This factor is close to that observed for stable Pb.

Table 4-8 summarizes the calculated concentrations at the site boundary for Case IIA'. At 10,000 years, concentrations for all radionuclides are very low; all are near or below the 10^{-16} kg/kg level. Only stable lead is present at higher concentrations (1.3 x 10^{-8} kg/kg). Stable lead is the only contaminant to reach the stock well in any concentration (5 x 10^{-12} kg/kg) greater than 10^{-16} kg/kg within 10,000 years (Figures 4-13 through 4-17).

Table 4-9 gives calculated integrated radionuclide releases at both the WIPP-site boundary (projected land-withdrawal boundary) and stock well for Case IIA'. The integrated release includes both spatial integration over the full width of the contaminant plume and temporal integration over 10,000 years at the selected location. Table 4-9 indicates that, in terms of the normalized releases defined in 40 CFR 191 (EPA, 1985), ^{226}Ra and ^{210}Pb register the largest releases (IR/RL ~ 10^{-6}). The resulting normalized sums of all radionuclides are 1.7 x 10^{-6} at the site boundary and 1.9 x 10^{-10} at the stock well (neglecting cuttings brought directly to the surface during drilling). These sums are negligible in comparison with the regulatory constraint that the sum of normalized releases of all radionuclides of interest must be less than or equal to 1.0 for releases with probabilities >0.1.

Evaluating the differences between the present Case-IIA' analysis and Case IIA of Lappin et al. (1989) provides additional insight into transport

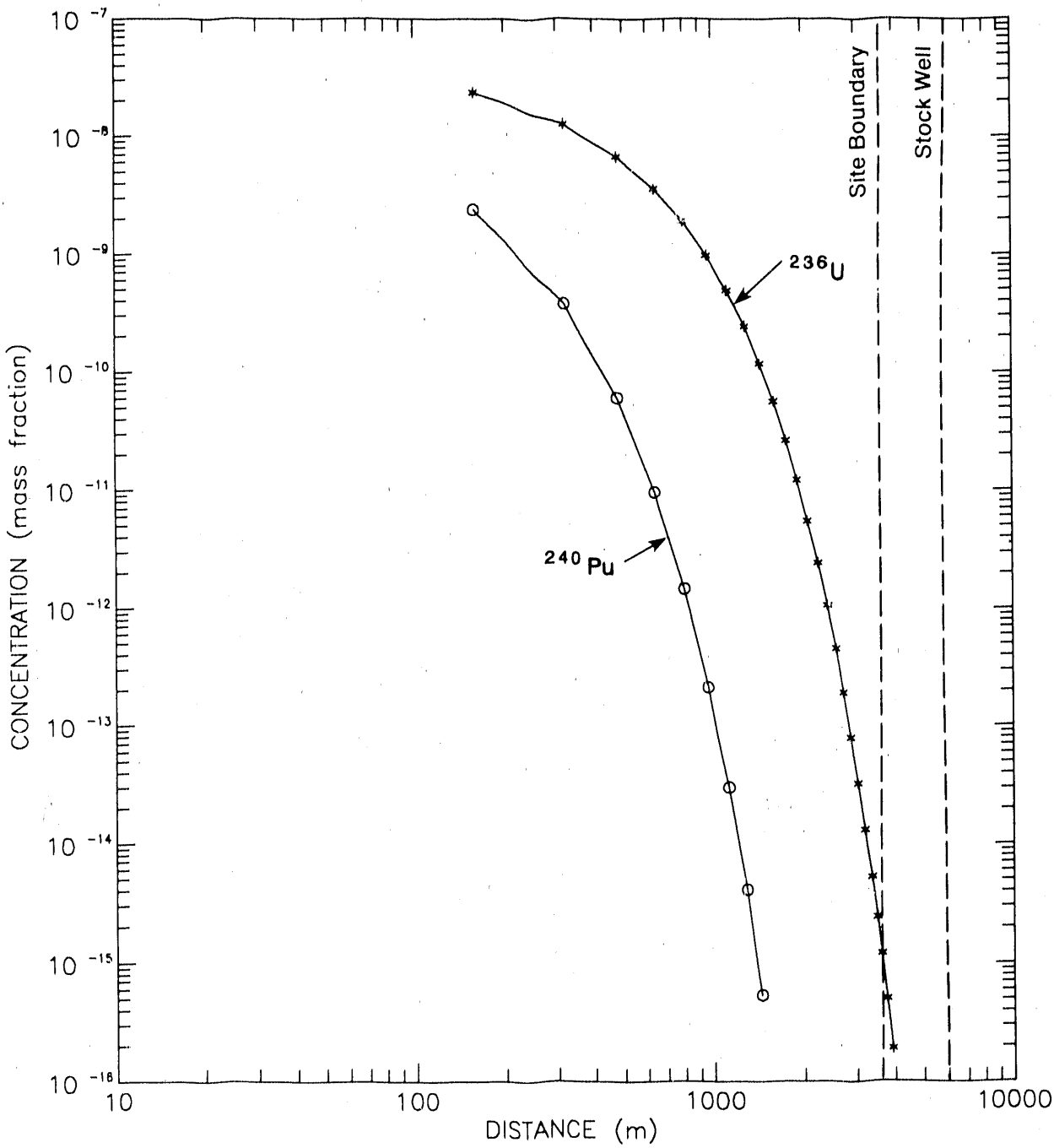

Figure 4-14. Concentration profiles along the plume centerline for the ^{240}Pu decay chain at 10,000 years, Case IIA'. Dashed vertical lines show the distance to the projected site boundary and the hypothetical stock well.

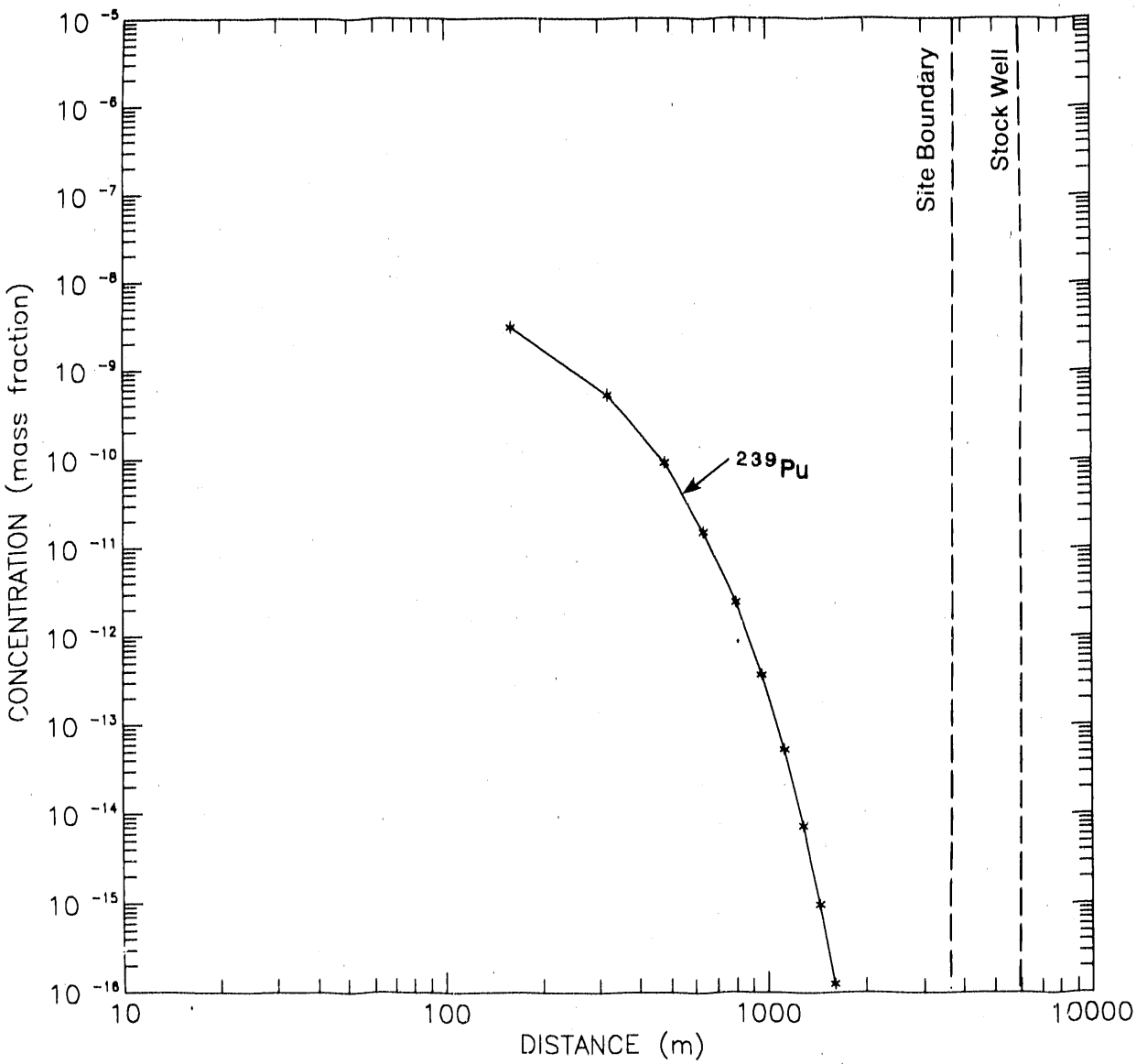

Figure 4-15. Concentration profiles along the plume centerline for the ^{239}Pu decay chain at 10,000 years, Case IIA'. Dashed vertical lines show the distance to the projected site boundary and the hypothetical stock well.

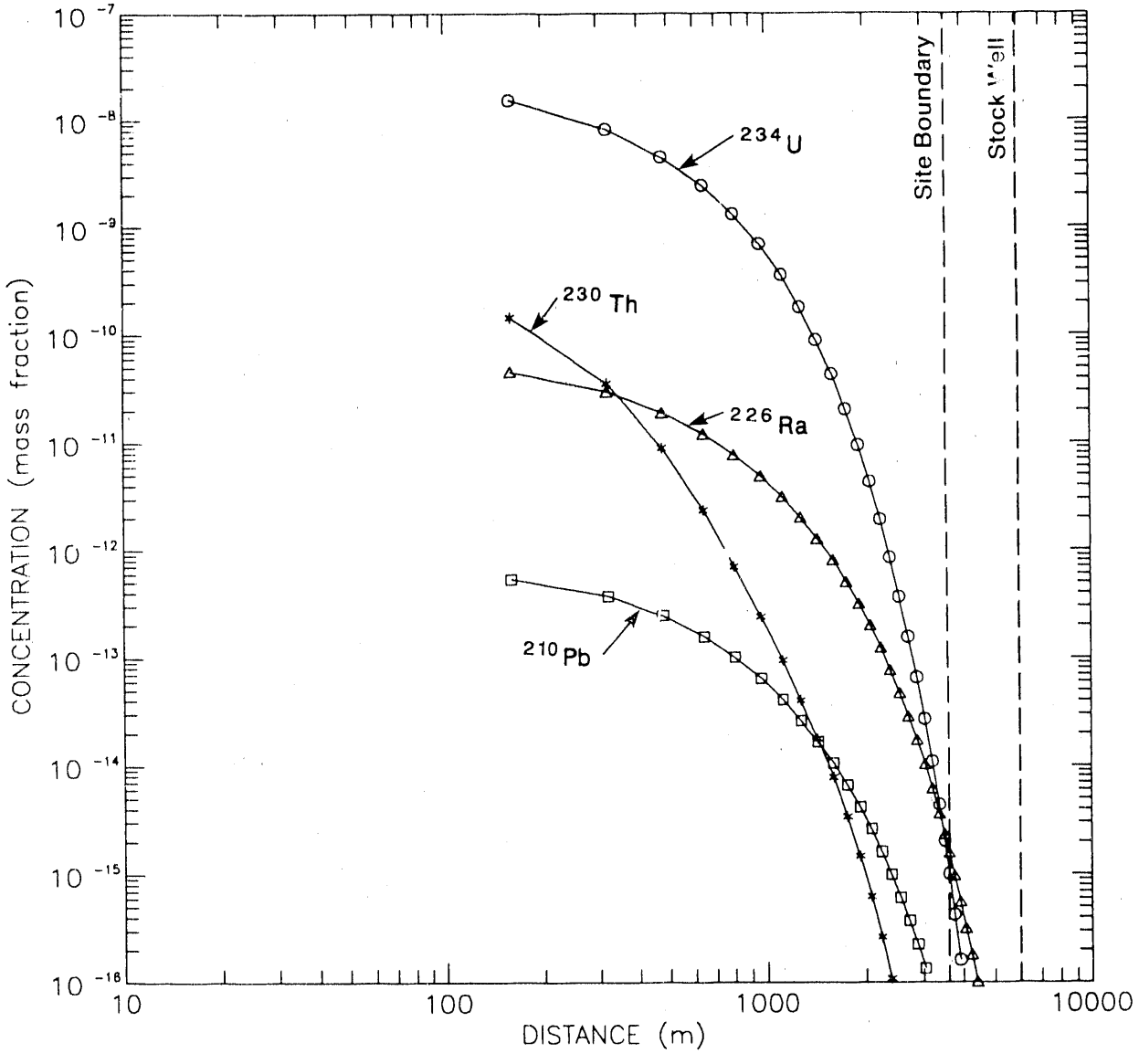

Figure 4-16. Concentration profiles along the plume centerline for the ^{238}Pu decay chain at 10,000 years, Case IIA' (cf. Lappin et al., 1989, Figure 7-4). Dashed vertical lines show the distance to the projected site boundary and the hypothetical stock well.

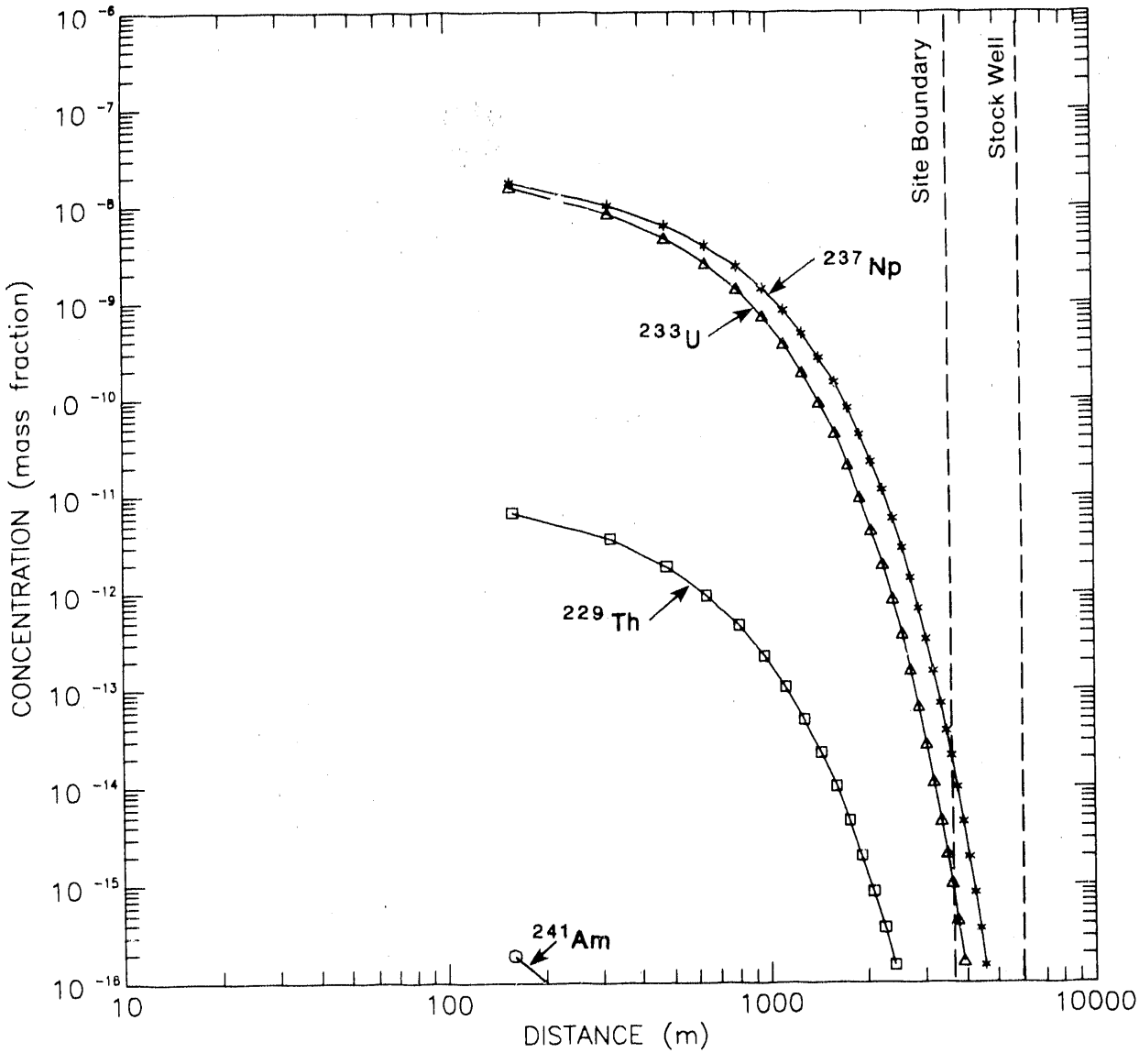

Figure 4-17. Concentration profiles along the plume centerline for the ^{241}Am decay chain at 10,000 years, Case IIA'. Dashed vertical lines show the distance to the projected site boundary and the hypothetical stock well.

Table 4-9. Normalized integrated release at site boundary and stock well at 10,000 years, Case IIA' (cf. DOE, 1989a, Table 5.62)

Radionuclide	Release Limit* (Ci) (RL)	WIPP-Site Boundary Integrated Release (IR) (kg)	WIPP-Site Boundary Integrated Release (IR) (Ci)	WIPP-Site Boundary IR(Ci) /RL**	Stock Well Integrated Release (IR) (kg)	Stock Well Integrated Release (IR) (Ci)	Stock Well IR(Ci) /RL**
^{240}Pu	660	-	-	$<1x10^{-13}$	-	-	$<1x10^{-13}$
^{236}U	660	$2.85x10^{-7}$	$1.84x10^{-8}$	$2.79x10^{-11}$	-	-	$<1x10^{-13}$
^{239}Pu	660	-	-	$<1x10^{-13}$	-	-	$<1x10^{-13}$
^{238}Pu	660	na	na	na	na	na	na
^{234}U	660	$2.44x10^{-7}$	$1.53x10^{-6}$	$2.31x10^{-9}$	-	-	$<1x10^{-13}$
^{230}Th	66	$1.89x10^{-11}$	$3.82x10^{-10}$	$5.78x10^{-12}$	-	-	$<1x10^{-13}$
^{226}Ra	660	$5.45x10^{-7}$	$5.39x10^{-4}$	$8.16x10^{-7}$	$6.19x10^{-11}$	$6.12x10^{-8}$	$9.28x10^{-11}$
^{210}Pb	660	$7.10x10^{-9}$	$5.42x10^{-4}$	$8.22x10^{-7}$	$8.05x10^{-13}$	$6.15x10^{-8}$	$9.32x10^{-11}$
^{241}Am	660	-	-	$<1x10^{-13}$	-	-	$<1x10^{-13}$
^{237}Np	660	$5.81x10^{-6}$	$4.10x10^{-6}$	$6.21x10^{-9}$	-	-	$<1x10^{-13}$
^{233}U	660	$2.53x10^{-7}$	$2.45x10^{-6}$	$3.71x10^{-9}$	-	-	$<1x10^{-13}$
^{229}Th	660	$2.76x10^{-11}$	$5.81x10^{-9}$	$8.81x10^{-12}$	-	-	$<1x10^{-13}$
			Sum:	$1.65x10^{-6}$		Sum:	$1.86x10^{-10}$

na means not applicable
* Calculated from Table 4-3 of this report and Table B-1 of the EPA (1985)
** Normalized integrated release, i.e., calculated integrated release (IR) divided by release limit (RL).

behavior within the Culebra under expected conditions. The largest difference is the significant reduction of centerline concentration that results from lateral dispersion that can be directly accounted for using the new two-dimensional transport-simulation approach. As noted above, comparing the present results with those of Lappin et al. (1989) indicates that lateral dispersion reduces centerline concentrations by about a factor of 10 for Case IIA'.

Another difference between this analysis and that of Lappin et al. (1989) is the use of species-specific diffusion coefficients. As discussed for the case of stable Pb, the distal segments of the concentration profiles show a substantial deviation between single- and double-porosity behavior, with a concentration difference of about one order of magnitude at the site boundary. This sensitivity to porosity effects implies a corresponding sensitivity to free-water diffusivity. However, the species-dependent diffusivities (Table 4-7) of this analysis assume only a maximum factor-of-3.8 variation from the Case-IIA value used by Lappin et al. (1989). Therefore, the impact of radionuclide-dependent diffusivities in Case IIA' should be less than the variation between single- and double-porosity behavior.

The last major difference between this analysis and that of Lappin et al. (1989) is the use of the revised flow field from the recently recalibrated model of LaVenue et al. (1990). The change in particle travel time for the present analysis is only 4.8% relative to that of Lappin et al. (1989), which used the previous flow field from LaVenue et al. (1988). Therefore, the change in stock-well location and Darcy velocities due to the recalibrated model of LaVenue et al. (1990) has relatively small impact on the Case-IIA' results. The dominant factor appears to be the implementation of the two-dimensional contaminant-transport methodology, which provides more realistic calculation of lateral dispersion.

4.3.4 Contaminant Transport for Case IIC'

Case IIC' uses a degraded set of parameters to characterize the repository-geosphere system under breach conditions. The simultaneous degradation of repository, borehole, and Culebra transport parameters used in Case IIC' is highly improbable. The approach here is to develop a deterministic "bounding" calculation, intended to lie largely outside the range of combinations of values that would be sampled randomly as part of a probabilistic calculation such as those required to evaluate compliance with 40 CFR 191. The limits on releases set by 40 CFR 191 vary with probability; the allowable normalized integrated release is 1.0 at probabilities >0.1 and 10.0 at probabilities between 0.001 and 0.1. No limit is set for releases with probabilities <0.001.

Like Case IIA', the Case-IIC' analysis has been modified to include lateral dispersion, species-specific diffusion, and the revised Culebra flow field. Borehole properties assigned for Case IIC' are listed in Table 4-2; repository parameters in Table 4-4; Culebra properties in Table 4-5; and free-water diffusion coefficients in Table 4-7. Resulting plume characteristics in the Culebra are summarized in Table 4-6.

4.3.4.1 Centerline Concentrations. This section describes contaminant concentrations along the centerline of the plume.

Stable Lead. Figures 4-18 and 4-19 show a spatial profile and stock-well breakthrough for stable Pb concentrations at the centerline of the contaminant plume. Both plots show reduced centerline concentrations relative to the results of Lappin et al. (1989), as a result of lateral dispersion. Near the point of release, i.e., within about 150 m of the injection well, the centerline profile (Figure 4-18) is reduced by a factor of 7.7 relative to the solubility-limited concentration (5.4×10^{-5} kg/kg) of the injected fluid. On a log-log scale, the double-porosity concentration profile shows a nearly linear decrease with distance. At the stock well, the breakthrough curve (Figure 4-19) shows a concentration of 1.5×10^{-6} kg/kg at 10,000 years, a reduction by a factor of 27 compared with the Case-IIC results of Lappin et al. (1989).

The breakthrough curve (Figure 4-19) has a new feature, a concentration peak at ~2,400 years. Many of the radionuclide breakthrough curves of Lappin et al. (1989) exhibit peaks as a result of inventory depletion. However, for stable Pb, the inventory does not deplete. The peak here is the result of a different effect. At early times, immediately following complete degradation of the borehole plug, the relatively large rate of release swells the plume width to 154 m. This wide plume provides some protection against lateral dispersion for contaminant concentrations at the plume centerline. When this maximum plume width reaches the stock well, it permits the centerline concentration there to reach its maximum value. Later reduction in plume width, resulting from brine-reservoir depressurization over time, permits more lateral dispersion and produces decreased centerline concentrations at late times in the absence of inventory depletion.

Figure 4-20 further illustrates the effect of lateral dispersion, showing calculated Pb concentration as it decreases from its centerline value at the stock well to about 4% of that value at a lateral distance of 950 m.

As discussed in Section 7.3.3 of Lappin et al. (1989), the degraded Culebra transport parameters used in Case IIC' (and Case IIC of the earlier report) diminish the effectiveness of the rock matrix in retarding the movement of contaminants. Therefore, one would expect a significant departure from a single-porosity transport calculation in which the rock matrix is assumed to be optimally effective. In order to provide this single- versus double-porosity comparison, a single porosity simulation was performed for stable lead using the degraded matrix-plus-fracture-porosity value of 0.07.

Both the centerline profile and the stock-well breakthrough plot (Figures 4-18 and 4-19) show a significant difference between the single- and double-porosity simulations. Figure 4-18 shows that an equivalent single-porosity calculation underestimates breakthrough concentration at the stock well at 10,000 years by almost three orders of magnitude relative to double-porosity calculations (calculated mass fractions of 3×10^{-9} and $\sim 1.5 \times 10^{-6}$). Comparing the areas under the two breakthrough curves in Figure 4-19 also illustrates that an equivalent single-porosity calculation for radionuclides would grossly underestimate integrated release at the stock well.

Figure 4-18 provides further insight into the large difference between single- and double-porosity simulations by focusing attention on the concentration maximum in the single-porosity simulation. This maximum, which has the same origin in both single-porosity and double-porosity calculations, breaks through at the stock well at about 2,400 years in the double-porosity

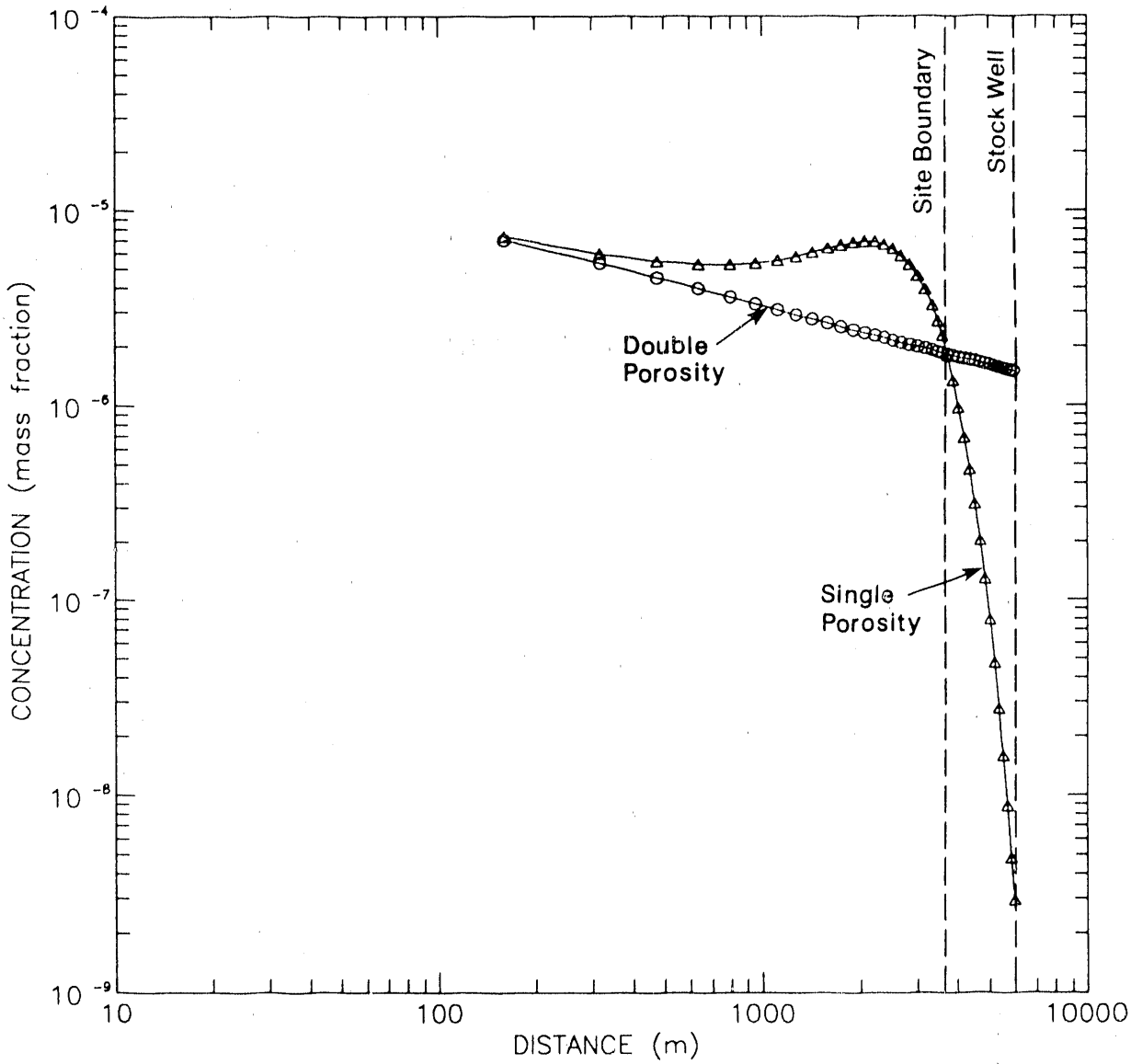

Figure 4-18. Concentration profiles along the plume centerline for stable Pb at 10,000 years, Case IIC' (cf. Lappin et al., 1989, Figure 7-15). Dashed vertical lines show the distance to the site boundary and the hypothetical stock well.

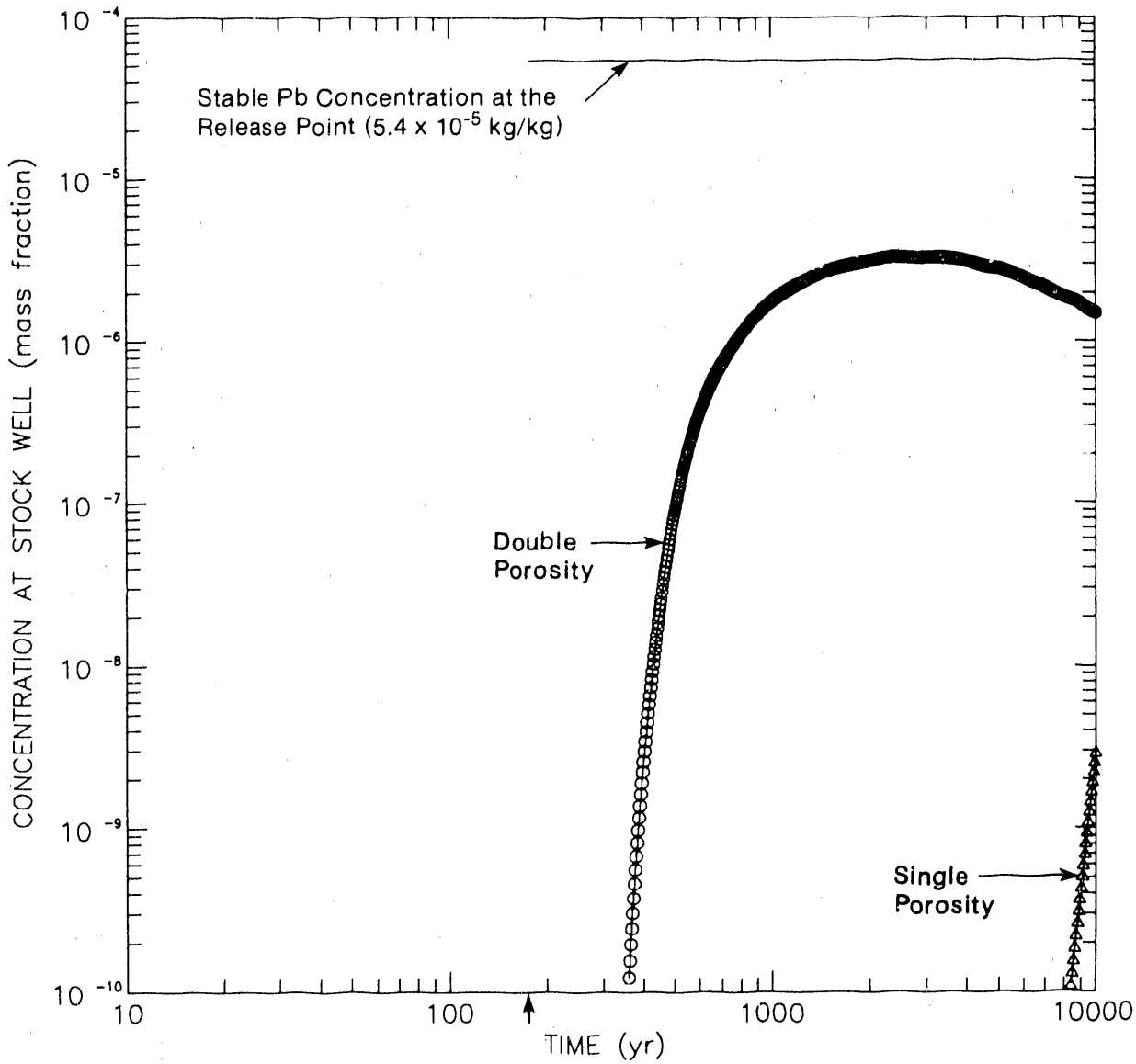

Figure 4-19. Breakthrough concentrations at stock well for stable Pb as a function of time, Case IIC' (cf. Lappin et al., 1989, Figure 7-16). The arrow on the horizontal axis indicates the starting time of the SWIFT-II calculation, 175 years after repository decommissioning.

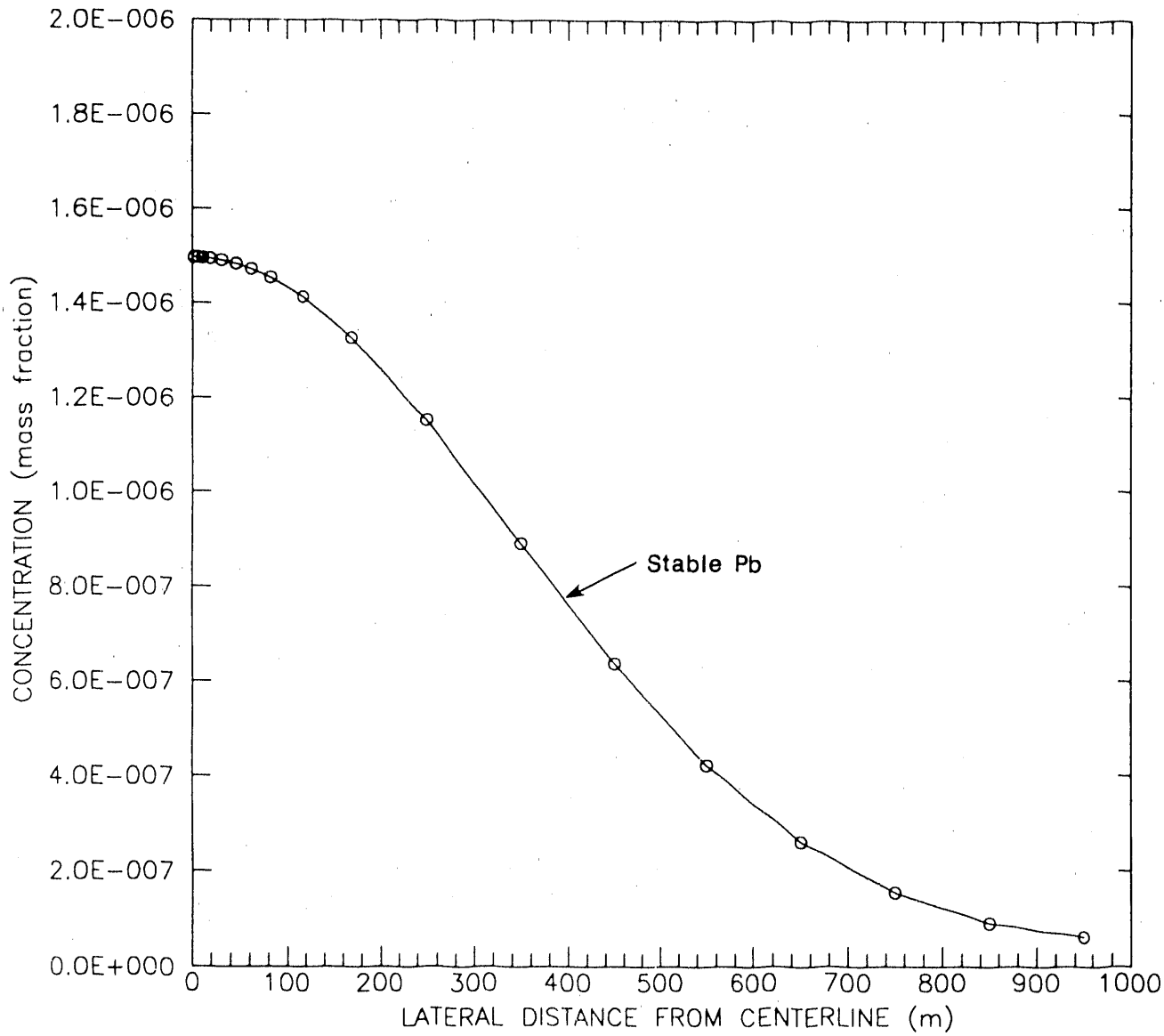

Figure 4-20. Lateral concentration profile across contaminant plume at stock well for stable Pb at 10,000 years, Case IIC'.

analysis (Figure 4-18), but has migrated only ~2,500 m in 10,000 years in the single-porosity analysis (Figure 4-18). Another approach to assessing the impact of single-versus-double-porosity assumptions on transport is to consider transport travel time. Consider a reference concentration of 10^{-10} kg/kg for stable lead. The time required for stable lead to reach this reference concentration at the stock well is slightly more than 8000 years (Figure 4-19) under single-porosity transport conditions. In contrast, stable lead reaches this reference concentration in only about 350 years under double-porosity transport conditions for the properties assigned for Case IIC'. Clearly, the single-porosity approach is nonconservative in assuming that the rock matrix will optimally retard contaminant migration.

Radionuclides. Figures 4-21 through 4-28 show concentration profiles and breakthrough curves for the ^{240}Pu, ^{239}Pu, ^{238}Pu, and ^{241}Am chains. Figures 4-21, 4-23, 4-25, and 4-27 are profiles of centerline concentration, and Figures 4-22, 4-24, 4-26, and 4-28 are breakthrough curves for the stock well. All show reduced concentrations relative to the results of Lappin et al. (1989).

The effects of inventory depletion and radioactive decay and production on the present Case-IIC' results are similar to those same effects in Case IIC of Lappin et al. (1989, Section 7.3.4). Therefore, the following paragraphs focus on the differences between the results of Lappin et al. (1989) and this analysis.

To examine the significance of radionuclide-dependent free-water diffusivities, the transport of the ^{238}Pu chain was also simulated using the same value (5.0×10^{-7} cm^2/s) for the free-water diffusion coefficient used by Lappin et al. (1989) (Figure 4-29). The ^{238}Pu chain was selected because the diffusion coefficient of ^{226}Ra used in these calculations (1.9×10^{-6} cm^2/s, Table 4-7), one of the daughter products in the chain, has the largest deviation from the previously used value. Concentrations of ^{226}Ra, the third daughter, will also contain effects that result from the deviations of the diffusivities of its parent ^{230}Th and its grandparent ^{234}U from the nominal value of Lappin et al. (1989). Figure 4-29 compares ^{226}Ra breakthroughs at the stock well. Relative to those of Lappin et al. (1989), the currently adopted values (Table 4-7) of the free-water diffusion coefficients do not significantly reduce centerline concentrations at 10,000 years, but do reduce concentration about one order of magnitude at early times as a result of enhanced diffusion into and within the matrix blocks.

The major differences between the Case-IIC' results and the results for Case IIC of Lappin et al. (1989) are caused by lateral dispersion, which is fully simulated using the two-dimensional transport model developed for this study. For stable Pb, breakthrough concentrations at the stock well were reduced by a factor of 27 at 10,000 years. Although this reduction also derives from changes in the calibrated flow field, the latter are assumed to be small relative to the reduction caused by lateral dispersion, as discussed for Case IIA'. For the radionuclides, breakthrough concentrations at the stock well at 10,000 years were reduced by factors ranging from 11 for ^{226}Ra to 120 for ^{240}Pu. Although these reductions also reflect the effects of radionuclide-dependent diffusivities, the above discussion indicates that most of the reduction results from lateral dispersion.

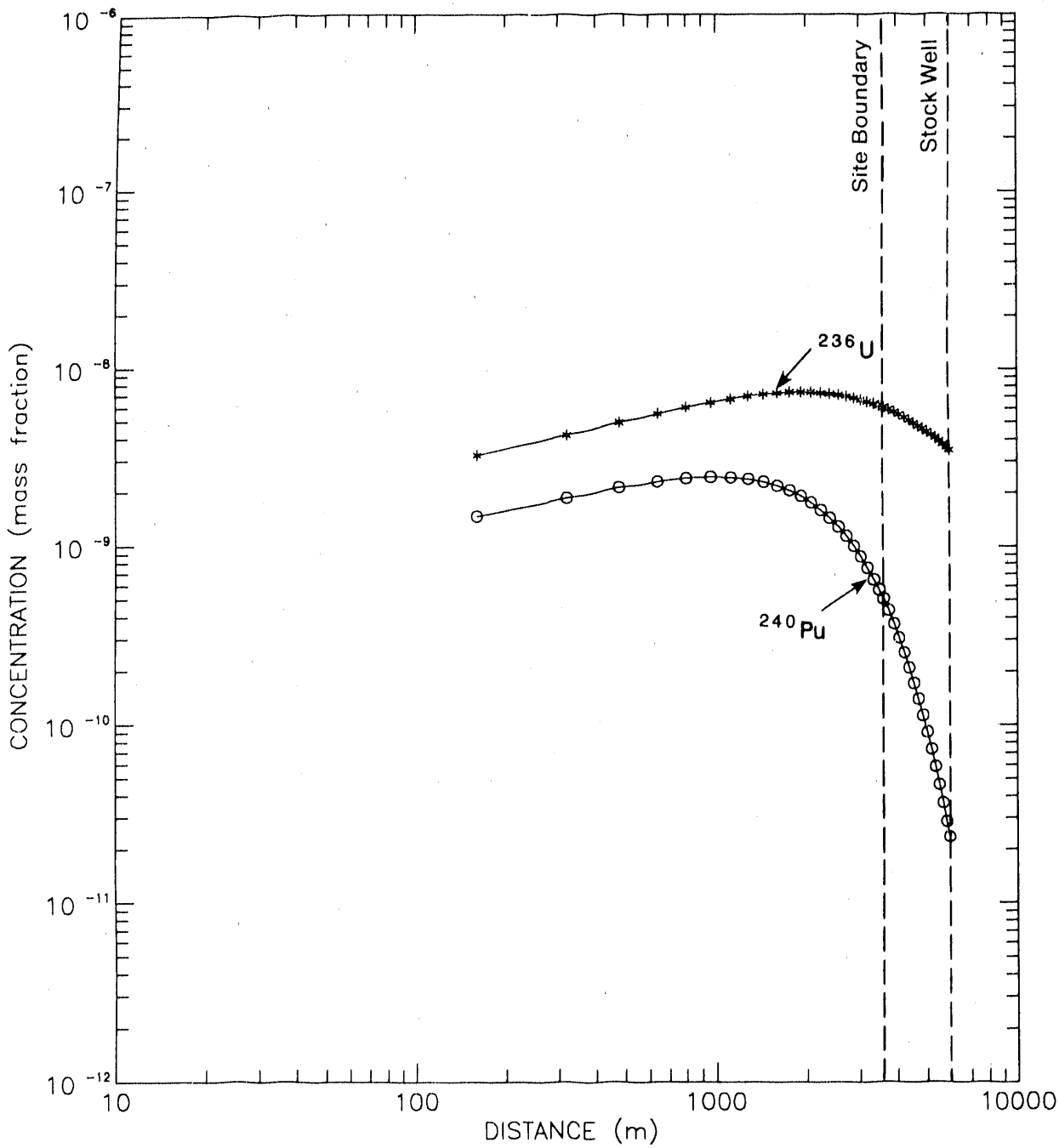

Figure 4-21. Concentration profiles along the plume centerline for the ^{240}Pu decay chain at 10,000 years, Case IIC' (cf. Lappin et al., 1989, Figure 7-17). Dashed vertical lines show the distance to the projected site boundary and the hypothetical stock well.

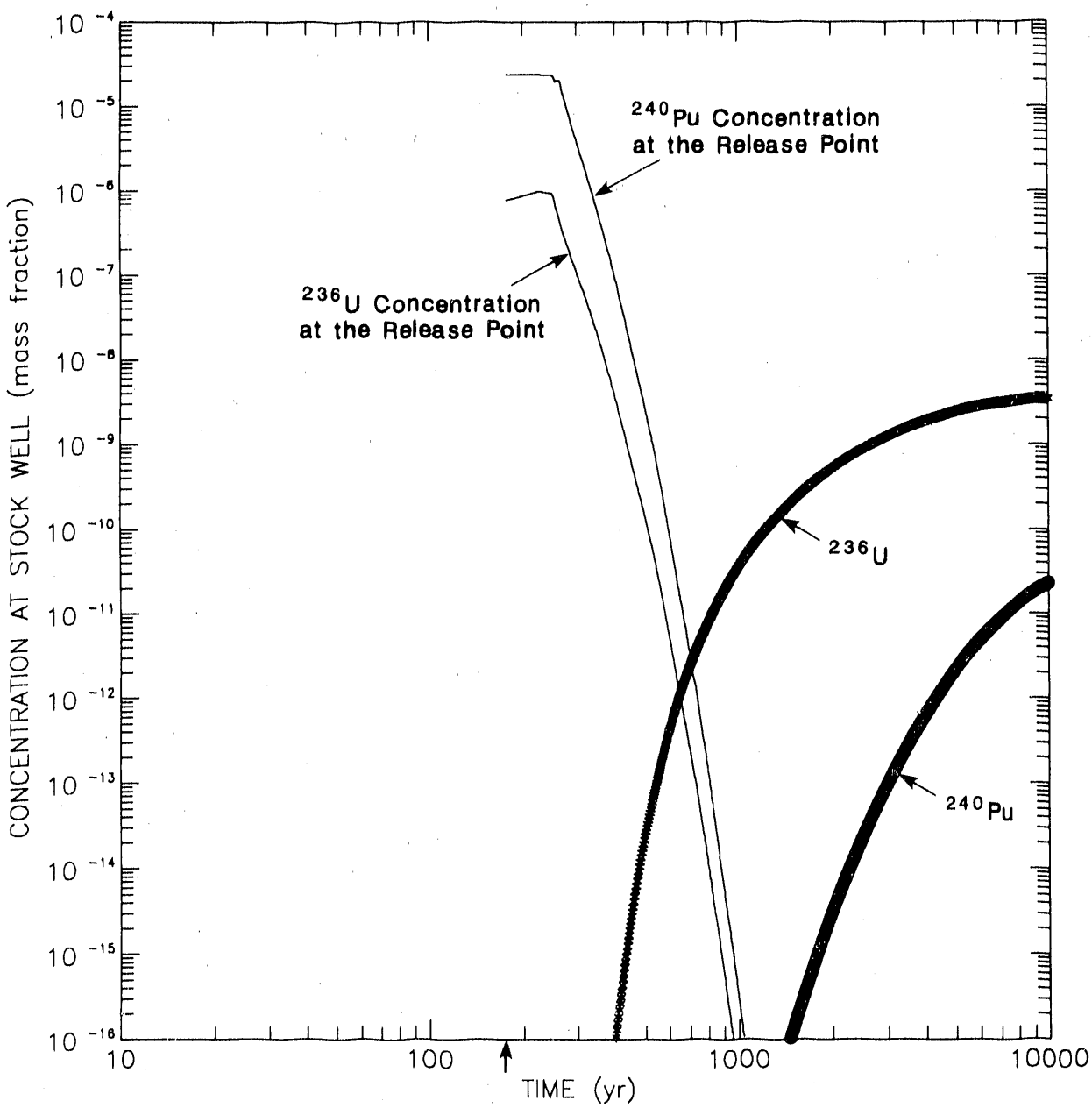

Figure 4-22. Breakthrough concentrations at stock well for the ^{240}Pu decay chain as a function of time, Case IIC' (cf. Lappin et al., 1989, Figure 7-18). The arrow on the horizontal axis indicates the starting time of the SWIFT-II calculation, 175 years after repository decommissioning.

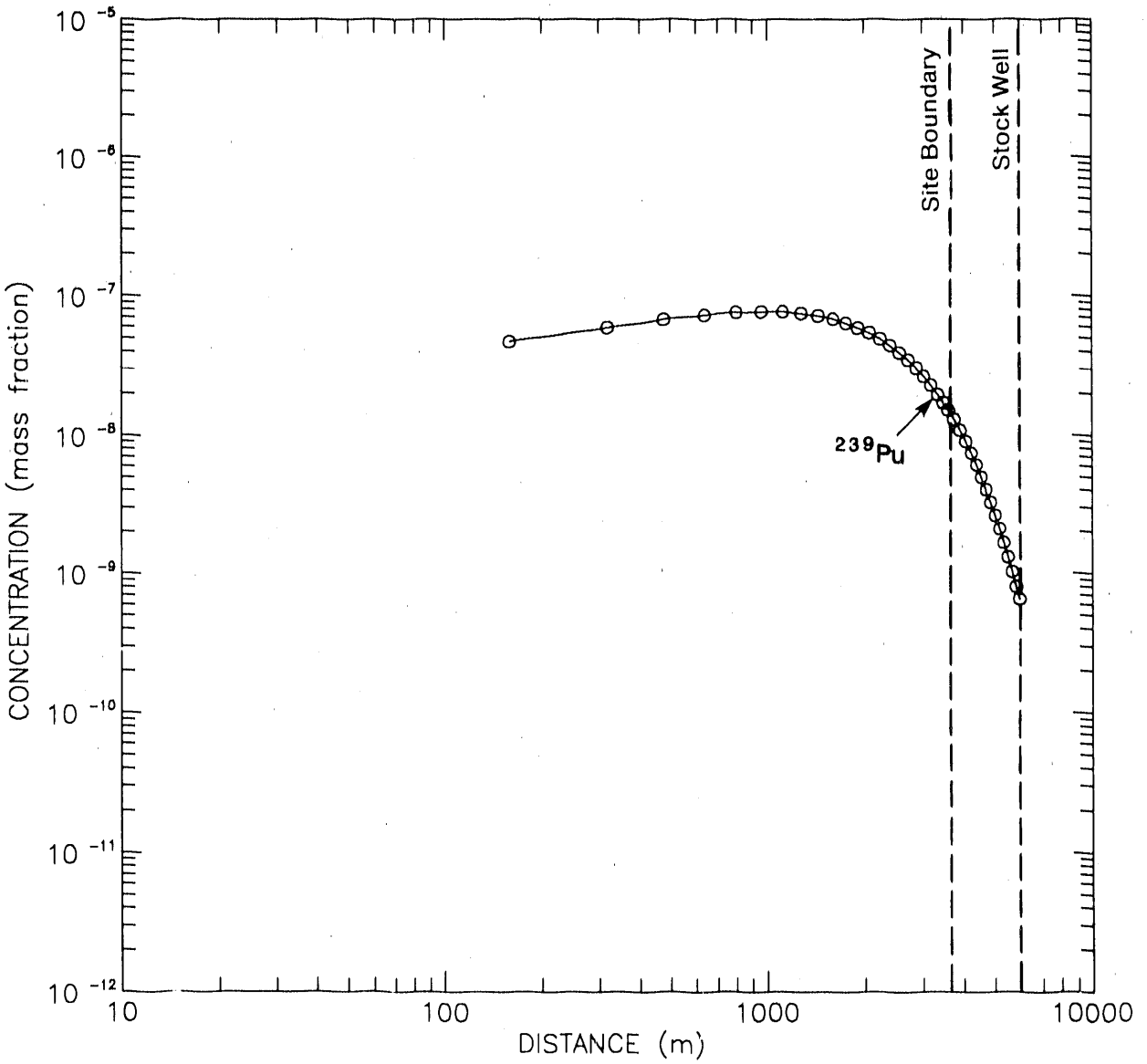

Figure 4-23. Concentration profiles along the plume centerline for the ^{239}Pu decay chain at 10,000 years, Case IIC' (cf. Lappin et al., 1989, Figure 7-19). Dashed vertical lines show the distance to the projected site boundary and the hypothetical stock well.

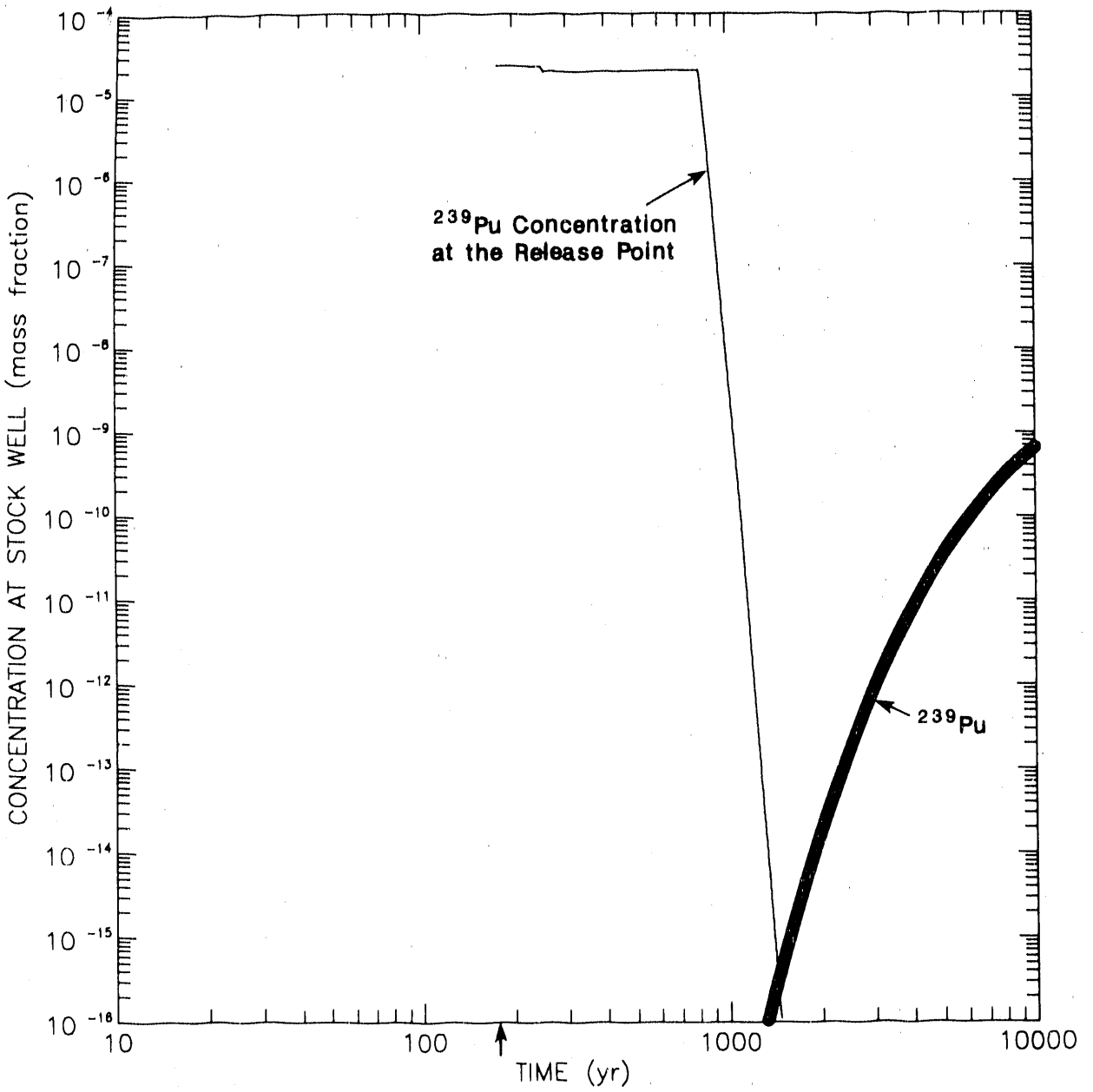

Figure 4-24. Breakthrough concentrations at stock well for the ^{239}Pu decay chain as a function of time, Case IIC′ (cf. Lappin et al., 1989, Figure 7-20). The arrow on the horizontal axis indicates the starting time of the SWIFT-II calculation, 175 years after repository decommissioning.

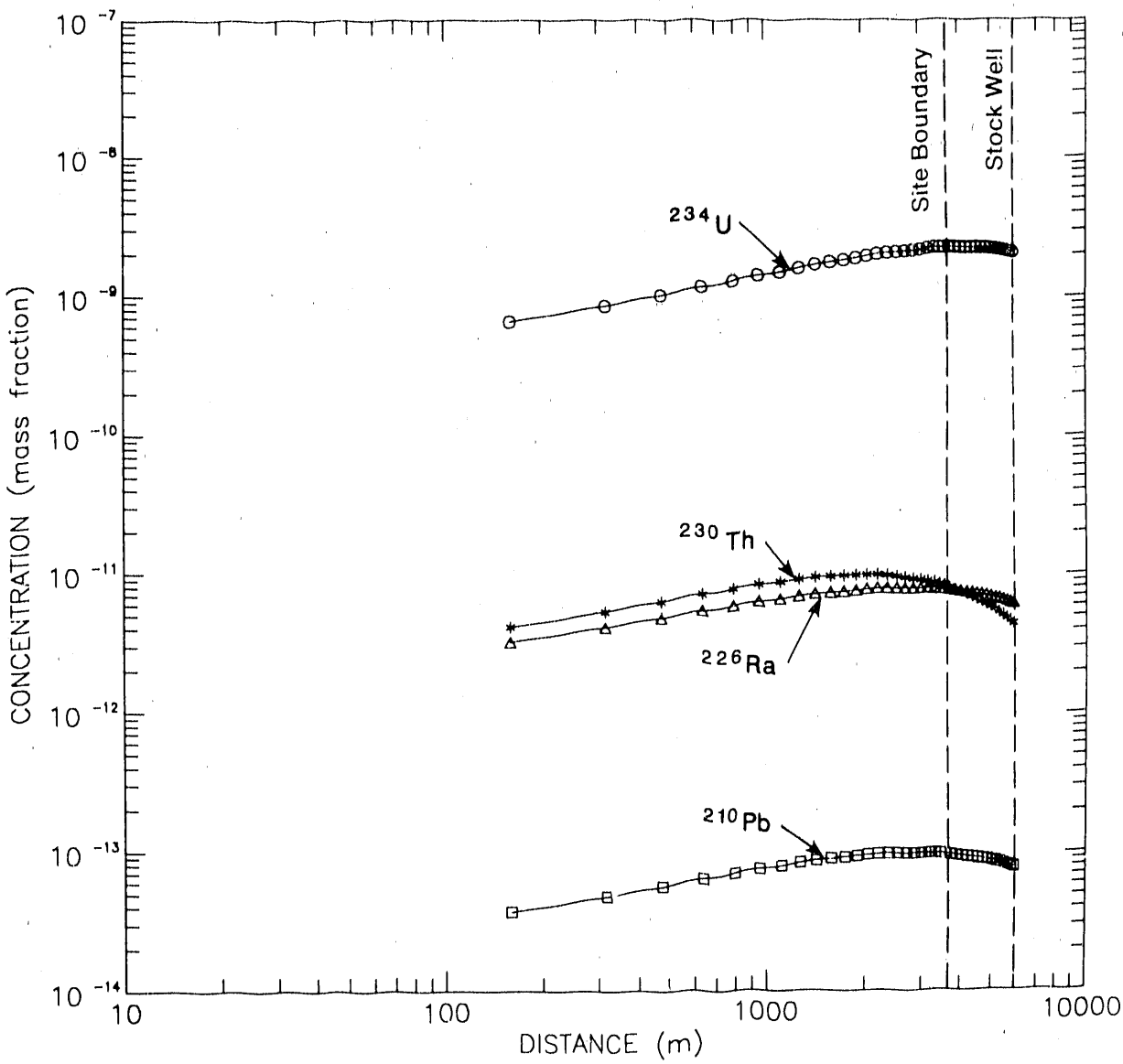

Figure 4-25. Concentration profiles along the plume centerline for the ^{238}Pu decay chain at 10,000 years, Case IIC′ (cf. Lappin et al., 1989, Figure 7-21). Dashed vertical lines show the distance to the projected site boundary and the hypothetical stock well.

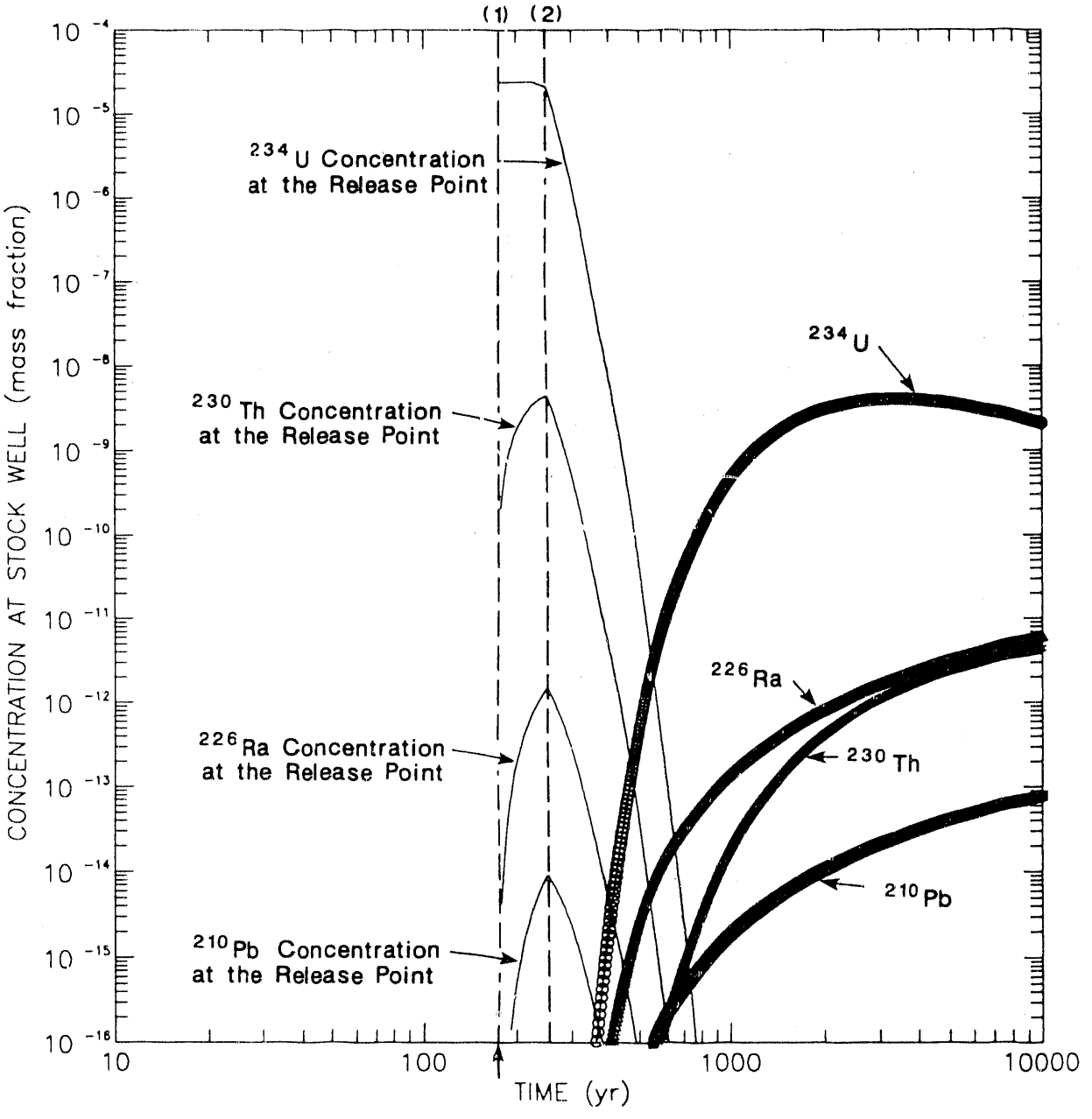

Figure 4-26. Breakthrough concentrations at stock well for the ^{238}Pu decay chain as a function of time, Case IIC' (cf. Lappin et al., 1989, Figure 7-22). (1) Daughters are produced within the repository at a rate faster than they are discharged up the borehole during 125 to 150 years of borehole degradation. (2) After 150 years, i.e., after complete borehole degradation, borehole permeability is high enough to discharge daughters from the repository faster than they can be produced through decay. The arrow on the horizontal axis indicates the starting time of the SWIFT-II calculation, 175 years after repository decommissioning.

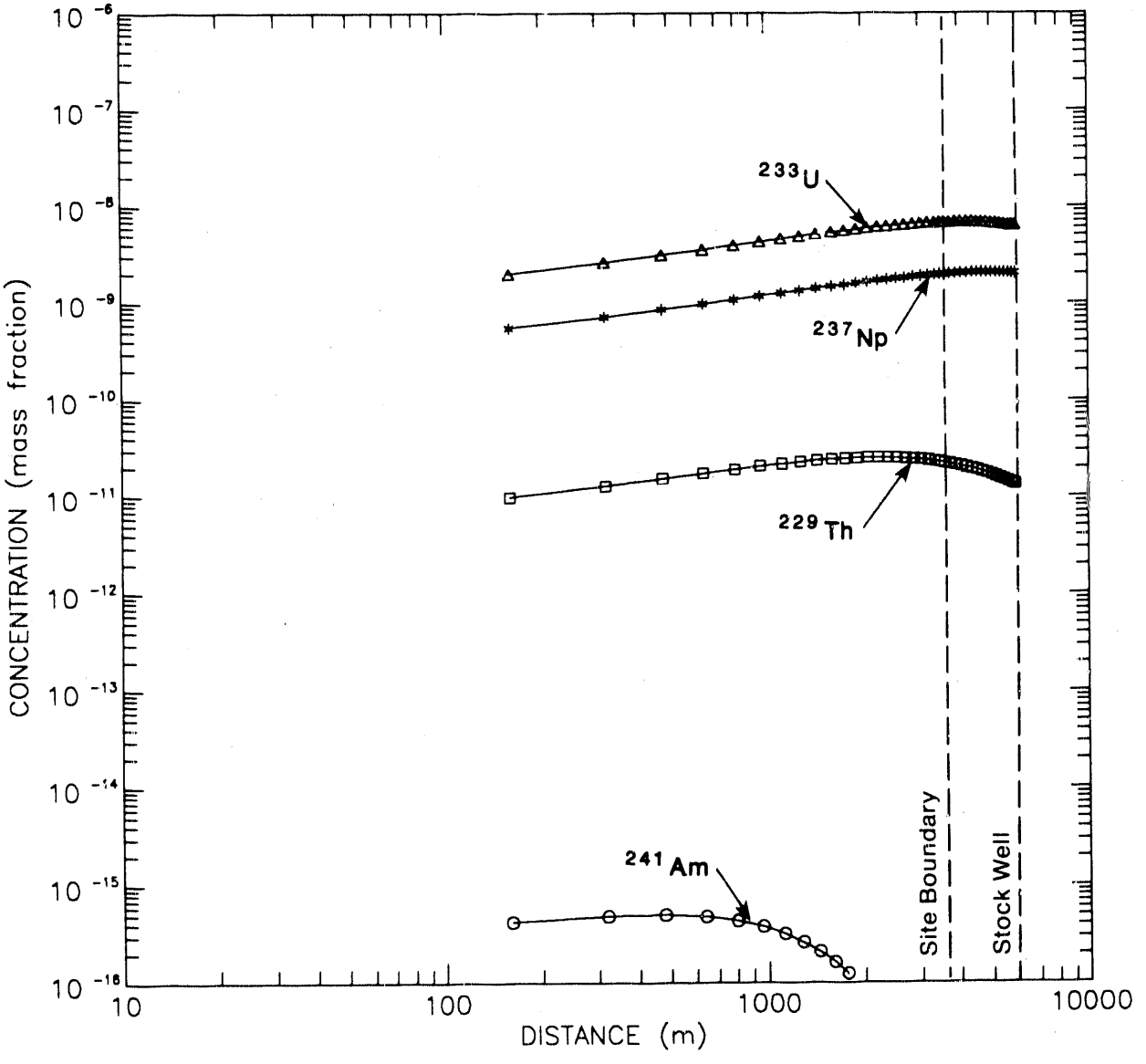

Figure 4-27. Concentration profiles along the plume centerline for the ^{241}Am decay chain at 10,000 years, Case IIC' (cf. Lappin et al., 1989, Figure 7-23). Dashed vertical lines show the distance to the projected site boundary and the hypothetical stock well.

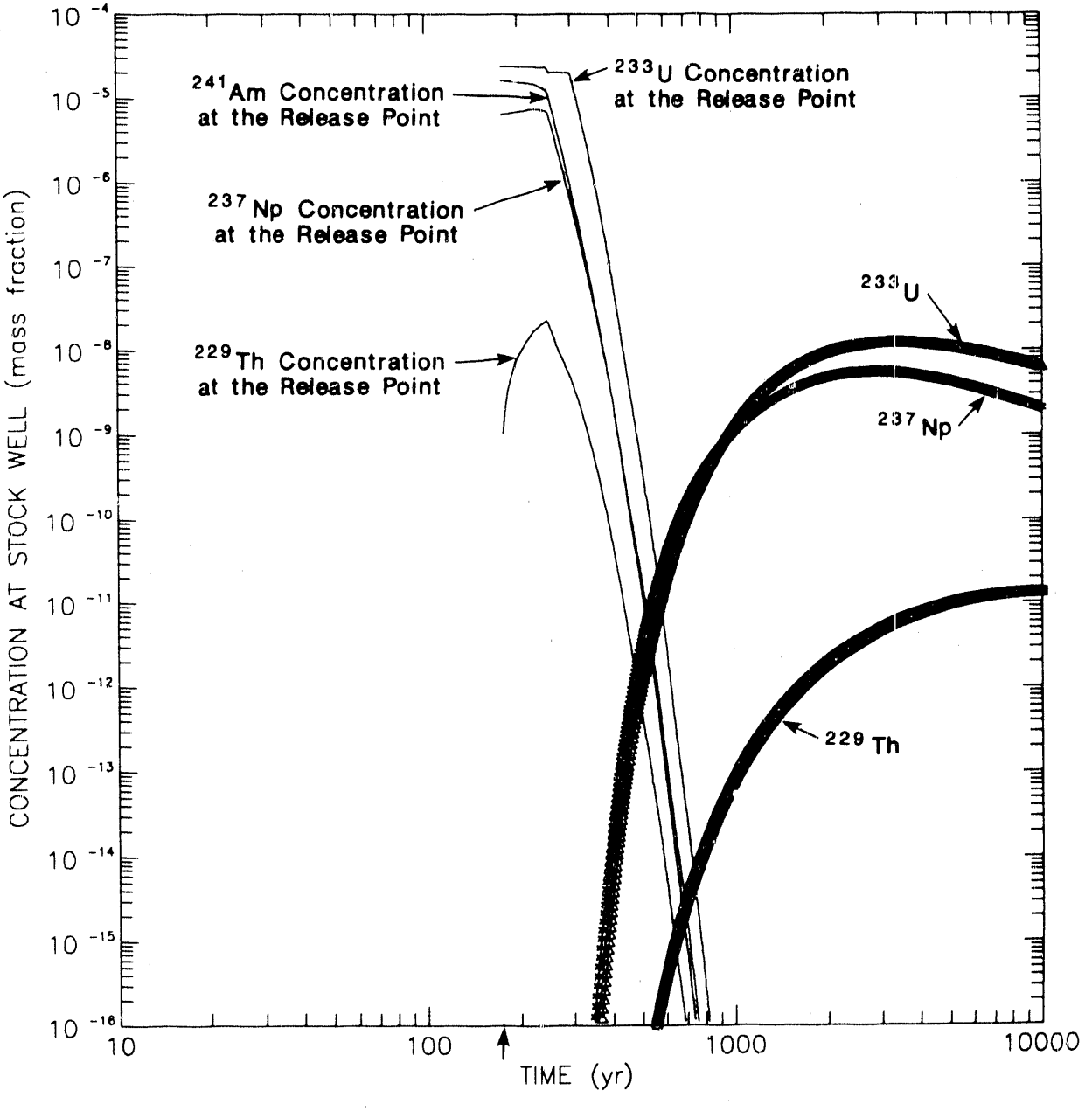

Figure 4-28. Breakthrough concentrations at stock well for the ^{241}Am decay chain as a function of time, Case IIC' (cf. Lappin et al., 1989, Figure 7-24). The arrow on the horizontal axis indicates the starting time of the SWIFT-II calculation, 175 years after repository decommissioning.

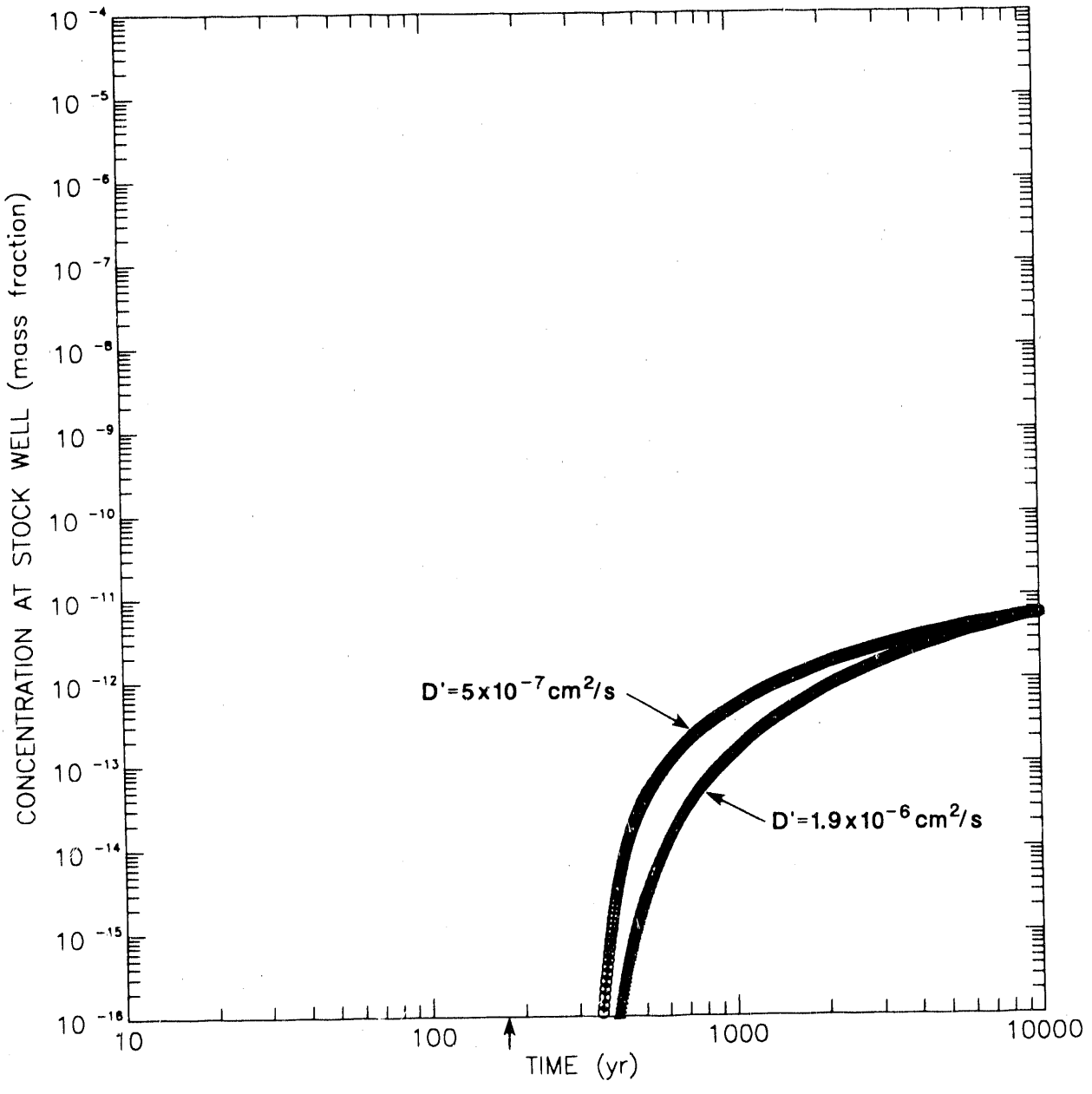

Figure 4-29. Breakthrough concentrations at stock well for ^{226}Ra as a function of free-water diffusivity, Case IIC'. The arrow on the horizontal axis indicates the starting time of the SWIFT-II calculation, 175 years after repository decommissioning.

4.3.4.2 Integrated Releases of Radionuclides. Table 4-10 provides integrated releases at the site boundary and at the distance of the stock well for Case IIC'. The results indicate that the net effect of changes considered here, especially a realistic treatment of contaminant transport within the Culebra Dolomite, is to reduce the integrated release at the distance of the stock well (5.04 km straight line) to 0.7, which is below the 40 CFR 191 limit of 1.0 for releases with probabilities greater than 0.1. This (0.7) is between the bounding upper and lower estimates for Case IIC of Lappin et al. (1989). In contrast to Case IIA', the normalized integrated-release sums are significant for Case IIC'. At the stock well, the normalized integrated release sum is 0.7. At the site boundary, the normalized integrated-release sum is 3.2. Analogous values for Case IIA' are 1.9×10^{-10} and 1.7×10^{-6}. The combination of degraded parameter values used for Case IIC' is unlikely to occur. For releases with probabilities less than 0.1, 40 CFR 191 sets the allowable sum for normalized integrated release at 10. The results for Case IIC' suggest that WIPP can comply with 40 CFR 191.

4.3.4.3 Radiation Doses. Lappin et al. (1989, p. 7-1) calculated doses for four human-intrusion cases:

> Case IIA incorporates representative flow and transport properties for geosphere transport coupled with the design-basis waste form and backfill. Case IIB incorporates degraded geosphere-transport properties, increased radionuclide solubility, and compaction of the waste prior to emplacement that eliminates Castile brine flow through the repository. Case IIC is similar to Case IIB, except that Case IIC assumes that waste is not precompacted and that Castile brine therefore flows through the repository. Case IID incorporates degraded geosphere-transport properties, representative values for radionuclide solubility (same as Case IIA values), and generic engineered modifications of the waste and backfill that eliminate Castile brine flow through the repository and reduce Salado brine-inflow rates to the penetrating borehole.

Of these four cases, transport calculations for IIA and IIC have been revised above, and the results are presented as Cases IIA' and IIC'. As a result of more-realistic transport simulation, the calculated concentrations of most radionuclides in the ground water at the stock well has decreased relative to the earlier calculations. Table 4-11 gives the radionuclide concentrations in ground water at the stock well for Cases IIA, IIB, IIC, and IID of Lappin et al. (1989) and for Cases IIA' and IIC' from Table 4-8.

Doses have been recalculated for Cases IIA' and IIC'. The calculational techniques used were identical to those used by Lappin et al. (1989). Table 4-12 compares the results of dose calculations for Cases IIA, IIB, IIC, and IID of Lappin et al. with those of IIA' and IIC' from the current study.

The new calculations with the more-comprehensive, two-dimensional transport model show an average decrease in concentrations at the stock well by about a factor of 6 for Case IIC' and by about a factor of 200 for Case IIA' (Table 4-11). The decreases in concentrations result from the improved stream-tube model, as discussed above. Because Cases IIB, IIC, and IID of Lappin et al. (1989) used the same constant correction factor (4.2), in an attempt to correct for lateral dispersion, Cases IIB and IID would also be

Table 4-10. Normalized integrated release at site boundary and stock well over 10,000 years, Case IIC'. The release at the stock well would be allowable under 40 CFR 191 at any probability; the release at the site boundary would be allowable at probabilities <0.1.

Radio-nuclide	Release Limit (RL)	WIPP-Site Boundary Integrated Release (IR) (kg)	(Ci)	IR(Ci) /RL	Stock Well Integrated Release (IR) (kg)	(Ci)	IR(Ci) /RL
^{240}Pu	660.0	8.49×10^{-1}	1.93×10^{2}	2.93×10^{-1}	2.06×10^{-2}	4.69	7.11×10^{-3}
^{236}U	660.0	1.62×10^{1}	1.05	1.59×10^{-3}	7.95	5.15×10^{-1}	7.80×10^{-4}
^{239}Pu	660.0	1.92×10^{1}	1.19×10^{3}	1.81	4.81×10^{-1}	2.99×10^{1}	4.53×10^{-2}
^{238}Pu	660.0	na	na	na	na	na	na
^{234}U	660.0	1.80×10^{1}	1.12×10^{2}	1.70×10^{-1}	1.05×10^{1}	6.56×10^{1}	9.95×10^{-2}
^{230}Th	66.0	1.78×10^{-2}	3.59×10^{-1}	5.44×10^{-3}	8.51×10^{-3}	1.72×10^{-1}	2.60×10^{-3}
^{226}Ra	660.0	1.38×10^{-2}	1.36×10^{1}	2.06×10^{-2}	1.21×10^{-2}	1.19×10^{1}	1.81×10^{-2}
^{210}Pb	660.0	1.72×10^{-4}	1.31×10^{1}	1.99×10^{-2}	1.54×10^{-4}	1.18×10^{1}	1.78×10^{-2}
^{241}Am	660.0	3.96×10^{-7}	1.36×10^{-3}	2.06×10^{-6}	6.09×10^{-12}	2.09×10^{-8}	3.17×10^{-11}
^{237}Np	660.0	1.94×10^{1}	1.37×10^{1}	2.07×10^{-2}	1.29×10^{1}	9.11	1.38×10^{-2}
^{233}U	660.0	5.54×10^{1}	5.35×10^{2}	8.10×10^{-1}	3.22×10^{1}	3.11×10^{2}	4.71×10^{-1}
^{229}Th	660.0	6.26×10^{-2}	1.32×10^{1}	1.99×10^{-2}	3.08×10^{-2}	6.48	9.82×10^{-3}
			Sum:	3.17		Sum:	6.86×10^{-1}

na means not applicable

Table 4-11. Radionuclide concentrations (kg/kg brine) in the Culebra aquifer at the stock well at 10,000[a] years for all cases (data for Cases IIA, IIB, IIC, and IID from Lappin et al., 1989, Table 7-9)

Nuclide	IIA	IIA'	IIB	IIC	IIC'	IID
^{237}Np	br	4.91×10^{-20}	3.52×10^{-8}	1.26×10^{-7}	2.01×10^{-9}	1.08×10^{-9}
^{210}Pb	2.82×10^{-17}	3.12×10^{-21}	5.05×10^{-13}	1.64×10^{-13}	7.80×10^{-14}	6.14×10^{-15}
^{239}Pu	br	br	3.51×10^{-09}	1.11×10^{-13}	6.54×10^{-10}	2.76×10^{-12}
^{240}Pu	br	br	4.51×10^{-10}	6.18×10^{-14}	2.34×10^{-11}	1.61×10^{-12}
^{226}Ra	2.02×10^{-15}	2.40×10^{-19}	3.62×10^{-11}	1.18×10^{-11}	6.12×10^{-12}	4.40×10^{-13}
^{229}Th	br	2.31×10^{-26}	1.53×10^{-10}	6.17×10^{-11}	1.33×10^{-11}	6.37×10^{-13}
^{230}Th	br	1.43×10^{-26}	3.78×10^{-11}	1.39×10^{-11}	4.37×10^{-12}	5.04×10^{-13}
^{233}U	br	3.00×10^{-22}	1.23×10^{-7}	3.61×10^{-7}	6.29×10^{-9}	1.07×10^{-9}
^{234}U	br	2.67×10^{-22}	3.34×10^{-8}	1.21×10^{-7}	2.05×10^{-9}	1.07×10^{-9}
^{236}U	br	3.02×10^{-22}	3.24×10^{-8}	3.42×10^{-8}	3.47×10^{-9}	3.11×10^{-10}

a Peak concentrations at 1345 years for Case IIC are compared with maximum calculated concentrations at 10,000 years for Case IIC'. The concentration for Case IIC' continues to rise after 10,000 years.
br below resolution of calculations

Table 4-12. Maximum 50-year committed effective dose equivalent after a 1-year exposure to contaminated beef (mrem/50 yr) (data for Cases IIA, IIB, IIC, and IID from Lappin et al., 1989, Table 7-13). Individuals were assumed to ingest 86 g/d beef. All maximum doses occur at 10,000 years, except in Case IIC, which has a maximum dose at 1345 years.

Nuclide	IIA	IIA'	IIB	IIC	IIC'	IID
^{237}Np	nd	1.36×10^{-11}	2.5	9.1	5.55×10^{-1}	7.8×10^{-2}
^{210}Pb	1.8×10^{-4}	6.65×10^{-7}	2.8×10^{1}	9.2	$1.66 \times 10^{+1}$	3.4×10^{-1}
^{239}Pu	nd	nd	2.2×10^{-1}	7.1×10^{-6}	1.60×10^{-1}	1.8×10^{-4}
^{240}Pu	nd	nd	1.1×10^{-1}	1.4×10^{-5}	2.09×10^{-2}	3.8×10^{-4}
^{226}Ra	3.0×10^{-5}	1.19×10^{-7}	4.7	1.5	3.04	5.7×10^{-2}
^{229}Th	nd	1.88×10^{-16}	3.3×10^{-1}	1.3×10^{-1}	1.08×10^{-1}	1.4×10^{-3}
^{230}Th	br	1.68×10^{-18}	1.2×10^{-3}	4.3×10^{-4}	5.12×10^{-4}	1.5×10^{-5}
^{233}U	br	2.86×10^{-13}	3.1×10^{1}	9.0×10^{1}	6.00	2.7×10^{-1}
^{234}U	br	1.58×10^{-13}	5.2	1.9×10^{1}	1.22	1.7×10^{-1}
^{236}U	nd	1.78×10^{-15}	5.0×10^{-2}	5.3×10^{-2}	2.05×10^{-2}	4.8×10^{-4}
Total	2.1×10^{-4}	7.85×10^{-7}	$7.2 \times 10^{+1}$	$1.3 \times 10^{+2}$	$2.78 \times 10^{+1}$	9.1×10^{-1}

likely to show similar reductions in concentrations if lateral diffusion were included in the model as calculations IIB' and IID'

In Cases IIA, IIA', IIB, IIC', and IID, the maximum calculated committed dose occurs at the end of the 10,000-year period. In Case IIC of Lappin et al. (1989), however, a maximum calculated dose occurs 1345 years after borehole abandonment; this maximum is the one shown in Table 4-12. The relative maximum of the Case-IIC dose at 1345 years is caused by the occurrence of the peak contribution of ^{233}U at 1345 years, exceeding the peak contribution of ^{210}Pb. Some time after 10,000 years, ^{210}Pb would cause a larger dose than the 1345-year relative maximum. Thus, in all cases the actual maximum will occur later than 10,000 years. This is not surprising, because a key purpose of geological disposal is to delay the appearance of contaminants in the accessible environment for very long times. Calculations could be extended past 10,000 years, but they become less meaningful; increasing uncertainty of an adequate model results from increasingly unreliable assumptions of steady-state flow within the Culebra at longer times.

Comparison of the human-intrusion cases (Table 4-12) indicates that Case IIC is the most severe. The maximum Case-IIC 50-year dose commitment was 130 mrem at 1345 years; the dose falls to 82 mrem at 10,000 years (Figure 4-30a). The revised calculations (Figure 4-30b) show that the peak at 1345 years is an artifact of the conservative assumptions made in Case IIC. Case IIC', the more accurate calculation of the most severe case, yields a maximum dose of 27.8 mrem at 10,000 years (Table 4-12 and Figure 4-30b). This is the committed dose that a person would receive during the next 50 years as the result of one year's ingestion of 86 g/d of contaminated beef from cattle watered at the stock well. This person receives an average annual exposure of 0.56 mrem from one year's commitment. If this person continues to eat contaminated beef at this rate, he will receive a 27.8 mrem radiation dose in his 50th year of eating beef. This dose is about 30% of the 100-mrem average annual background in the United States.

Only the stream-tube model of Lappin et al. (1989) has been used to simulate all four human-intrusion cases. Comparing the Case-IIC dose of 82 mrem at 10,000 years with the Case-IIC' dose of 27.8 mrem at 10,000 years suggests that the stream-tube model of Lappin et al. (1989) gives about 3 times larger a dose. The integrated releases of the individual radionuclides in the DSEIS (DOE, 1989a) were, on average, 6 times larger. Qualitatively similar reductions would likely be seen for Cases IIB and IID, if the more accurate model were used in new calculations. The reduction factor for Case IIA' is larger, perhaps as large as 200, but it is not determined precisely, because both the Case IIA and IIA' releases are negligible.

4.4 Other Consequences of Human Intrusion

In addition to the doses arising from the ingestion of contaminated beef, Lappin et al. (1989, Section 7.2) calculated possible exposures resulting from two pathways that began with releases of radioactive material to the surface at the top of an intruding well. These calculations have not been revised during the current study, but the results are summarized here for completeness. The maximum external radiation exposure was assumed to be received by the drilling-crew member who examines cutting chips for a period of one hour at a distance of one meter. The exposure rate from natural background

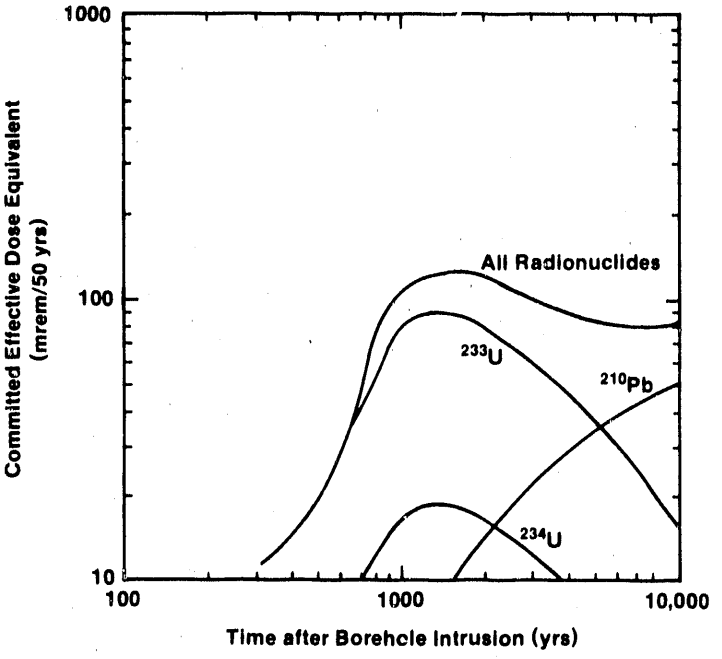

a. Doses calculated based on the model of Lappin et al. (1989) (DOE, 1989a, Figure 5.15)

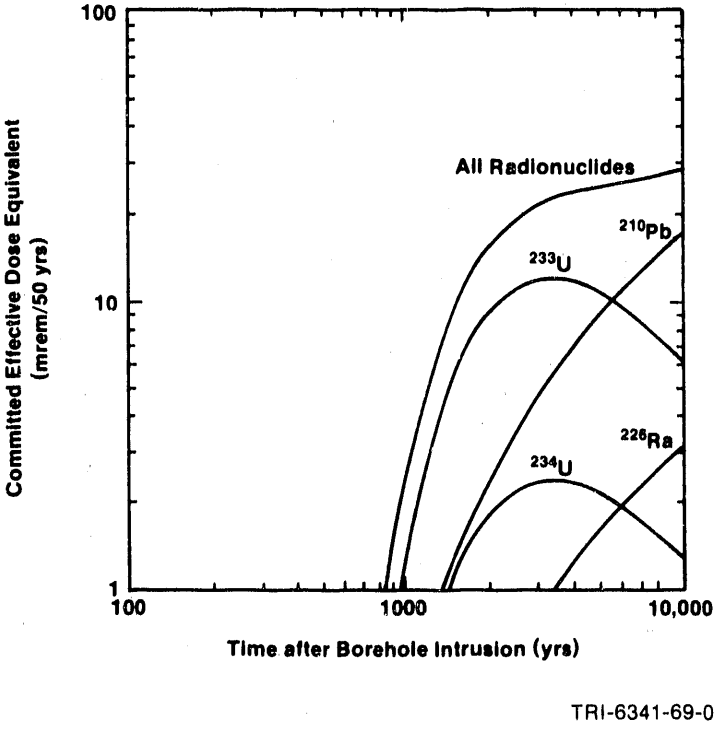

b. Doses calculated based on the updated model of this report.

Figure 4-30. Radiation doses to individuals who ingest contaminated beef from cattle watered at the stock well, Cases IIC and IIC'.

radiation is ~0.01 milliroentgen per hour (mR/hr) (100 mrem/yr); Lappin et al. (1989) estimated the exposure rate from chip examination to be eight times the background exposure rate, but the incremental dose was only 0.08 mR/yr, because the exposure only lasted for one hour. After drilling operations cease, radioactive material remains in the drilling-mud settling pond and is available for transport through airborne or surface-water pathways. Doses to a hypothetical farm family living 500 m downwind from the settling pond were calculated by Lappin et al. (1989). The pathways considered included inhalation of contaminated air and ingestion of foods (meat, milk, and above- and below-surface food crops) produced on the farm. Estimated doses to a member of this farm family were assumed to be the same for all variants of Case II. The 50-year committed dose equivalent from inhalation, primarily from ^{238}Pu and ^{241}Am, was 0.77 mrem. The estimated 50-year committed dose from ingestion of contaminated food products was negligible.

Lappin et al. (1989) also calculated the amount of radon present in the repository at 5000 and 10,000 years. They used single-precision arithmetic (7 significant digits) in the computer calculations; the results showed that only 2×10^{-4} Ci of radon would be present at 5000 years and only 1×10^{-3} Ci would be present at 10,000. The results of the single-precision calculations contained errors caused by loss of significance. The calculations have been repeated for this study, using double-precision arithmetic (14 significant digits), showing much larger amounts of radon present: 35 Ci at 5000 years and 91 Ci at 10,000 years. Radon has such a short half-life, 3.8 days, that only human intrusion would result in the release of radon to the surface. Because it is spread throughout the repository, even human intrusion would release only a very small amount to the surface. No doses arising from radon have been calculated.

5.0 SUMMARY

The results of this report fall into two broad categories. First, the disturbed rock zone is described in greater detail than it was by Lappin et al. (1989). Second, long-term radionuclide-transport behavior at the WIPP, both under undisturbed conditions and in response to human intrusion, is modeled using updated input-parameter values, and, in the latter case, a more realistic, two-dimensional implementation of transport. Human intrusion is assumed to connect a reservoir of pressurized brine in the Castile Fm. with both the WIPP repository and the overlying Culebra Dolomite. Only two of the six cases analyzed by Lappin et al. (1989) have been recalculated.

5.1 Disturbed Rock Zone

The far-field mechanical response of the Salado Formation to construction of the WIPP underground workings is expected to be dominated by creep closure of a coherent rock mass; however, a disturbed rock zone develops near the underground openings. The DRZ at the WIPP is currently 2 to 4 m thick. It should reach its maximum extent in twenty years or less. With the possible exception of the marker beds, the connectivity of the DRZ is expected to be greatly reduced in the long term in response to far-field creep closure and backpressure exerted by the waste and backfill. Although the DRZ is important during the transient phases of repository behavior, it is not expected to affect the final state of the WIPP repository significantly.

The origin of the DRZ is a function of dilation and rapid strain rates near the excavation. Several processes are apparently involved in forming the DRZ: strain-dependent brittle fracturing; dilatant microfracturing and increase in pore volume in response to fluid expansion or exsolution of gas; and partial brine desaturation. These processes lead to the development of a volume of disturbed rock within an "active opening" somewhat larger than the geometric opening.

The DRZ is expected to have several potential effects. Gas or brine may bypass emplaced panel seals and escape from waste-emplacement panels into adjacent portions of the WIPP underground workings. This might decrease internal gas pressures, but it might also increase the effective foot-print of the WIPP for performance assessment. The DRZ may alter fluid-flow behavior within the Salado Formation near the repository and may allow increased flow of brine into the repository. Fractures within the DRZ should also provide significant storage capacity for gases that may be generated as a result of brine inflow. In the long term, partial saturation of the matrix within the DRZ may result in a zone of relatively decreased brine permeability near the repository.

5.2 Cases IA′ and IB′, Undisturbed Performance

In Cases IA′ and IB′, no radionuclide migration to either the Culebra Dolomite or the surface occurs within 10,000 years under the assumed conditions, and therefore no doses to human beings are possible. This result, similar to that of Lappin et al. (1989), was obtained in spite of a modification to the calculation that tends to promote an earlier release of waste:

modeling the northern equivalent panel instead of Panel 1. The calculations were also improved in several other ways. Lithostatic and hydrostatic driving pressures for flow were used to provide upper and lower bounds. The porosity of Marker Bed 139 and the cross-sectional area of the path through it have been increased to reflect an improved understanding of the disturbed rock zone and more accurately reflect seal geometry. Finally, a more realistic threshold value was used to describe the first release of waste to the stock well.

5.3 Cases IIA' and IIC', Effects of Human Intrusion

The human-exposure pathways for the two cases considered here begin with release to the surface at the head of the intrusion well or at a stock well in the Culebra Dolomite, located down gradient from the repository. Only releases and doses arising from releases to the stock well have been recalculated; the effects of releases at the head of the intrusion well calculated by Lappin et al. (1989) are reported unchanged.

5.3.1 Doses Arising from Releases at the Head of the Intrusion Well

Lappin et al. (1989) calculated the highest external dose received by a drill-crew member, assumed to be a geologist who examined the cuttings. The geologist was calculated to receive a total incremental dose of 0.08 mR during a one-hour exposure to the cuttings. They also calculated the committed dose equivalent received by a member of a hypothetical farm family living 500 m downwind of the intruding bore hole. The total ingested dose was negligible. The total inhaled committed dose equivalent received after a one-year exposure was 0.77 mrem/50 yr.

5.3.2 Doses Arising from Ingestion of Contaminated Beef

The starting point for calculations of doses arising from ingestion of contaminated beef is the hypothetical stock well in the Culebra Dolomite. The calculations presented here are revised from those of Lappin et al. (1989) in several ways. First, a revised transmissivity distribution (LaVenue et al., 1990) was used in the ground-water-flow modeling; this revised distribution gave rise to a slightly different location for the stock well and a slightly different flow-path length. Second, the new calculations incorporate more realistic, two-dimensional contaminant transport, which reduces centerline concentrations in the contaminant plume. Finally, both single-porosity and double-porosity transport times have been calculated and compared.

The concentrations of the radionuclides at the stock well, which are reduced from those of Lappin et al. (1989), were highest at 10,000 years. In the calculations of Lappin et al., the highest concentrations, which came at 10,000 years for Case IIA and at 1345 years for Case IIC, were used for the dose calculations. The estimated doses calculated for a person consuming 86 g/d of beef contaminated by radionuclides from the stock pond are reported in Table 4-12. The 50-year committed effective dose equivalents are lower than those calculated by Lappin et al. (1989) as a result of the reduced concentrations in the stock well: 7.85×10^{-7} mrem for Case IIA', as opposed to 2.1×10^{-4} mrem for Case IIA at 10,000 years; and 27.8 mrem at 10,000 years for Case IIC', as opposed to 130 mrem for Case IIC at 1,345 years.

5.3.3 Integrated Releases

For expected conditions within the Castile brine occurrence, the WIPP repository, and the Culebra Dolomite (Case IIA'), integrated releases at the WIPP-site boundary at 10,000 years are several orders of magnitude below those allowed by the present form of 40 CFR 191. The integrated release at 10,000 years is calculated to be 1.7×10^{-6} times the allowed release. The integrated release at the distance of the hypothetical stock well (5 km) is 1.9×10^{-10} times the allowed release. Calculated radionuclide concentrations for this case are still rising at the site boundary at 10,000 years, the maximum that must be considered under 40 CFR 191.

The two highest contributors to the integrated release are ^{226}Ra and ^{210}Pb. However, the integrated release of each radionuclide is less than 10^{-6} times its allowed release. At the 5-km distance of the hypothetical stock well, ^{226}Ra and ^{210}Pb are the only radionuclides calculated to have broken through significantly. Again, however, the integrated release of each isotope is less than 1×10^{-10} times the allowed release (Table 4-9). The results of Case IIA' indicate that, if both repository and Culebra properties are near those expected, there is a high degree of confidence that far-field contaminant transport within the Culebra will result in highly reliable performance of the WIPP.

For degraded flow-and-transport conditions within the repository and the Culebra Dolomite (Case IIC'), integrated releases at the WIPP-site boundary at 10,000 years are calculated to be 3.2 times the limit presently set by 40 CFR 191 for releases with probabilities >0.1 and 0.32 times the limit set for releases with probabilities between 0.1 and 0.001. The three greatest contributors to integrated release for Case IIC' are ^{239}Pu, ^{233}U, ^{240}Pu, and ^{234}U (Table 4-10). The estimated release of ^{239}Pu alone is 1.8 times the allowed release at probabilities >0.1. Calculated radionuclide concentrations are still increasing at the site boundary at 10,000 years, but releases are only regulated for 10,000 years.

The calculated release at 5 km for Case IIC' is only 0.7 times the limit for releases with probabilities >0.1. The four greatest contributors to release at the distance of the stock well are ^{233}U, ^{234}U, ^{239}Pu, and ^{226}Ra. They are influenced by greater flow distances and greater potential for rock-water interactions, i.e., by effects due to low K_d. One radionuclide, ^{233}U, contributes 0.5 of the total allowed integrated release.

These results indicate that there is appreciable potential for radionuclide storage within the Culebra Dolomite between the site boundary and the distance of the hypothetical stock well and that the relative importance of a given radionuclide depends on the length of the flow path to the point of evaluation. Even for degraded flow-and-transport properties within the repository and the Culebra Dolomite, it appears likely that the WIPP could satisfy 40 CFR 191, because this combination of properties is most likely to be significantly less probable than 0.1. Including the interval between the present land-withdrawal boundary and the 5-km limit within an administratively controlled zone might provide significant advantages if additional assurance is needed for compliance.

6.0 REFERENCES

Argüello, J. G., and T. Torres, 1988. WIPP Panel Entryway Seal--Numerical Simulation of Seal Component/Formation Interaction for Preliminary Design Evaluation, SAND87-2591. Sandia National Laboratories, Albuquerque, NM.

Baar, C. A., 1977. Applied Salt-Rock Mechanics 1: The In-Situ Behavior of Salt Rocks. Elsevier, Amsterdam.

Barrows, L. J., S.-E. Shaffer, W. B. Miller, and J. D. Fett, 1983. Waste Isolation Pilot Plant Site Gravity Survey and Interpretation, SAND82-2922. Sandia National Laboratories, Albuquerque, NM.

Bear, J., 1972. Dynamics of Fluids in Porous Media. American Elsevier Publishing Company, NY.

Beauheim, R. L., 1987. Interpretations of Single-Well Hydraulic Tests Conducted At and Near the Waste Isolation Pilot Plant (WIPP) Site, 1983-1987, SAND87-0039. Sandia National Laboratories, Albuquerque, NM.

Beauheim, R. L., 1989. Interpretation of H-11b4 Hydraulic Tests and the H-11 Multipad Pumping Test of the Culebra Dolomite at the Waste Isolation Pilot Plant (WIPP) Site, SAND89-0536. Sandia National Laboratories, Albuquerque, NM.

Beauheim, R. L., and G. J. Saulnier, 1990. Interpretation of Brine-Permeability Tests of the Salado Formation at the Waste Isolation Pilot Plant Site: First Interim Report, SAND90-0083. Sandia National Laboratories, Albuquerque, NM.

Bechtel National Inc., 1986. Quarterly Geotechnical Data Report, DOE-WIPP-221. U.S. Department of Energy, Carlsbad, NM.

Bertram-Howery, S. G., and R. L. Hunter, eds., 1989. Preliminary Plan for Disposal-System Characterization and Long-Term Performance Evaluation of the Waste Isolation Pilot Plant, SAND89-0178. Sandia National Laboratories, Albuquerque, NM.

Borns, D. J., 1985. Marker Bed 139: A Study of Drillcore From a Systematic Array, SAND85-0023. Sandia National Laboratories, Albuquerque, NM.

Borns, D. J., and J. C. Stormont, 1988a. An Interim Report on Excavation Effect Studies at the Waste Isolation Pilot Plant: The Delineation of the Disturbed Rock Zone, SAND87-1375. Sandia National Laboratories, Albuquerque, NM.

Borns, D. J., and J. C. Stormont, 1988b. "Dilatancy and Fracturing in the Disturbed Rock Zone and Its Contribution to the Total Observed Closure in WIPP Excavations," Memorandum to distribution, Sandia National Laboratories, Albuquerque, NM. October 7, 1988.

Borns, D. J., and J. C. Stormont, 1989. "The Delineation of the Disturbed Rock Zone Surrounding Excavations in Salt," in A. Wahab Khair, ed., Rock Mechanics as a Guide for Efficient Utilization of Natural Resources: Proc. 30th U.S. Symposium. A. A. Balkema, Rotterdam.

Brace, W. F., B. W. Paulding, and C. Scholz, 1966. "Dilatancy in the Fracture of Crystalline Rocks," Journal of Geophysical Research, vol. 71.

Brady, B. H. G., and E. T. Brown, 1985. Rock Mechanics for Underground Mining. George Allen and Unwin, London.

Brush, L. H., 1988. Feasibility of Disposal of High-Level Radioactive Wastes Into the Seabed: Review of Laboratory Investigations of Radionuclide Migration Through Deep-Sea Sediments, SAND87-2438. Sandia National Laboratories, Albuquerque, New Mexico.

Case, J. B., 1989. Communication regarding the effects of mining the test alcoves in Panel 1 at WIPP to U.S. Department of Energy, WIPP Project Office, Carlsbad, NM, June, 1989.

Case, J. B., P. C. Kelsall, and J. L. Withiam, 1987. "Laboratory Investigation of Crushed Salt Consolidation," in I. W. Farmer, J. J. K. Daemen, C. S. Desai, C. E. Glass, and S. P. Neuman, eds., Rock Mechanics: Proc. 28th U.S. Symposium. A. A. Balkema, Rotterdam.

Coates, D. F., 1981. "Rock Mechanics Principles," CANMET, Energy Mines and Resources Canada, Monograph 874, Ottawa.

Costin, L. S., and W. R. Wawersik, 1980. Creep Healing of Fractures in Rock Salt, SAND80-0392. Sandia National Laboratories, Albuquerque, NM.

Deal, D. E., J. B. Case, R. M. Deshler, P. E. Drez, J. Myers, and J. A. Tyburski, 1989. Brine Sampling and Evaluation Program Phase II Report, DOE-WIPP-87-010. U.S. Department of Energy, Carlsbad, NM.

Dusseault, M. B., L. Rothenburg, and D. Z. Mraz, 1987. "The Design of Openings Using Multiple Mechanism Viscoplastic," in I. W. Farmer, J. J. K. Daemen, C. S. Desai, C. E. Glass, and S. P. Neuman, eds., Rock Mechanics: Proc. 28th U.S. Symposium, pp. 633-642. A. A. Balkema, Rotterdam.

Gonzales, M. M., 1989. Compilation and Comparison of Test-Hole Location Surveys in the Vicinity of the Waste Isolation Pilot Plant (WIPP) Site. SAND88-1065. Sandia National Laboratories, Albuquerque, NM.

Higgo, J. J., L. V. C. Rees, T. G. Coles, and D. S. Cronan, 1987. Diffusion of Radionuclides Through Deep-Sea Sediments, DOE/RW87.053. Department of the Environment, London.

Holcomb, D. J., and M. E. Shields, 1987. Hydrostatic Creep Consolidation of Crushed Salt with Added Water, SAND87-1990. Sandia National Laboratories, Albuquerque, NM.

Ibrahim, A. W., D. J. Borns, and Y. Jung, 1989. Mapping Fractures in Salt at WIPP with the Seismic Method, SAND89-7074A. For presentation at the Society of Exploration Geophysics, Sandia National Laboratories, Albuquerque, NM.

Kelley, V. A., and J. F. Pickens, 1986. Interpretation of the Convergent-Flow Tracer Tests Conducted in the Culebra Dolomite at the H-3 and H-4 Hydropads at the Waste Isolation Pilot Plant (WIPP) Site, SAND86-7161. Sandia National Laboratories, Albuquerque, NM.

Lambert, S. J., 1983. Dissolution of Evaporites in and Around the Delaware Basin, Southeastern New Mexico and West Texas, SAND82-0461. Sandia National Laboratories, Albuquerque, NM.

Lambert, S. J., 1987. Feasibility Study: Applicability of Geochronologic Methods Involving Radiocarbon and Other Nuclides to the Groundwater Hydrology of the Rustler Formation, SAND86-1054. Sandia National Laboratories, Albuquerque, NM.

Lambert, S. J., and J. A. Carter, 1987. Uranium-Isotope Systematics in Groundwaters of the Rustler Formation, Northern Delaware Basin, Southeastern New Mexico, SAND87-0388. Sandia National Laboratories, Albuquerque, NM.

Lappin, A. R., 1988. Summary of Site-Characterization Studies Conducted From 1983 Through 1987 at the Waste Isolation Pilot Plant (WIPP) Site, Southeastern New Mexico, SAND88-0157. Sandia National Laboratories, Albuquerque, NM.

Lappin, A. R., and R. L. Hunter, eds., D. P. Garber, P. B. Davies, assoc. eds., 1989. Systems Analysis, Long-Term Radionuclide Transport, Dose Assessments, Waste Isolation Pilot Plant (WIPP), Southeastern New Mexico; March 1989, SAND89-0462. Sandia National Laboratories, Albuquerque, NM.

LaVenue, A. M., A. Haug, and V. A. Kelley, 1988. Numerical Simulation of Ground-Water Flow in the Culebra Dolomite at the Waste Isolation Pilot Plant (WIPP) Site: Second Interim Report, SAND88-7002. Sandia National Laboratories, Albuquerque, NM.

LaVenue, A. M., B. S. RamaRao, and M. Reeves, 1990. Ground-Water Flow Modeling of the Culebra Dolomite at the Waste Isolation Pilot Plant (WIPP) Site, Vol. 1, Model Calibration, Vol. 2, Data Base, SAND89-7068/1, SAND-7068/2. Sandia National Laboratories, Albuquerque, NM.

Li, Yu., and S. Gregory, 1974. "Diffusion of Ions in Seawater and in Deep-Sea Sediments," Geochimica et Cosmochimica Acta, vol. 38, pp. 703-714.

Longsine, D. E., E. J. Bonano, and C. P. Harlan, 1987. User's Manual for the NEFTRAN Computer Code, NUREG/CR-4766, SAND86-2405. Sandia National Laboratories, Albuquerque, NM.

Morgan, H. S., 1987. "Estimate of the Time Needed for TRU Storage Rooms to Close." Memorandum to D. E. Munson, Sandia National Laboratories, Albuquerque, NM, June 2, 1987.

Mraz, D., 1980. "Plastic Behavior of Salt Rock Utilized in Designing a Mining Method," CIM Bulletin, vol. 73, pp. 11-123.

Munson, D. E., A. F. Fossum, and P. E. Senseny, 1989. Advances in Resolution of Discrepancies Between Predicted and Measured In Situ WIPP Room Closures, SAND88-2948. Sandia National Laboratories, Albuquerque, NM.

National Academy of Science--National Research Council, 1957. The Disposal of Radioactive Waste on Land: Report of the Committee on Waste Disposal of the Division of Earth Sciences, Publication 519. NAS, Washington, DC.

Natural Resources Defense Council v. U.S. Environmental Protection Agency, 824 F.2d 1258 (1st Cir. 1987).

Patrick, W. C., 1987. "Room Conditions in the WIPP Underground." Memorandum to R. Eastmond, Acting Chief, U.S. Department of Energy, Engineering and Experiments Branch, WIPP Project Office, Westinghouse, Memorandum WD:87:00439. U.S. Department of Energy, Carlsbad, NM, March 25, 1987.

Peng, S. S., 1978. Coal Mine Ground Control. John Wiley and Sons, NY.

Peterson, E. W., P. L. Lagus, and K. Lie, 1987. Fluid Flow Measurements of Test Series A and B for the Small-Scale Seal Performance Tests, SAND87-7041. Sandia National Laboratories, Albuquerque, NM.

Rechard, R. R., 1989. Review and Discussion of Code Linkage and Data Flow in Nuclear Waste Compliance Assessments, SAND87-2833. Sandia National Laboratories, Albuquerque, NM.

Reeves, M., D. S. Ward, N. D. Johns, and R. M. Cranwell, 1986a. Data Input Guide for SWIFT II, the Sandia Waste-Isolation Flow and Transport Model for Fractured Media, Release 4.84, SAND83-0242, NUREG/CR-3162. Sandia National Laboratories, Albuquerque, NM.

Reeves, M., D. S. Ward, N. D. Johns, and R. M. Cranwell, 1986b. Theory and Implementation for SWIFT II, the Sandia Waste-Isolation Flow and Transport Model for Fractured Media, Release 4.84, SAND83-1159, NUREG/CR-3328. Sandia National Laboratories, Albuquerque, NM.

Reeves, M., V. A. Kelley, and J. F. Pickens, 1987. Regional Double-Porosity Solute Transport in the Culebra Dolomite: An Analysis of Parameter Sensitivity and Importance at the Waste Isolation Pilot Plant (WIPP) Site, SAND87-7105. Sandia National Laboratories, Albuquerque, NM.

Skokan, C., J. Starrett, and H. T. Andersen, 1988. Final Report: Feasibility Study of Seismic Tomography to Monitor Underground Pillar Integrity at the WIPP Site, SAND88-7096. Sandia National Laboratories, Albuquerque, NM.

Stormont, J. C., E. W. Peterson, and P. L. Lagus, 1987. Summary of and Observations About WIPP Facility Horizon Flow Measurements through 1986, SAND87-0176. Sandia National Laboratories, Albuquerque, NM.

Sutherland, H. J., and S. Cave, 1978. Gas Permeability of SENM Rock Salt, SAND78-2287. Sandia National Laboratories, Albuquerque, NM.

Torstenfelt, B., H. Kipatsi, K. Anderson, B. Allard, and U. Olofsson, 1982. "Transport of Actinides Through a Bentonite Backfill," in W. Lutze, ed., Scientific Basis for Radioactive Waste Management V. Elsevier Science Publishing Co., New York, NY, pp. 659-668.

U.S. Department of Energy, 1980. Final Environmental Impact Statement, Waste Isolation Pilot Plant, DOE/EIS-0026. U.S. Department of Energy, Washington, DC.

U.S. Department of Energy, 1988. Geotechnical Field Data and Analysis Report, June 1986 June 1987, Waste Isolation Pilot Plant, DOE-WIPP-87-0127. U.S. Department of Energy, Carlsbad, NM.

U.S. Department of Energy, 1989a. Draft Supplement, Environmental Impact Statement, Waste Isolation Pilot Plant, DOE/EIS-0026-DS. U.S. Department of Energy, Washington, DC.

U.S. Department of Energy, 1989b. Geotechnical Field Data and Analysis Report, June 1987 June 1988, Waste Isolation Pilot Plant, DOE/WIPP 88-009. U.S. Department of Energy, Carlsbad, NM.

U.S. Department of Energy, 1990a. Final Supplement, Environmental Impact Statement, Waste Isolation Pilot Plant, DOE/EIS-0026-FS. U.S. Department of Energy, Washington, DC.

U.S. Department of Energy, 1990b. Geotechnical Field Data and Analysis Report, DOE/WIPP-90-006. U.S. Department of Energy, Carlsbad, NM.

U.S. Department of Energy and State of New Mexico, 1981, as modified. "Agreement for Consultation and Cooperation," modified 11/30/84 and 8/4/87. U.S. Department of Energy, Albuquerque, NM.

U.S. Environmental Protection Agency, 1985. "Environmental Standards for the Management and Disposal of Spent Nuclear Fuel, High-Level and Transuranic Radioactive Waste; Final Rule," 40 CFR Part 191, Federal Register, vol. 50, pp. 38066-38089.

Weart, W. D., 1983. Summary Evaluation of the Waste Isolation Pilot Plant (WIPP) Site Suitability, SAND83-0450. Sandia National Laboratories, Albuquerque, NM.

APPENDIX A:
UNPUBLISHED MEMORANDUM

April 7, 1987

ROUGH DRAFT

to: Distribution

from: The Performance Assessment Group

re: Early PA Scoping Calculations--To Help Refocus the Research, Development, and Engineering Parts of the WIPP Project, If Necessary

Introduction

Sufficient information has been amassed to begin scoping calculations of the consequences of some scenarios that do not require detailed transport calculations through the engineered barriers and the geologic formation of interest. Because of gaps in data, many assumptions have been necessary; these are identified in each section as appropriate. Some assumptions can be shown to be unimportant; others seem to have high relative importance. During the next few years, the Performance Assessment Task will focus the R & D on those questions that seem to be important.

This memo addresses some potential waste releases that can be bracketed by analytical mathematical calculations revolving mainly around drilling into the repository after the 100-year grace period. Until we can show that these potential releases do not violate 40 CFR 191, there is little reason to complete more detailed calculations of releases from more complex scenarios, using more complex, numerical models. This is because it can easily be shown that by following the guidance on human intrusion in Appendix B of the Standard, the assigned probability of the drilling scenario described here is very high. We note that small margins of safety for this scenario should not be cause for complacency: other scenarios at smaller probabilities may also give rise to projected releases, which when combined with the drilling scenario described here could easily give rise to an unacceptable CCDF (complementary cumulative distribution function).

The guidance suggests that, for WIPP, one must consider 30 drill holes/km^2 per 10,000 years. Of these, R. Hunter estimates that 4 drill holes will penetrate rooms. Because there are no criteria outlining the timing of drilling, we must assume that at least one drill hole will penetrate a room when the operating phenomena combine to produce the largest impact. The first phase of this performance assessment can be summarized as identifying (1) those "energy sources" that could move a quantity of waste sufficient to violate the standard from the repository horizon to the land surface, (2) the form the radionuclides are in at the time of interest, and (3) whether pathway exist through which the energy source can move the waste to the surface in quantities sufficient to be detrimental.

Four energy sources that have been identified are

A. The drill string and drilling fluids,
B. The gas generated by bacteria, thermal, and radiolytic decomposition and further compression by room closure,
C. A pressurized brine pocket beneath the repository, and
D. Hydraulic flow of upper-aquifer water through a U-tube.

Only A and B will be considered as energy sources in the following discussion. The makeup of the material that might be transported up the drill hole ranges from only liquid that has seeped into the room, through a solid/liquid mixture that we have called a slurry, to only solids.

Our conclusions are presented directly below. The overall conclusions are based on the detailed consideration of three cases (p. 2 to p. 6). The results of these three cases are supported by background calculations of inventory (p. 6), EPA release limits (p. 7), brine inflow (p. 8), room closure (p. 10), amounts of rust, bentonite, and void space in the room (p. 10), and gettering capacity of the backfill (p. 11). We also calculated the volumes of gas that might be generated and released from the repository (p. 12). Table 2 (p. 13) presents conversions and calculated values for many of the parameters discussed here.

Overall Conclusions

Based on the available data and analytical calculations and possible releases resulting from drilling, we conclude that

o If any appreciable amount of brine enters the repository before lithification occurs, the EPA 40 CFR 191 cannot be met, because releases resulting from human intrusion, which must be assumed under 40CFR191, guarantee noncompliance.

o Some chemical or mechanical conditions inside the room would ensure that certain specific human-intrusion cases would not violate the Standard.

o The only solution that addresses all cases requires the removal of most of the free volume in the first few years after decommissioning (10 or so years after closure). The free volume can be removed by both processing the waste and changing the backfill.

o Completing only one of the free-volume-reduction steps described above is not adequate to guarantee repository success.

A Detailed Discussion of Three Cases

Three cases are particularly important:

Case 1. Drilling into a room containing a slurry.
Case 2. Drilling into a dry lithified room.
Case 3. Drilling into a dry non-lithified room.

Case 1. Drilling into a Room Containing a Brine Slurry

How much brine or slurry can be released for different Pu solubilities? We considered several possible cases for releases caused by drilling into the repository after closure. Below, we calculate 1.1×10^6 liters of brine/room at 200 years. In Subcase 1, Pu is present in solution at a concentration of 10^{-3} moles/liter; in Subcase 2, Pu is present in solution at a concentration of 10^{-6} moles/liter; and in Subcase 3, Pu is present in solution at a concentration of 10^{-9} moles/liter. We think that these concentrations bracket the range of possible Pu concentrations in brine solutions. In Subcases 1a, 2a, and 3a, only brine is released. In Subcases 1b, 2b, and 3b, a slurry of brine and backfill is released.

Subcase 1a: 1×10^{-3} Moles Pu/liter brine; brine release

Without violating the standard, which allows the summed normalized release (described below) to be 1, we may release a number of liters which is the inverse of the summed normalized release for one liter, i.e., 6.7×10^2 liters or approximately 170 gallons of Subcase 1a brine. This is less than 0.0002% of the room volume.

Subcase 2a: 1×10^{-6} Moles Pu/liter brine; brine release

In the Subcase 2a brine, there is 10^{-6} moles Pu/liter brine. The allowable release thus increases by three orders of magnitude and is 6.7×10^5 liters of brine. This is 61% of the brine in the room.

Subcase 3a: 1×10^{-9} Moles Pu/liter brine; brine release

In the Subcase 3a brine, there is 10^{-9} moles Pu/liter brine. The allowable release thus increases by three orders of magnitude from Case 2a and is 6.7×10^8 liters of brine; however, only 1.1×10^6 liters of brine is present in the room. All the brine may be released without violating the EPA standard.

Subcase 1b: 1×10^{-3} Moles Pu/liter brine; slurry release

We estimate below that 3.6×10^5 g Pu is present in the room and that the volume of slurry in the room is 1.1×10^6 liters. This gives 0.22 g Pu/liter of slurry. The summed normalized release for Subcase 1b can be calculated by scaling from the concentration in one liter of Subcase 1a brine:

$$\frac{\text{0.239 g Pu/liter 1a brine}}{\text{0.22 g Pu/liter 1b slurry}} = 1.09$$

$1.09 \times 6.7 \times 10^2$ (the allowable release of 1a brine) = 728 liters or approximately 180 gallons allowable release of 1b slurry.

Subcases 2b and 3b: 10^{-6} and 10^{-9} Moles Pu/liter brine; slurry release

The change in concentration of Pu in the brine in Subcases 2b and 3b means that slightly more Pu will remain on the solids; however, the total Pu in a

liter of slurry will remain the same. Therefore the allowable releases for Subcases 2b and 3b are the same as for Subcase 1b.

ROUGH DRAFT

Distribution of Pu Among the Components

By assuming that the halite sorbs no Pu and that the bentonite and rust sorb equally, we can estimate the distribution of the Pu among the brine, bentonite, and rust. In the room there are 1.1×10^6 liters of brine, 1.3×10^5 liters of bentonite, and 9.6×10^4 liters of rust (see below). In addition, there are 1.5×10^3 moles Pu/room.

Subcase 1: Brine. 1.1×10^6 liters $\times 10^{-3}$ moles/liter = 1.1×10^3 moles Pu in brine, leaving 0.4×10^3 M Pu to distribute between rust and bentonite.

Bentonite.

$$\frac{1.3 \times 10^5 \text{ liters bentonite}}{(1.3 + 0.96) \times 10^5 \text{ liters (bentonite + rust)}} \times 0.4 \times 10^3 \text{ moles Pu}$$

$= 0.23 \times 10^3$ moles Pu on bentonite. Because we estimate below 3.4×10^5 kg bentonite/room, we obtain 6.8×10^{-4} moles Pu/kg bentonite.

Rust. $0.4 \times 10^3 - 0.23 \times 10^3 = 0.17 \times 10^3$ moles Pu on rust. Because we estimate below 3.2×10^5 kg rust/room, we obtain 5.3×10^{-4} moles Pu/kg rust.

Subcase 2: It can be similarly shown that for Subcase 2, there will be 1.1 moles Pu in the brine and 1.5×10^3 moles Pu on the solids, of which 8.6×10^2 moles Pu will be on the bentonite and 6.4×10^2 moles Pu will be on the rust. This is 2.5×10^{-3} moles Pu/kg bentonite and 2.0×10^{-3} moles Pu/kg rust.

Subcase 3: It can be similarly shown that for Subcase 3, there will be 1.1×10^{-3} moles Pu in the brine, which is negligible, and 1.5×10^3 moles Pu on the solids. The solids total 1.3×10^9 g/room, for 2.8×10^{-4} g Pu/g solids.

Finally, we determined how many grams of solids can be released if all the brine is released first:

670 liters (Subcase 1a brine allowable release) x 0.239 g/l = 160 g Pu allowable release of our mix.

$$\frac{160 \text{ g Pu}}{2.8 \times 10^{-4} \text{ g Pu/g solids}} = 5.7 \times 10^5 \text{ g solids allowable release.}$$

Although there are no data on the strengths of brine-saturated backfills, we have assumed that if there is more than 5% brine in the backfill (over and above the getting capacity of the backfill), it will have little strength, and drilling fluids will rapidly erode it. A 2000', 6-inch drill hole contains approximately 46 m^3 volume.

Summary, Case 1

ROUGH DRAFT

1. If the room is saturated prior to closure, the mixture is at chemical equilibrium at any solubility limit, either energy source A or B is used, and a drill hole penetrates a room, more than enough Pu could get out of the repository to violate 40 CFR 191 before dilution could occur. Because solids would also come to the surface, only 570 liters are needed for violation, which is 0.57/46 = 1% of the volume of the borehole.

2. The repository must remain dry, and getters cannot keep it dry. Thus the water-generation time (the time that the room is unlithified) must be drastically reduced, or the free volume of the room must be drastically reduced in the backfill and in the drums.

Case 2: Drilling into a Dry Lithified Room.

The release of the contents of how many bore holes will violate the standard? Case 2 assumes that the room is dry, i.e., contains less than 5% porosity and therefore no mobile brine, and lithified, i.e., the contents are of high enough strength that the drill hole will remove only the volume of the drill string. Assume a 6" bore hole and uniform distribution of waste in the room. Then from the calculations in Case 1, Subcase 1b, we know that we can remove 728 liters or 0.728 m^3 of mixture. If we assume that the lithified case scales as the initial volumes, then there is 0.26 m^3 of volume in each drum. Thus the equivalent of 0.726/0.26 = 2.8 drums will be the maximum number of drums that can be removed by drilling. Again, assuming that the drums are stacked 3 deep it would take

$$R^2_{drum}/R^2_{drill} = (2)^2/(0.50)^2 = 4/.25$$

= 16 holes to violate EPA 40CFR191.

Summary, Case 2

Recall that four bore holes are predicted to intercept rooms. Following EPA Guidelines, one will not violate 40CFR191 by drilling one to four holes into a dry reconsolidated room.

Case 3: Drilling Into a Room That Is Dry But Has Not Yet Lithified (Reached 95% of Density of Intact Rock)

Could one drill hole cause the standard to be exceeded? Assume that the barrels have been crushed, that 10% of the radionuclides (rather than all) have been or are capable of being mobilized very rapidly (minutes to hours), and that the backfill does not have appreciable strength. Also, assume that the weight of the drill hole full of fluid can and will exceed the strength of any backfill and will erode out a cavity. Then the allowable size of the breach cavity will be the quantity from Case 1, Subcase 3 times 10, or 5700 liters or 5.7 m^3

Because in Case 2 we calculated that there are 46 m^3 of volume in the drill pipe, 5.7 m^3 or 12% additional material would hardly be noticed. Even

for a condition of 1% mobile Pu the cavity need to be would only 57 m^3 or a space 4 m on a side to result in violation if there were complete return of drilling fluid. We estimate a room will be in an unconsolidated (erodable) condition for at least two-thirds of the time until closure, or 200 years after closure, which is 100 years after the 100-year protection period. The chance of violating the EPA standard at some time during the second 100 years is near unity.

Summary, Case 3

1. There will be a period after the 100 year grace period when a drill penetration into a room will violate the standard if there is not essentially complete loss of circulation.

2. The only solution for this case is to remove much of the free volume from the backfill and the drums so that lithification will occur before the 100 year protection period is over.

Background Calculations

Inventory

The IWOP table for Savannah River Operations (SRO) Isotopic Composition Wt. % (Joint Integration Office, 1987, correction dated 4/1/87) shows that Mix 1 is composed of 91.1% Heat Source Material and 7.9% Weapons Grade Material and Mix 2 is composed of 74.6% Heat Source Material, 13.7% Weapons Grade Material, and 10.9% "mostly Pu-241." Because SRO waste contains roughly half of the Pu from all generators (Hess, 1987, Table 1), we have chosen for these calculations to scale SRO Pu waste up to the total Pu inventory for 55 gallon drums (Hess, 1987, Table 1), according to the following method. Because we did not have adequate information for Am, U, and Np, at this time we have not calculated the impacts of these radionuclides; however, we know that the impacts cannot be lessened by their addition.

Table 1. Isotopic mix of plutonium, Savannah River Operations (B. C. Anderson, 1987)

Heat Source Material		Weapons Grade Material	
Pu-238	80 to 83%	Pu-239	93 to 94%
Pu-239	17 to 20%	Pu-240	6%
Pu-240, Pu-241	<1%	Pu-238, Pu-241, Pu-242, Am-241	<1%

Choose fixed percentage values to replace the ranges obtained from B. C. Anderson (Table 1): Heat Source Mix, Pu-238, 82%; Pu-239, 17%; Pu-240 and Pu-241, 0.5% each; Weapons Grade Material, Pu-238, 0.3%; Pu-239, 93%; Pu-240, 6%; Pu-241 and Pu-242, 0.3% each. Then determine the overall percentage of each isotope present in each mix, weighting the percentage in each mix by the percentage present in each type of material:

Mix 2:

Heat Source Material					Weapons Grade Material					241
238	239	240	241		238	239	240	241	242	
.746(.82	+ .17	+ .005	+ .005)	+	.137(.003	+ .93	+ .06	+ .003	+ .003)	+ .109
= (.612	+.127	+.0037	+.0037)	+	.00041	+.127	+.0082	+.00041	+.00041)	+ .109
= (.612	+.254	+.0119	+ .113)							

= 61.2% 238 + 25.4% 239 + 1.2% 240 + 11.3% 241 + 0.04% 242
(= 99.1% Pu as a check on the calculations)

Mix 1: Similar calculations give 75% 238 + 22% 239 + 1.0% 240 + 0.5% 241 + 0.02% 242 (= 98.5% Pu as a check) in Mix 1.

Total Pu Isotopic Mix: Weighting each Mix by percentages extracted from IWOP SRO Table A, p. 1 of 4, we obtain overall percentages of each Pu isotope in the SRO waste:
70.2% 238 + 23.4% 239 + +1.1% 240 + 4.0% 241 + 0.03% 242 (=98.7% as a check).

Using Table 1 (Hess, 1987) and these percentages of total Pu inventory, we obtain the first column below, Ci of each isotope. We use the specific activities in Ci/g to convert each isotope inventory to grams:

	Ci	Ci/g	g	kg
Pu-238	3.2×10^6	1.7×10	1.9×10^5	1.9×10^2
Pu-239	1.1×10^6	6.4×10^{-2}	1.8×10^7	1.8×10^4
Pu-240	5.0×10^4	~~5.47×10~~ .23	~~9.1×10^2~~ 2.17×10^5	~~9.1×10^{-1}~~ 2.17×10^2
Pu-241	1.8×10^5	1.0×10^2	1.8×10^3	1.8
Pu-242	1.4×10^3	3.93×10^{-3}	3.6×10^5	3.6×10^2

Thus the total normalized Pu inventory (NPI) is 1.9×10^4 kg.

Assuming that the NPI is evenly distributed among the 3.6×10^5 drums (Hess, 1987, Table 1), then we have 55 g Pu/drum or 2.3×10^{-1} moles Pu/drum.

Rooms at the WIPP are currently planned to be 300' x 33' x 13', and drums are 2' in diameter and 3' high, leading to a total of 150 x 15 x 3 = 6750 drums/room. At 55 g Pu/drum, this gives 3.6×10^5 g Pu/room or 1.5×10^3 moles Pu/room.

EPA Release Limits

For WIPP, the EPA release limit for an isotope is calculated based on the total TRU inventory according to a rule discussed in detail by Hunter (1987).

For the present calculations, we were unable to obtain an inventory suitable for calculating the release limits in the usual way. Instead, we scaled the release limit of 696 Ci for Pu calculated by Hunter based on the complete inventory of Harville (1986) to the NPI determined above. The NPI release limit is 1.8×10^{3} Ci for each of Pu-238, -239, -240, and -242. There is no release limit for Pu-241, because it has a half life less than 20 years.

Because the remainder of the release calculations have been carried out in grams or moles, we converted the EPA release limits in curies to a more useful unit, release limits in grams. This was done for each isotope by dividing the release limit in curies by the specific activity in curies/gram:

	specific activity in Ci/g	release limit in g
Pu-238	1.7×10	1.1×10^{2}
Pu-239	6.2×10^{-2}	2.9×10^{4}
Pu-240	5.47×10	3.3×10
Pu-242	3.93×10^{-3}	4.6×10^{5}

The release limit for each isotope is the amount that could be released without violating the EPA standard, if only that isotope and no other is released.

Because there is no way in the repository to fractionate the isotopes, they will be released in the same proportions that they are present. Thus we must normalize releases of each isotope to its release limit. We first determined how much of each isotope would be present in a liter of brine with a Pu concentration of 10^{-3} M (the Subcase 1a brine discussed above):

	0.01 x % isotope in mix		total Pu in solution		g isotope/liter
Pu-238	0.702	x	0.239 g Pu/l	=	0.17 g
Pu-239	0.234	x	0.239	=	0.056
Pu-240	0.011	x	0.239	=	0.0026
Pu-242	3×10^{-4}	x	0.239	=	7.2×10^{-5}

Normalizing by dividing each mass in g by the release limit in g and adding, we obtain

$$\begin{array}{cccccccc} & 238 & & 239 & & 240 & & 242 \\ & \frac{0.17}{110} & + & \frac{0.056}{29000} & + & \frac{0.0026}{33} & + & \frac{7.2 \times 10^{-5}}{4.6 \times 10^{5}} \end{array}$$

$$= 1.5 \times 10^{-3} + 1.9 \times 10^{-6} + 7.9 \times 10^{-5} + 1.6 \times 10^{-10}$$

$$= 1.5 \times 10^{-3}.$$

This figure is the summed normalized release for one liter of Subcase 1a brine. Because the summed normalized release may be 1, 670 liters x 10^{-3} moles/liter x 239 g/mole = 160 gm Pu can be released.

Brine Inflow

Two end member calculations have been made for brine inflow: direct scaling and 1/r scaling of D. Deal's field inflow data.

Direct Scaling. Direct scaling of brine inflow based on surface areas of the bore holes for which data are available and of the room should estimate the maximum volume of brine that could reasonably be expected to enter the room. The surface area of a room is 3,066 yd^2. From D. Deal's data, two holes that are being monitored as part of the Brine Sampling and Evaluation Program (BSEP) were chosen as representative: A3X02 and A3X02. (When time allows, an average of all holes will be used.) Their lengths were about 50 ft, diameters about 4 inches, and brine inflows about 0.03 liters/ day. Brine flow then will be 2 liters/yd^2/yr or 1.85 liter/ m^2/yr.

The flow into the room then would be 3000 yd^2 x 2 liter/yd^2/yr or 6000 liters/yr/room or about 5.8 m^3/yr/room. If the rooms do not repressurize for 200 years (the approximate crossover point for room closure and brine inflow), there will be approximately 1200 m^3 of brine in the room.

Approximate 1/r Scaling

From D. Deal's data for holes A3X01 and A3X02, there is an inflow of 0.03 liter/day for a 50-ft hole. Radial scaling of these data from bore hole scale to to repository scale should approximate the smallest volume of water that could reasonably be predicted to enter the repository. If we assume that the hole length is the length of the room, then the quantity of brine flowing into the room is

0.03 liter/day x 365 day/yr x 300/50 = 66 liter/yr/room

For a 200-year closure time, the amount of brine in the room will be 13,200 liter or 13 m^3.

For the calculations described above, a brine influx rate of 1.8 liters/ m^2/yr was used. This influx rate was assumed to be constant, on an areal basis, regardless of the radius of the opening into which the brine flows. Thus the brine influx rate for a room of a given length was assumed to be much greater than the influx rate for a borehole of the same length because the total surface area of the room is much larger than that of the borehole.

Another reasonable model for the brine influx rate assumes that inflow into a cylindrical opening is constant per unit length of the opening regardless of its radius and its total surface area. This model, which we refer to as the radially scaled brine influx model, results in much lower inflow rates than the one described above, and can be considered to be a reasonable lower bound on the brine influx rate for a room-size excavation (E. J. Nowak, personal communication). For this model, we chose a brine influx rate of about 0.03 liters/day from the 50'-long holes A3X01 and A3X02. Because a room would be 300' long, we multiplied 0.03 liters/day x 6 to obtain an influx rate of 0.18 liters/day for a room. This is equivalent to 365 day/yr x 0.18 liters/ day or 66 liters/day or 0.066 m^3/year of brine per room. Assuming that a

room closes in 1000 years and that the closure rate is constant, the volume of the room in m^3 as a function of time in years is given by the equation y = 3,644 - 3.644x, where y is the volume and x is the time. The volume of brine in m^3 in the room as a function of time is given by y = 0.066x. Both these equations describe straight lines, and they can be solved simultaneously to give the porosity of the room at the time of resaturation. For a room that is completely empty at t = 0 (no drums, no backfill), resaturation occurs at t = 982 years, at which time the porosity is about 2%. For a room that initially contains 65% void space (approximately the situation if the room is filled with 6,750 drums that are each 50% full, and a 70% halite/30% bentonite backfill with a porosity of 75%), resaturation occurs at t = 638 years, at which time the porosity is also 2%. If one assumes that each drum is completely full with no porosity at all (this could be approached by filling the drums with concrete), resaturation occurs at 393 years and a residual porosity that is still 2%.

All of the calculations based on the radially scaled brine influx model predict that resaturation would not occur until the void space in the room decreases to about 2%. This is slightly below the level of 5%, a level below which we feel it would be highly unlikely that the brine, halite, rust, and bentonite could form a slurry and transport significant quantities of Pu up a borehole. Nevertheless, this result is not very reassuring, because our estimates of some of the parameters used in our calculations are preliminary and could easily lead to errors of 3%, which in turn places the void space at the time of resaturation at 5% or greater. Moreover, we have only considered Pu in these calculations, and have not included Am, Np, and U, elements that we think are present in significant quantities in the TRU inventory.

We therefore calculated the initial porosity of the backfill that would be required, assuming no void space in the drums, to achieve a porosity of 5% by t = 100 years, the first time at which the EPA suggests in 40CFR191 that drilling be considered. Using the linear closure and inflow equations given above, we calculated an initial backfill porosity of 20%. This porosity apparently can be achieved by fabricating the halite-bentonite backfill mixture into bricks, but it is unclear whether these bricks can be fabricated to fit into the spaces between the drums.

Room Closure

From D. Munson's data on closure of an empty room, we estimate that there will be at least 100 years after the 100-year grace period during which the strength of the backfill and contained brine will be negligible. During most of the closure time, the pressure in the room will be very low, without back pressure to retard the flow of brine into the room.

Rust, Bentonite, and Void Space in the Room

Each drum contains about 30 kg of iron, which will oxidize to 48 kg of rust (Fe_2O_3). At 6750 drums, this is 3.2×10^5 kg rust/room.

Assuming a backfill mixture of 70% halite and 30% bentonite by volume, and densities of 2.16 g/cc for halite and 2.6 g/cc for bentonite, the weighted

particle density for the backfill is 2.3 g/cc. We have assumed 75% void space in the backfill: backfill will be blown in and therefore will be loosely packed and may have large air gaps near the ceiling and below drums. Deep-sea clay sediments have porosities of about 75%. This gives a bulk density of the backfill (including air gaps) of 0.58 g/cc.

The total room volume is 3.7×10^3 m^3. Each drum has a volume of 0.26 m^3. With 6750 drums, the total volume inside the drums is 1755 m^3 and outside the drums is 1945 m^3. Multiplying the backfill bulk density of 0.58 g/cc by the volume outside the drums, we obtain 1.13×10^6 kg as the mass of backfill in a room. The mass of bentonite in the room is 1.13×10^6 kg x $0.3 = 3.4 \times 10^5$ kg. The mass of salt in the room backfill is 1.13×10^6 kg x $0.6 = 7.9 \times 10^5$ kg.

The free volume or void space in the backfilled part of the room is 0.75×1945 $m^3 = 1459$ m^3. Assuming 50% void space inside the drums, the free volume inside drums is 0.26 m^3/drum x 6750 drums x 0.5 = 877 m^3. Total void space in the room is therefore about 2300 m^3. The total room volume is 3700 m^3, for a total room free volume of 62%.

Finally, we determined the volume percentage of each component in the slurry. First we calculated the mix of solids and brine in one liter of homogeneous slurry.

Rust: 3.2×10^8 g rust/room at 3.5 g/cc gives 9.1×10^7 cc rust/room or 9.1×10^4 liters rust/room.

Bentonite: 3.4×10^5 kg bentonite/room at 2.6 g/cc gives 1.3×10^8 cc bentonite/room or 1.3×10^5 liters bentonite/room.

Halite: Halite is present in a 7:3 volume ratio with bentonite. Therefore there are 1.3×10^5 liters x (7/3) or 3.0×10^5 liters of halite/room.

Brine: We assumed that the volume of the room will be reduced by half at 200 years, when all void space is filled by brine. Therefore the brine volume will be 31% of the initial room volume. Thus 3700 m^3 x 0.31 = 1147 m^3 = 1.1×10^6 liters of brine.

Total: The total volume of slurry is 1.6×10^6 liters/room. Dividing each component's volume by the total to obtain percentages gives 6% rust, 8% bentonite, 19% halite, and 69% brine.

Gettering of the Brine

Bentonite. Commercial bentonite will getter approximately 0.14 g brine/g bentonite before it turns into a slime. For a 70% salt, 30% bentonite backfill, there will be 3.4×10^5 kg bentonite in a room. The bentonite in a room will be able to getter 4.8×10^4 liters of brine. For the 1/r scaling of brine inflow, the bentonite can getter all of the water (4.8×10^4 liter getter capacity compared with 1.32×10^4 liters brine) with only 27% of the gettering capacity. If, however, the scaling factor is linear, the available bentonite can getter only 4% of the available brine. If the

backfill were all bentonite, it would only be able to getter 16% of the available brine. Because the amount of brine that will flow into the rooms is clearly not known at this time, relying on the capability of a getter to reduce releases seems very risky.

Other Possible Getters. A cursory review of some of some commen getters shows that anhydrous $CuSO_4$ will getter about as much water as any material: $CuSO_4$ $CuSO_4$ $5H_2O$, Two of the waters of hydration are very tightly bound; the other three are quite mobile. A little more water turns the getter into a liquid. It would thus require 1.7×10^9 g $CuSO_4$ powder to getter the brine from the direct scaling case described above. If the powder had a density of 0.58 g/cc (the same as the salt/bentonite backfill), then the quantity of $CuSO_4$ needed to getter the brine would be 2.9×10^3 m^3. There is available 1945 m^3 of volume for getter. Thus the getter could collect at most about 70% of the brine.

Parametric Variations in Biodegradable CH_2O Per Drum

We considered several cases for gas generation: 1, 10, and 100 kg biodegradable CH_2O per drum. The biodegradable CH_2O may be present not only inside the drums as part of the waste, but outside the drums as well.

One kg biodegradable CH_2O/drum is equivalent to 33 M of CH_2O and CO_2 per drum. From the TRUPACII document (Joint Integration Office, 1986), we see that 4.2 moles/drum/yr gas generation by bacteria is expected. Thus the biodegradable CH_2O will be used up in (33 moles/drum)/(4.2 moles/drum/yr) = 8 years. Similarly, 10 kg biodegradable CH_2O/drum will be used up in 80 years, and 100 kg biodegradable CH_2O/drum will be used up in 800 years. From Stormont's work (1987), we see that at 10 psig, 2.5 cc/m^2/minute of gas can flow into the formation. We assume that this flow rate is valid for all our calculations. The room is 10.1 m x 4 m x 92 m, for a surface area of 2674 m^2. Thus 2674 m^2 x 2.5 cc/m^2/minute leaks out of the room, equivalent to 6.7 liters/minute of gas leakage.

This is equaivalent to

$$\frac{6.7 \text{ liters/min}}{22.4 \text{ liters/mole}} = 0.3 \text{ moles/min} = 1.6 \times 10^5 \text{ moles/yr/room gas leakage}$$

At 4.2 moles/drum/yr x 6750 drums, we get 28,350 moles/yr/room of bacterially generated CO_2 from organic matter.

In addition, there is 17,550 moles/yr/room thermally generated CO_2 from organic matter.

The total generated gas is therefore 5.0×10^4 moles/yr/room.

If only the ceiling and floor leak gas out of the repository, the amount leaking out is

$$\frac{1858 \text{ m}^2}{2674 \text{ m}^2} \times 1.6 \times 10^5 \text{ mole/yr/room}$$

Therefore it appears that all the generated gas can leak out for the 1 kg biodegradable CH_2O case, without creating high pressures in the repository as a result of gas buildup. In the other two cases, we assume that gas generation will proceed at the same rate and pressures, and that only the time at which generation stops will change. Therefore, the repository will continue to leak gas as fast as it is produced, and gas pressurization will not occur.

Table 2. Conversions and calculated values

$1\ m^3 = 10^3$ liters

$1\ yd^3 = 0.8\ m^3$

Total repository Pu inventory (NPI) = 1.9×10^4 kg Pu

55 gm Pu/drum = 2.3×10^{-1} mole/drum

Amount of Pu to violate standard = 160 gm Pu/room

Room surface area = $3.066 \times 10^3\ yds^2$

Room volume = $3.7 \times 10^3\ m^3$

Drums/room = 6750

Room dimensions = 33' x 13' x 300'

Drum dimensions = 2' diameter, 3' high

Rust/drum = 48 kg/drum

Rust/room = 3.2×10^5 kg/room

Bentonite backfill/room (30%) = 3.4×10^5 kg/room

Salt backfill/room (70%) = 7.9×10^5 kg/room

Salt & bentonite/room = 1.13×10^6 kg/room

Void space in backfill/room = $1459\ m^3$

Void space in drum/room = $877\ m^3$

Bulk density of blown-in backfill = 0.58 gm/cc

Volume of drum = $0.26\ m^3$

Total void space/room = $2300\ m^3$

% initial room free volume = 62%

Room free volume = 62%

Brine flow in room (direct scaling 2 liters/gm/m^2) = $3700\ m^3$ or
1.1×10^6 liters at 200 yr.

Brine flow in room (1/r scaling) = 66 liters/yr/room

Time to 95% room closure, unfilled = 500, 1000 yrs

Time to 95% room closure, filled = 310, 620 yrs

Brine in room at closure (1/r scaling) = $13\ m^3$ at 200 yrs or $20\ m^3$ at 300 yrs

Summed normalized release of Pu, 1 liter of Case 1 brine = 1.5×10^{-3} gm

Gas generation/room = 5.0×10^4 moles/yr

Gas leak rate/room = 1×10^5 moles/yr

Brine gettered by bentonite/room = 4.8×10^4 liters

Volume of a 6"-diameter, 2000-ft drill hole = $1570\ ft^3$ or $58\ yds^3$ or $46\ m^3$

References

B. C. Anderson, Joint Integration Office, 1987, telephone conversation, 4/1/87.

Harvill, Joe P., 1986, Letter to Jon Myers, "Projected Radionuclide Inventories for the Waste Isolation Pilot Plant," 4/29/86.

E. G. Hess, Joint Integration Office, 1987, Letter to Michael McFadden, "Subject, Average Curie," 3/13/87.

R. L. Hunter, 1987, Memo to Distribution, "Two Scenarios for the Exercise of Codes for the WIPP Performance Assessment," 2/16/87 (Draft).

Joint Integration Office, 1987, Memo to Larry Kapinos, "Waste Information Based on 1985 IWOP Data," 3/16/87.

Joint Integration Office, 1986, "Proposed TRUPACT-II Criteria For Gas Generation," DRAFT.

J. C. Stormont, E. W. Peterson, and P. L. Lagus, 1987, Summary of and Observations about WIPP Facility Horizon Flow Measurements Through 1986, SAND87-0176, Sandia National Laboratories.

END

DATE FILMED

03 / 04 / 91